Universitat Ramon Llull

DOCTORAL THESIS

Title	**Singlet Oxygen in Antimicrobial Photodynamic Therapy: Biological effects, Mechanistic Studies and Future Directions**
Presented by	**Xavier Ragàs Amalrich**
Centre	**Escola Tècnica Superior IQS**
Department	**Organic Chemistry**
Directed by	**Prof. Santi Nonell Marrugat** **Prof. Montserrat Agut Bonsfills**

C. Claravall, 1-3
08022 Barcelona
Tel. 936 022 200
Fax 936 022 249
E-mail: urlsc@sec.url.es
www.url.es

C.I.F. G: 59069740 Universitat Ramon Lull Fundació Privada. Rgtre. Fund. Generalitat de Catalunya núm. 472 (28-02-90)

Per la meva família i amics.

Per la Carla.

"It was mid-1800s in France. The father looked at the teacher. Would he help?

The teacher looked at the father. He did not want to say no. He did not want to disappoint the father of one of his pupils. But, how could he possibly help? What did he, a science teacher, know about turning beetroots into alcohol?

But the father was looking so hopefully. Surely (his gaze seemed to say) you will come and look. You, Monseiur Pasteur, have set the boys of our city of Lille on fire with your fascinating lessons about the wonders of natural world.

Surely you, of all people, can solve our terrible problem at the sugarbeet factory?"

From: "Pasteur's fight against microbes"

We see in nature not words,
but rather only the first letters of words,
and if we then wish to read,
we discover that the new so-called words
are again merely first letters of others.

Georg Christoph Lichtenberg

AKNOWLEDGEMENTS

All the work presented in this thesis involves many different people, from different places, but all of them contributed in different but important ways:

Primer de tot, gràcies al Dr. Nonell i a la Dra. Agut per permetrem començar una nova línea “antimicrobiana” que espero sigui un bon punt d’inici per nous treballs. Donar també les gràcies al Santi i a la Montse pels bons moments dins i fora la universitat, per haver sabut trobar un equilibri idoni en la codirecció, i haver sabut crear una figura de “pare” i “mare” científics difícil d’oblidar.

Secondly, but not least, I’d like to thank Prof. Hamblin for accepting me during six months in his laboratory. Working with animals had been one of the goals of my thesis and I’m really glad that it finally has been accomplished.

Likewise, I’d like to thank everybody in MGH: Pawel, Ying Ying, Tianhong, Liyi, Marcus, Divya, Casey, etc. You’ve all been part of my trip, showing me the way things work in US. Special thanks to Andrea, who helped me from beginning to end without saying NO any single time…

Agraïr també al Dr. Sànchez García la síntesi del porficè catiònic donat que sense ell, el viatge a Boston no hagués tingut sentit. Tot viatge té un objectiu i aquest porficè era part indispensable en ell. I al David, per haver-me animat en situacions on l’experiència era de gran ajuda.

A la Dra. Flors, por proveernos con la proteína fluorescente. A Cris por, desde un principio y sin saberlo, ser parte de esta tesis. Si nos lo llegan a decir en Monzón, de verdad que no lo creo… Sabes que me hace mucha ilusión!

To Prof. Geddes for proving us the silver island films.

To Prof. Rocha Gonsalves for providing us the ACS268 porphyrin.

A l’empresa SORISA, i en concret al Dr. Amat, pel préstec de la font de llum SORISA Photocare®.

Al Dr. Tomàs per l’ajuda amb tots els dubtés de la part estadística del present treball.

Al Dr. Borrell per permetrem intentar retrobar un camí perdut en el món de la síntesi durant els primers 6 mesos de feina… Qui m’ho hagués dit a mi… Per suposat, a tota la gent de la secció de síntesi des de l’Ofir fins al Gonzalo i la Maria, els últims a arribar. Moltes estones divertides, moltes xerrades (futbolístiques o no), consells, experiències (qui ens treurà Llavorsí), cafès… etc. Per tot, GRÀCIES!

To Xin He and Miquel Duràn (l’estudiant de 2n) for helping me during a few months with my studies. I hope each of you learned as much as I did trying to explain you, not to teach you, how and why we did all those experiments. Thanks!

A les noies de microbiología, Helena, Anna i Patri, per soportar tot el caos que pugui haver generat anant d'un costat a l'altre… Cada laboratori és diferent i conseqüenment funciona de diferent manera… Espero no haver estat cap "molèstia" durant aquest temps!

A la Judith per tots els grandíssims moments que hem viscut junts al laboratori de 3r… Ha estat molt de temps fent d'auxiliars o companys junts. Gràcies per deixar-me viure l'experiència docent!

Als Fotoq's 1, i permeteu-me la separació temporal, Ana, Mireia i Lourdes. Vam passar molts bons moments que de veritat no podré oblidar. Primero a Ana, sabes cuanto te quiero, aunque nos veamos muy poco, y cuanto hiciste por esta tesis (muchas charlas, muchos ratos juntos, muchos experimentos fallidos… pero tal y como dijiste, al final, todo sale!). Mireia i Lourdes, Lourdes i Mireia… Quins farts de riure al lab, quins grans moments... Molts secrets, vivències, cafès i xerrades que marquen a una persona! Per tot, GRÀCIES!

Als Fotoq's 2, Adaya, María, Rubén, Ignasi, Marta, Miki i Roger. Increibles! Amb això ho dic tot… És extrany quan te n'adones que ets el més antic en un lloc… espero haver sabut transmetre el que havia de transmetre en aquest sentit. En qualsevol cas, tots vosaltres m'heu fet sentir realitzat al acabar… Diuen que no es deixa mai d'aprendre i això s'ha vist amb vosaltres… M'heu fet aprendre moltíssim des del primer dia que vau arribar! Podria dir moltes coses de cada un, però crec que tots sabeu el que penso de vosaltres!

A tot el grup de dinars, en especial a la Tere i l'Anna que encara no han sortit… portem molts anys junts i molts més que espero que passin, si no treballant al mateix lloc, amb els sopars com el de casa l'Anna! Suposo que tots trobarem a faltar en algún moment aquesta hora de Psicòleg en les que hem arreglat el món tantes vegades! Oi?

Als Piltras, tots vosaltres ja sabeu com importants heu estat… molts anys comentant el viatge i per fi ja té un final feliç. Moltíssimes gràcies pel vostre interés en tot moment, per si les coses sortien o no. Persones com vosaltres són necessàries! A resaltar sobre tots, al Juan i la Imma. Sabeu que tot i no estar presents heu patit col·lateralment aquesta tèsi i tot el que ha comportat! Gràcies per ser com sou i poder tenir-vos al costat!

Y en especial, a mis compañeros de viaje… Xavi, Manu y Quique… Quique desde el CSIC con sus problemas computacionales… Xavi, perdón, Dr. Berzosa, con sus dilemas sínteticos… Manu, con tus dudas metodológicas y analíticas… Si es que lo tenemos todo para montar una empresa!!!! Sabeis tan bien como yo que cada uno de vosotros ha sido parte indispensable en esto. MUCHAS MUCHÍSIMAS GRACIAS!!!

Al Dani, la Maria i el Nacho… Tota taula té 4 potes sobre les que s'aguanta, i vosaltres serieu també una d'elles. Fa molts molts anys que ens coneixem i compartim bons moments… De vegades més a sovint, de vegades menys del que deuriem… Però si hi ha una cosa que tinc clara amb vosaltres és que la distancia no importa. Ja formeu part de mi i anireu sempre, com heu estat fent durant aquest viatge, amb mi! Moltes gràcies!

Al meu germà Sergi, la meva cunyada Míriam i com no, a la meva futura neboda. Sou un exemple per mi a seguir des del primer moment… De vegades lamento tenir-vos "tan" lluny i no poder veure'us més sovint. En qualsevol cas, m'heu demostrat que la distancia no és un obstacle, encara que hi hagi l'Atlàntic pel mig!!! I m'heu fet tiet, que més puc demanar?? Sou els millors, i tal com us vaig dir en un dels dies més importants de la vostra vida, us estimo!

Als meus pares. Recordo que quan us vaig comentar la possibilitat de fer la tèsi només em vau dir una cosa… El que vulguis, però si la comences, l'acabes! Doncs aquí està… Aquest és el meu regal per vosaltres i el vostre regal cap a mi… uns anys de la meva vida que mai podré oblidar. Mai us podré tornar tot el que heu fet i el que m'heu ajudat! Us estimo!

I finalment, a la Carla (també als teus pares i al teu germà)… Des del primer moment has estat al meu costat en aquest viatge. M'has ajudat escoltant-me, aconsellant-me, i animant-me quan ha calgut. Ara tu has començat el teu viatge, i puc prometre des del primer moment que no et fallaré tal i com tu no ho has fet … T'estimo!

The development of this thesis has been possible thanks to a predoctoral FI fellowship and BE fellowship from the *Departament d'Universitats, Recerca i Societat de la Informació* of the Catalonian government and from the *Fons Social Europeu*, to the Spanish Ministry of Science and Technology (BCQ2007-67763-C03/BQU), and to the Escola Tècnica Superior IQS.

SUMMARY

In this thesis, the use of antimicrobial photodynamic therapy as alternative to antibiotics has been assessed. First, the potential of phenothiazinium dyes, and specifically new methylene blue, to inactivate multidrug-resistant strains has been demonstrated against *Acinetobacter baumanii in vitro* and in a mouse burn model. In this regard, it also has been investigated the potential of aryl cationic porphycenes as photosensitizing drugs in APDT *in vitro* and *in vivo*, successfully inactivating different gram-positive and negative bacteria, and fungal cells.

Second, the kinetics of singlet oxygen ($^1O_2$) production and fate in *E. coli* have been investigated by means of an ultrasensitive near-infrared spectrometer with submicrosecond time resolution. The results allowed us to gain insight into the mechanism of APDT, *i.e.*, the localization of the photosensitiser (PS) in the bacteria and the reactivity of $^1O_2$. On one hand, the microenvironment of the PS changes when the distribution of the cationic charges changes. On the other hand, depending on the site of production, $^1O_2$ reacts with the nearest microenvironment or is able to escape out of the cells.

Third, the ability of fluorescent proteins (GFPs), as genetically-encoded photosensitisers, to produce reactive oxygen species has been studied by means of fluorescent probes and time-resolved techniques. Thus, for the first time, the quantum yield of $^1O_2$ production of some of the studied proteins has been calculated showing a value similar to that of the synthetic GFP chromophore.

Finally, the plasmonic effect of silver island films on $^1O_2$ has been investigated using the near-infrared spectrometer, demonstrating a maximum enhancement of the $^1O_2$ luminescence signal at 1270 nm *ca.* 30-fold in some cases.

RESUMEN

En esta tesis se ha evaluado el uso la terapia fotodinámica antimicrobiana (APDT) como alternativa a los antibióticos. Inicialmente, se ha demostrado, *in vitro* y en un modelo de quemaduras en ratón, el potencial de las fenotiazinas, y más concretamente del nuevo azul de metileno, para inactivar una bacteria resistente a antibióticos como *Acinetobacter baumanii*. Además, también se ha investigado el potencial de los porficenos aril catiónicos como agentes fotosensibilizadores para APDT *in vitro* e *in vivo*, inactivando exitosamente distintos tipos de bacterias gram positivas y negativas, así como hongos.

Por otro lado, se ha estudiado las cinéticas de formación y decaimiento de oxígeno singlete ($^1O_2$) en *E. coli* mediante un espectrofotómetro ultrasensible en el infrarrojo cercano con resolución temporal por debajo del microsegundo. Los resultados nos permiten profundizar en el mecanismo de la APDT, es decir, en la localización del fotosensibilizador (PS) en la bacteria y la reactividad del $^1O_2$. Por un lado, el entorno del PS cambia cuando la distribución de las cargas catiónicas varía. Por otro lado, en función del lugar de formación, el $^1O_2$ reacciona con el entorno cercano o es capaz de escapar fuera de las células.

En tercer lugar, también se ha estudiado, mediante sondas fluorescentes y técnicas con resolución temporal, la habilidad de una proteína fluorescente para producir especies reactivas de oxígeno, actuando pues como agentes fotosensibilizadores genéticamente codificados. Así, se ha calculado por primera vez el rendimiento cuántico de formación de $^1O_2$ mostrando un valor similar al del cromóforo sintético de las GFP.

Finalmente, se ha investigado mediante el espectrofotómetro en el infrarojo cercano el efecto plasmon producido por films de islas de plata sobre $^1O_2$, observando un incremento máximo de la luminiscencia de $^1O_2$ a 1270 nm alrededor de 30 veces en algunos casos.

RESUM

En aquesta tèsi s'ha avaluat l'ús de la teràpia fotodinàmica antimicrobiana (APDT) com a alternativa als antibiòtics. Inicialment, s'ha demostrat *in vitro* i en un model de cremades en ratolins el potencial de les fenotiazines, i més concretament del nou blau de metilè, per inactivar un bacteri resistent a antibiòtics com *Acinetobacter baumanii*. A més, també s'ha investigat el potencial dels porficens aril catiònics com a agents fotosensibilitzadors per a APDT *in vitro* i *in vivo*, inactivant exitosament diferents tipus de bacteris gram positius i negatius, així com fongs.

Per altra banda, s'han estudiat les cinètiques de formació i decaïment d'oxigen singlet ($^1O_2$) en *E. coli* mitjançant un espectrofotòmetre ultrasensible a l'infraroig proper amb resolució temporal per sota del microsegon. Els resultats ens permeten profunditzar en el mecanisme de l'APDT, és a dir, en la localització del fotosensibilitzador (PS) en el bacteri i la reactivitat de l'$^1O_2$. Per un costat, l'entorn del PS canvia quan la distribució de les càrregues catiòniques varia. Per l'altre, en funció del lloc de formació, l'$^1O_2$ reacciona amb l'entorn proper o és capaç d'escapar fora de les cèl·lules.

En tercer lloc, també s'ha estudiat, mitjançant sondes fluorescents i tècniques amb resolució temporal, l'habilitat d'una proteïna fluorescent per produir espècies reactives d'oxigen, actuant com a agents fotosensibilitzadors genèticament codificats. Així, s'ha calculat per primera vegada el rendiment quàntic de formació d'$^1O_2$ obtenint un valor similar al del cromòfor sintètic de les GFPs.

Finalment, s'ha investigat mitjançant l'espectrofotòmetre en l'infraroig proper l'efecte plasmó produït per films d'illes de plata sobre l'$^1O_2$, demostrant un increment màxim en la luminescència d'$^1O_2$ a 1270 nm al voltant de 30 vegades en alguns casos.

LIST OF ABBREVIATIONS

APDT	antimicrobial photodynamic therapy
ALA	Δ_5-aminolevulinic acid
BSA	bovine serum albumin
CALI	chromophore-Assisted Light Inactivation
CFU	colony forming units
DHE	dihydroethidium
DMMB	dimethylmethylene blue
DNA	deoxyribonucleic acid
D-PBS	deuterated phosphate buffered saline
EDTA	ethylenediaminetetraacetic acid
EGFP	enhanced green fluorescent protein
F	fluorescence
GFP	green fluorescence protein
HBDI	4-hydroxybenzylidene-1,2-dimethylimidazoline
IC	internal conversion
IR	infrared
IRF	Instrument’s response function
ISC	intersystem crossing
k_q	quenching rate constant
LPS	lipopolysaccharides
MB	methylene blue
MEA	2-mercaptoethylamine
MDPyTMPyP	5-mono(*N*-decyl-4-pyridyl)-10,15,20-tri(*N*-methyl-4-pyridyl)-21*H*,23*H*-porphine
MDRs	multidrug resistance pumps
MRSA	methicillin-resistant *Staphylococcus aureus*
NIR	near infrared radiation
NMB	new methylene blue N
$^1O_2$, O_2 ($a^1\Delta_g$)	singlet oxygen
$O_2^{\bullet -}$	superoxide radical
OPA	optical parametric amplifier
OPO	optical parametric oscillator
P	phosphorescence
PBS	phosphate buffered saline
PDI	photodynamic inactivation

PDT	photodynamic therapy
PMT	photomultiplier tube
PN	phenalenone
PS	photosensitiser
^{3}**PS**	triplet excited state of the photosensitiser
ROS	reactive oxygen species
SDS	sodium dodecyl sulphate
SOSG	singlet oxygen sensor green
τ_Δ	singlet oxygen lifetime
TBO	toluidine blue O
TCSPC	time-correlated single photon counting
TMPyP	5,10,15,20-tetrakis(*N*-methyl-4-pyridyl)-21*H*,23*H*-porphine
TRPD	time-resolved phosphorescence detection
τ_T	triplet lifetime
UV	ultraviolet
VIS	visible
VR	vibrational relaxation

INDEX

1. CHAPTER 1: *Introduction*

1.1. The “antibiotic” era 23
1.2. Antimicrobial photodynamic therapy 25
  1.2.1. Molecular basis of photodynamic therapy . . . 25
  1.2.2. Advantages of antimicrobial photodynamic therapy . . 28
  1.2.3. Possible applications of antimicrobial photodynamic therapy 28
1.3. Antibacterial photodynamic therapy 29
  1.3.1. Gram positive and negative bacteria . . . 30
  1.3.2. Photosensitisers 32
  1.3.3. Selectivity 34
  1.3.4. Mechanisms of bacterial inactivation . . . 34
1.4. Objectives 37
1.5. References 38

2. CHAPTER 2: *General Techniques and Methods*

2.1. Steady-state optical techniques 47
  2.1.1. Absorption and transmitance 47
  2.1.2. Emission 47
2.2. Time-resolved optical techniques 49
  2.2.1. UV-VIS nanosecond laser flash photolysis . . . 49
  2.2.2. Time-Correlated Single Photon Counting . . . 50
  2.2.3. Time-Resolved NIR Phosphorescence Detection . . 51
  2.2.4. Bioluminescence imaging 53
2.3. Microbiological techniques 54
  2.3.1. Microbial strains 54
  2.3.2. Culture conditions 54
  2.3.3. Photosensitiser uptake and quantification . . . 55
  2.3.4. Spectroscopic measurements in cell suspensions . . 55
  2.3.5. Spheroplasts formation 56
  2.3.6. Photodynamic inactivation experiments *in-vitro* . . 56
  2.3.7. *In-vivo* burn infection model 57
  2.3.8. Photodynamic inactivation experiments *in-vivo* . . 58
  2.3.9. Mouse follow-up 58
2.4. References 59

3. **CHAPTER 3:** ***Photodynamic inactivation of Acinetobacter baumannii using phenothiazinium dyes***

3.1. Introduction 63
3.2. Experimental section. 65
3.3. Results 66
3.4. Discussion 70
3.5. Conclusions 73
3.6. References 74

4. **CHAPTER 4:** ***A tricationic porphycene as potential photosensitiser in antimicrobial photodynamic therapy***

4.1. Introduction 81
4.2. Experimental section 83
4.3. Results 84
4.4. Discussion 90
4.5. Conclusions 93
4.6. References 94
4.7. Annex 98

5. **CHAPTER 5:** ***Singlet oxygen in E. coli: new insights for antimicrobial photodynamic therapy***

5.1. Introduction 101
5.2. Experimental section 103
5.3. Results 104
5.4. Discussion 110
5.5. Conclusions 115
5.6. References 116

6. **CHAPTER 6:** ***Mechanistic aspects of antimicrobial photodynamic therapy in E. coli: Photosensitiser-dependent singlet oxygen formation and decay***

6.1. Introduction 123
6.2. Experimental section 125
6.3. Results 126
6.4. Discussion 131
6.5. Conclusions 135

6.6. References 136
6.7. Annex 140

7. **CHAPTER 7:** ***Singlet oxygen photosensitisation by the fluorescent probe Singlet Oxygen Sensor Green***

7.1. Introduction 145
7.2. Experimental section 147
7.3. Results 148
7.4. Discussion 155
7.5. Conclusions 157
7.6. References 158
7.7. Annex 161

8. **CHAPTER 8:** ***Genetically-encoded singlet oxygen production by a red fluorescent protein***

8.1. Introduction 167
8.2. Experimental section 169
8.3. Results 170
8.4. Discussion 174
8.5. Conclusions 176
8.6. References 177
8.7. Annex 180

9. **CHAPTER 9:** ***Singlet oxygen enhancement by silver islands films***

9.1. Introduction 183
9.2. Experimental section 185
9.3. Results 186
9.4. Discussion 191
9.5. Conclusions 193
9.6. References 194

10. **CHAPTER 10:** ***General Discussion***

10.1. General discussion 199
10.2. References 203

11. CHAPTER 11: ***Conclusions*** 209

List of contributions to other articles 211

Chapter 1

Introduction

A general introduction to the subject of this thesis and the aim of this work is given in this chapter. The history and the basis of antimicrobial photodynamic therapy are reviewed and new perspectives for this therapy are also presented.

1.1. THE "ANTIBIOTIC" ERA

Since the discovery of penicillin by Fleming in 1928, many different families of antibiotics have been approved in the EU and in the US (Fig 1), being the cell wall and the protein synthetic processes the most important targets.

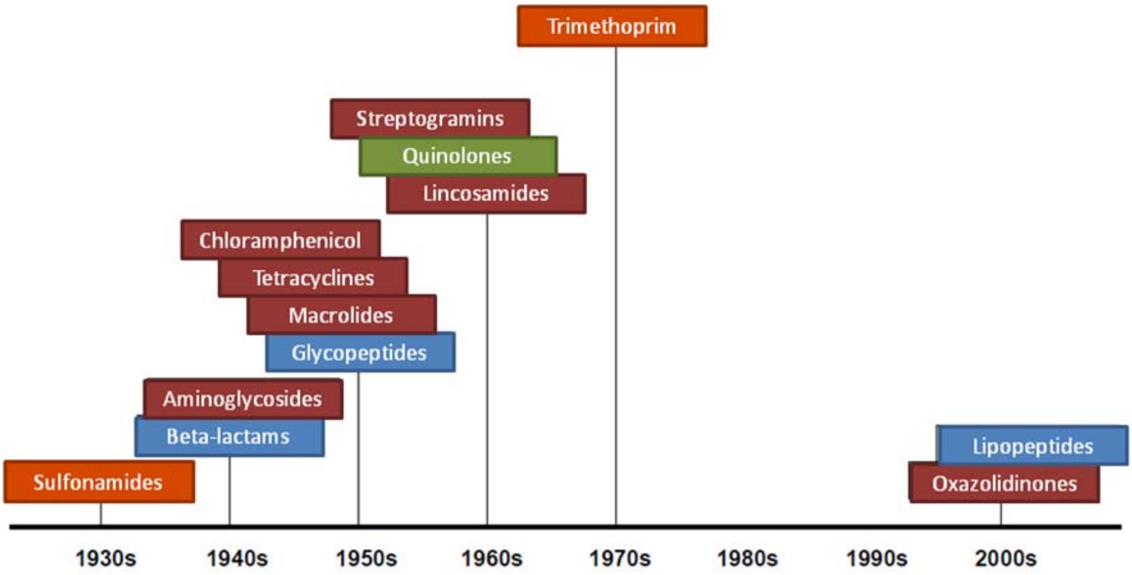

Fig. 1: Discovery of new classes of antibiotics. Color refers to the principal target. Orange: Inhibition of folic acid synthesis. Blue: Inhibition of cell wall synthesis. Maroon: inhibition of protein synthesis. Green: inhibition of DNA or RNA synthesis. Modified from [1].

Antibiotics have become the "panacea" of medicine and are being used to treat even the most common and trivial types of infections, many of these non-bacterial in nature. However, during the last decades, the number of clinical drug-resistant isolates –such as methicillin-resistant *Staphylococcus aureus* (MRSA), cephalosporin-resistant *Escherichia coli*, carbapenem-resistant *Pseudomonas aeruginosa,* etc.– has significantly increased and grown to be a global pandemic and unavoidable problem in hospitals (Fig. 2) [2-4].

Even Alexander Fleming, in 1945, warned that the inappropriate use of penicillin could lead to the selection of resistant "mutant forms" of *S. aureus* [5]. Transferable genetic elements such as plasmids encoding resistance enzymes and efflux pumps that can be transferred between species, the inappropriate prescription of antibiotics and the failure of some patients to complete their treatment regimen, the widespread use of antibiotics in livestock feedstuff; all of them are causes by which the most resistant strain is selected [3].

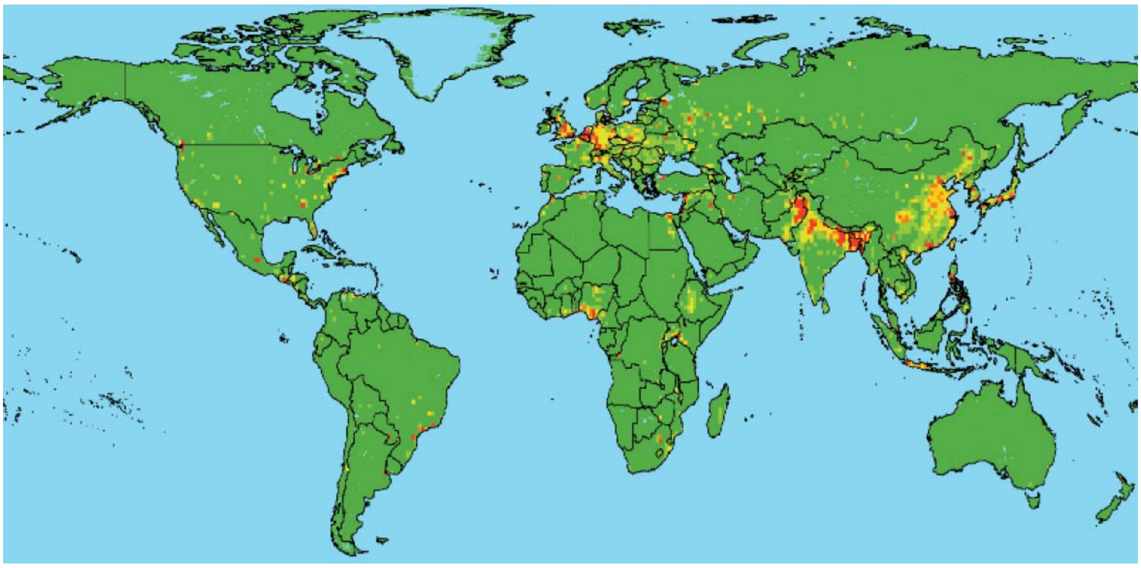

Fig. 2: Global distribution of relative risk of an emerging infectious disease event caused by drug-resistant pathogens. Relative risks mapped on a linear scale from green (lower values) to red (higher values). From [6].

As a result, infections by a drug or, in some cases a pandrug-resistant bacteria –strains that are resistant to all available antibiotics– result in extra health care costs and productivity losses of at least 1.5 billion euros in the EU and 5 billion dollars in the US per year. What is even more important is that, each year, about 25000 patients in the EU and 90000 patients in the US die from an infection caused by these bacterial strains.

The problem of increased resistance is not only restricted to bacteria. Some fungal strains such as *Candida albicans* and *Kodamaea ohmeri* have already developed resistance to antifungal agents such as amphotericin B, flucytosine and fluconazole [7-10]. As regards protozoan parasites, it has been clinically demonstrated that uncompleted treatments of leishmaniasis with meglumine antimoniate and sodium stibogluconate induces selection of the drug-resistant strains increasing 10 to 17 fold the 50% inhibitory concentration for *L. mexicana* and *L. braziliensis* isolates.

Therefore, an important research effort is being made to find alternative antimicrobial therapies to which these “superbugs” cannot easily develop resistance. Examples of these relatively novel therapies are bacteriophages [11], naturally occurring or synthetic antimicrobial peptides [12,13], and photodynamic therapy (PDT) [14].

1.2. ANTIMICROBIAL PHOTODYNAMIC THERAPY

Among all the alternative treatments to antimicrobial agents, antimicrobial photodynamic therapy (APDT) seems to be a promising one. Indeed, the first recorded observations using photodynamic processes to inactivate microbial cells were made by Raab *et al.* more than 100 years ago [15]. They observed that low concentrations of acridine orange were able to kill *Paramecium caudatum* in the presence of sunlight, whereas in darkness these microorganisms survived.

Two main advantages have to be highlighted about PDT. On one hand, it has been demonstrated that drug-resistant microorganisms are as susceptible to APDT as their native counterparts [16], or even more susceptible [17]. On the other hand, it has not been possible to artificially induce resistance to APDT yet [18-20], presumably because of the short-lived species related to the photodynamic effect and the non-specific nature of the photooxidative damage that leads to cell death.

1.2.1. Molecular basis of photodynamic therapy

Photodynamic therapy (PDT) involves the administration of a photoactive dye that is able to produce *reactive oxygen species* (ROS) upon irradiation with light. Thus, when the dye absorbs a photon, an electron is promoted from its ground state to an electronically-excited state that returns the energy through three main pathways (Fig. 3) [21]:

a) Non-radiative processes. The excited state species release the excess of energy as heat by three different processes:

- *Vibrational relaxation* (VR): the excited molecule decreases its vibrational energy within a single electronic state.
- *Internal conversion* (IC): transition between two electronic states with the same spin multiplicity, generally followed by vibrational relaxation.
- *Intersystem crossing* (ISC): transition between two electronic states with different spin multiplicity, generally followed by vibrational relaxation.

b) Radiative processes. The excited state species return the excess of energy as electromagnetic radiation. Divided in two kinds of processes:

- *Fluorescence* (F): spontaneous emission of radiation upon transition between two electronic states with the same spin multiplicity.

- *Phosphorescence* (P): spontaneous emission of radiation upon transition between two electronic states with different spin multiplicity.

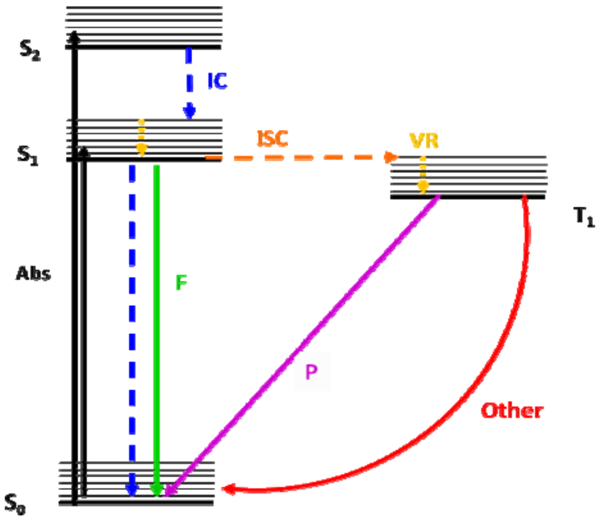

Fig. 3: Jablonski diagram depicting the possible photophysical processes.

c) Other deactivation processes. The excited state molecules can undergo photochemical or photophysical reactions or photosensitisation.

Photosensitisation is the process by which a photochemical or photophysical alteration occurs in one molecular entity (A) as a result of initial absorption of radiation by another entity called photosensitiser (PS) [22]. It can schematically be represented as follows:

$$PS + h\nu \rightarrow PS^*$$

Photochemical: $PS^* + A \rightarrow PS' + B$

Photophysical: $PS^* + A \rightarrow PS + A^*$

When molecular oxygen is involved in photosensitisation, such process is termed “photodynamic action” and two different mechanisms are possible:

- *Type I mechanism:* the PS in its singlet or triplet excited state reacts with a substrate *via* (a) electron transfer or (b) hydrogen abstraction to yield free radicals, which will readily react with oxygen to form peroxides radicals, and in turn starting a radical chain reaction.

$$PS + h\nu \rightarrow PS^*$$

a) $PS^* + R \rightarrow PS^{\bullet -} + R^{\bullet +}$ b) $PS^* + RH \rightarrow PSH^{\bullet} + R^{\bullet}$

$PS^{\bullet -} + {}^3O_2 \rightarrow PS + O_2^{\bullet -}$ $R^{\bullet} + {}^3O_2 \rightarrow ROO^{\bullet}$

$R + O_2^{\bullet -} \rightarrow R^{\bullet -} + {}^3O_2$ $ROO^{\bullet} + RH \rightarrow ROOH + R^{\bullet}$

- *Type II mechanism:* in this process, the sensitiser in its excited state (commonly in its triplet state) transfers its energy to ground-state molecular oxygen, giving rise to the PS in its ground state and singlet oxygen ($^1O_2$), a very reactive oxygen species towards electron rich substrates such as alquenes, aromatic rings, phenols, amines and thioethers [23].

$$PS + h\nu \rightarrow PS^*$$
$$PS^* + {}^3O_2 \rightarrow PS + {}^1O_2$$

In general, in biological media, the photodynamic effect occurs simultaneously by either the two mechanisms (Fig. 4). The relative importance of one mechanism over the other depends, among other factors, on the substrate and oxygen concentrations and on the distance between the PS and the substrate. However, both mechanisms can produce the photooxidation of relevant biomolecules, such as aminoacids, nucleic bases and lipids, which leads to damage on proteins, DNA and membranes, *i.e.*, leading to cell death.

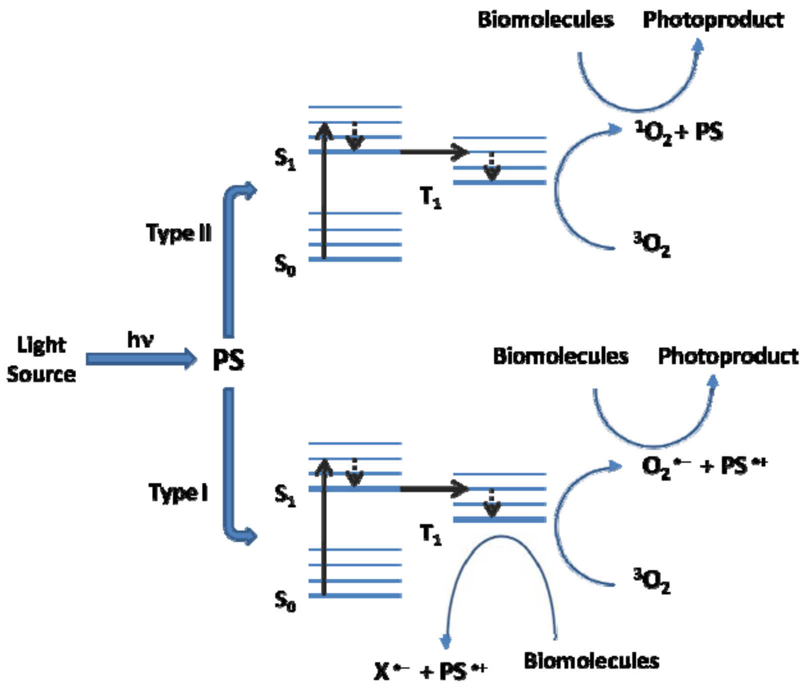
Biomolecules
Photoproduct
$^1O_2$+ PS
S_1
T_1
Type II
S_0
$^3O_2$
Light Source
hν
PS
Biomolecules
Photoproduct
$O_2^{•-}$ + PS$^{•+}$
Type I
S_1
T_1
$^3O_2$
S_0
X$^{•-}$ + PS$^{•+}$
Biomolecules

Fig. 4: Mechanisms of ROS generation by combination of light, photosensitiser (PS) and ground-state oxygen. Ground-state photosensitiser (S_0) is irradiated with visible light generating excited-state photosensitiser (S_1). S_1 can relax back to excited-triplet PS state (T_1), generating radicals (Type I mechanism) and / or singlet oxygen (Type II mechanism).

1.2.2. Advantages of antimicrobial photodynamic therapy

One of the greatest hits of photodynamic therapy is the double selectivity obtained by targeting (1) the PS, derived from its high affinity for microbial cells, and (2) the light, implying that only the infected area is irradiated and, consequently, treated. However, many other advantages can be found compared to antimicrobial drugs [24,25]:

- *Practical advantages:* APDT is safe for human tissue as the PS typically shows a higher affinity against microbial cells. The results are instantaneous while antibiotics take several days to act. It can be used to treat damaged or dead tissue, e.g. burns.

- *Effective:* The therapeutic window of APDT is broader than other antimicrobial therapies, even against pathogenic biofilms. Because of the high reactivity of ROS, secreted virulence factors can be destroyed as these are commonly proteins, enzymes or aminoacid residues. Besides, APDT cannot easily induce the development of microbial resistance.

1.2.3. Possible applications of antimicrobial photodynamic therapy

As previously said, one of the main advantages of APDT versus other antimicrobial agents is the broader therapeutic window. Hence, it can be applied to many different infectious diseases as presented in Fig. 5.

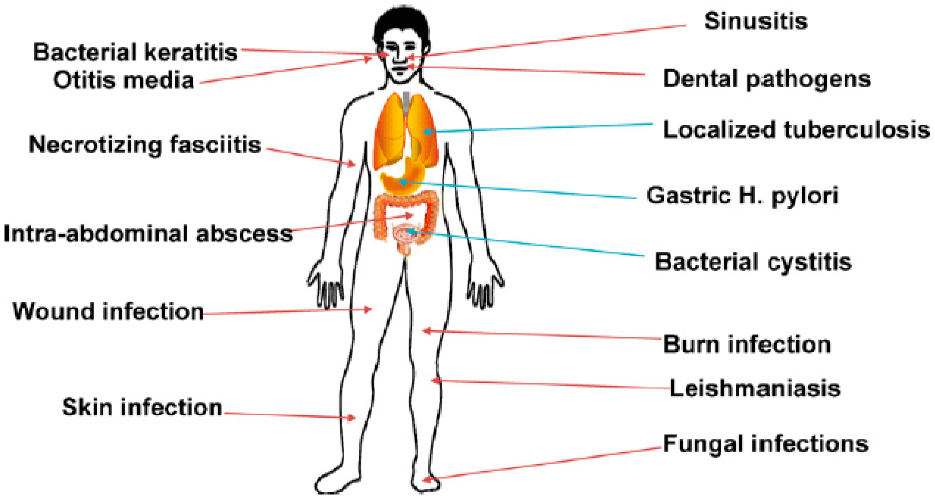
Sinusitis
Bacterial keratitis
Otitis media
Dental pathogens
Localized tuberculosis
Necrotizing fasciitis
Gastric H. pylori
Intra-abdominal abscess
Bacterial cystitis
Wound infection
Burn infection
Leishmaniasis
Skin infection
Fungal infections

Fig. 5: Candidate infectious diseases for PDT. A wide variety of localized infections could be clinically treated by antimicrobial PDT. From [24].

Thus, there are many different possible applications of APDT against a wide range of pathogenic microorganisms, some of them in clinical trials. Herein, a brief summary with examples of possible applications for different microbial cells is presented:

- *Antibacterial photodynamic therapy:* Dental infections are the largest growth area of clinical antibacterial PDT. Indeed, three different companies in North America, Austria and UK use APDT with phenothiazinium dyes and red light to treat periodontitis, endodontics and caries. This field will be more extensively treated in the following section.
- *Antifungal photodynamic therapy:* Teichert *et al.* [26] demonstrated in a mouse model that methylene blue mediated PDT can efficiently inactivate *C. albicans* upon irradiation with red light in order to treat mucocutaneous oropharyngeal candidiasis. Also, APDT was used clinically by Calzavara-Pinton *et al.* [27] to treat interdigital mycosis of the feet by *Candida* or *Tricophyton* species by means of an Δ_5-aminolevulinic acid (ALA) preparation and red light.
- *Antiprotozoan photodynamic therapy:* The most important application in this field is the use of APDT to treat leishmaniasis. PDT was shown to be more effective than tropical paromomycin and methylbenzethonium chloride in the therapy of cutaneous leishmaniasis [28-30].
- *Antiviral photodynamic therapy:* Although virus are not microorganisms because they are not considered living cells, it has been demonstrated the efficiency of APDT against them [31]. Diseases such as herpesvirus infections and papillomatosis are susceptible to be treated with APDT. However, the most general application in this field is blood sterilization. Mohr *et al.* [32,33] reported the inactivation of hepatitis B and C viruses, human immunodeficiency virus, parvovirus B19 and west nile virus with phenothiazinium dyes in blood products or plasma.

1.3. ANTIBACTERIAL PHOTODYNAMIC THERAPY

As mentioned above, the first recorded observations of photodynamic processes in medicine refer to the inactivation of microorganisms [15]. However, the potential of PDT against diseases of microbial origin was not exploited for several decades, largely for two reasons: (a) the discovery of antibiotics; (b) early discouraging results that some well known pathogens, especially gram-negative bacteria, were poorly responsive to PDT with the most traditional photosensitising agents.

1.3.1. Gram positive and negative bacteria

The domain *Bacteria* is divided in two groups based on the cell's reaction to a staining method called *Gram stain*. The differences between gram-positive and gram negative bacteria relate to differences in their cell wall structure and chemical composition.

Thin sections of gram-positive bacteria reveal thick walls, almost uniformly dense layers (Fig. 6; left). In contrast, the cell walls of gram-negative bacteria are much more complex, because in addition to a peptidoglycan layer they have another layer, called an outer membrane. The structural differences between the cell walls of both kinds of bacteria reflect differences in biochemical composition.

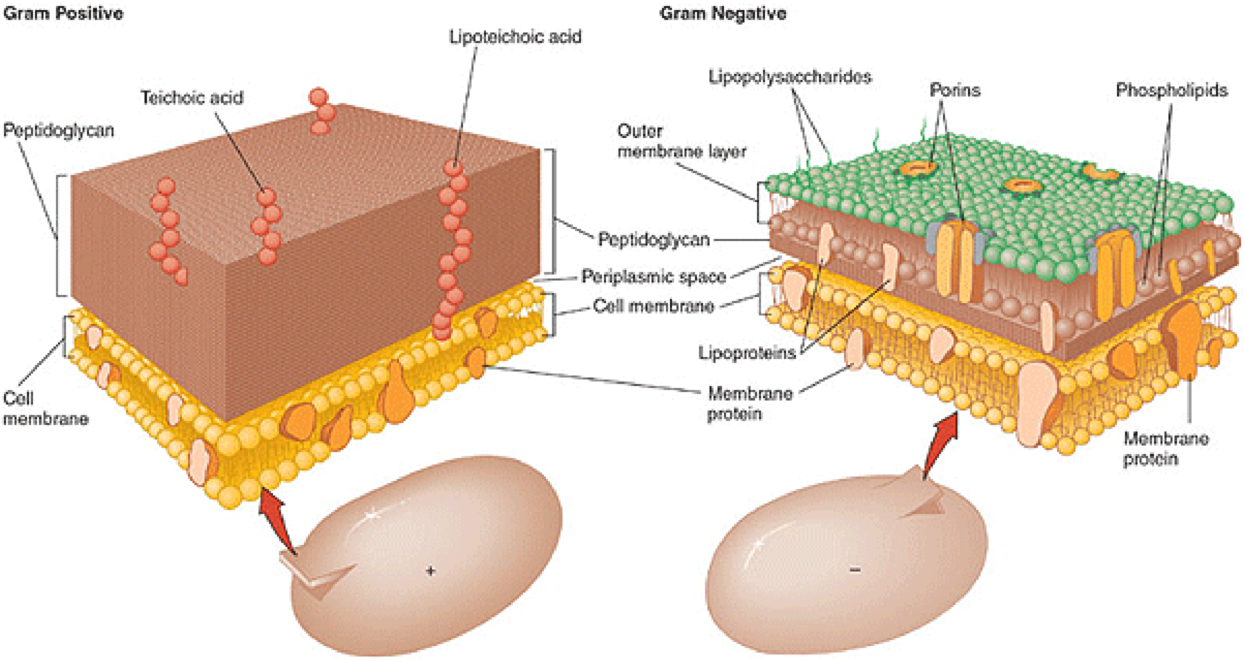
Gram Positive
Gram Negative
Lipoteichoic acid
Teichoic acid
Peptidoglycan
Cell membrane
Lipopolysaccharides
Porins
Phospholipids
Outer membrane layer
Peptidoglycan
Periplasmic space
Cell membrane
Lipoproteins
Membrane protein
Membrane protein
+
–

Fig. 6: Schematic representation of the cell wall and cytoplasmic membrane structure in gram positive (left) and negative bacteria (right).

Peptidoglycan is the major constituent of the cell wall of gram-positive bacteria. This is made up by chains of the amino sugar backbone *glycan* (*N*-acetylglucosamine and *N*-acetylmuranic acid linked) that are held together by peptide bridges. It makes up about 40% to 80% of the cell wall weight depending on the species and has a tensile strength similar to that of reinforced concrete. *Teichoic* and *teichuronic acids* are also constituents of gram-positive cell walls. Teichoic acids are polyol phosphate polymers, such as polyglycerol phosphate and polyribitol phosphate. Sugars (e.g., glucose and galactose), amino sugars (e.g., glucosamine), and the amino acid *D*-alanine are found in some of these compounds. Teichuronic acids are polymers of two or more repeating subunits, one of which is always a uronic acid (such as glucuronic acid), or the uronic acid of an amino sugar (such as aminoglucuronic acid). Both teichoic and teichuronic acids are linked covalently to peptidoglycan.

In gram-negative bacteria (Fig. 6; right), *peptidoglycan* is present, but it makes up a much smaller portion of the cell wall composition. In contrast to gram-positive bacteria, which have several layers of peptidoglycan encasing the cell, gram-negative have only a single or a few macromolecular sheets. Indeed, the peptidoglycan makes up about 5% by weight of the gram-negative cell wall, but it still plays an important role as a rigid barrier outside the cell membrane.

The outer membrane of gram-negative cells seems similar to the cell membrane: there is a predominance of lipids and proteins, but there are polysaccharides that extend into the aqueous environment as well. As in the cell membrane, the outer membrane has two leaflets, each of them consisting of lipid molecules with their hydrophilic moieties facing away from the membrane toward the aqueous environment, and their hydrophobic portions facing inward and holding the two leaflets together. Lipid A attaches to the outer leaflet of the membrane and is bound covalently to a polysaccharide forming a complex. This complex lipid-polysaccharide is called *lipopolysaccharide* (LPS). LPS is a high-molecular-weight, strongly negatively charged molecule. The outer membrane of gram-negative bacteria contains less proteins than the cell membrane. The most prevalent protein is a small polypeptide that contains a lipid moiety. This *lipoprotein* is joined covalently to the diaminoacid of the peptidoplycan forming a complex called *peptidoglycan-lipoprotein*. Therefore, the lipoprotein is the bridge that joins the outer membrane to the cell wall peptidoglycan layer. Other important proteins are those that serve as transport proteins (*porins*), which allows the passage of molecules through the outer membrane.

There are two main features of outer membrane structure that influence its functioning as a selective permeability barrier. The first is given by *porins*, which form water-filled channels that work as general or substrate-selective conduits for free diffusion of certain hydrophilic molecules, such as sugars and amino acids, as well as inorganic ions. The second is the high net negative charge on LPS molecules, which provides a polyanionic external surface that is partly neutralised by divalent cations, such as Mg^{2+} and Ca^{2+}, and can be considered to bridge adjacent LPS molecules [34].

The space between the cell wall and the cell membrane is called the *periplasm*. This is important to the cell because, although small, a great enzymatic activity takes place inside.

1.3.2. Photosensitisers

A good photosensitising agent with potentially optimal properties for APDT (Fig. 7) should be endowed with specific features in addition to the expected photophysical characteristics [35,36]. Such features include the possibility to identify a therapeutic window which allows (a) the extensive killing of the disease-inducing microbial cells with minimal damage to the host tissue in the area of infection, and (b) the prevention of the regrowth of the pathogens after the treatment [25].

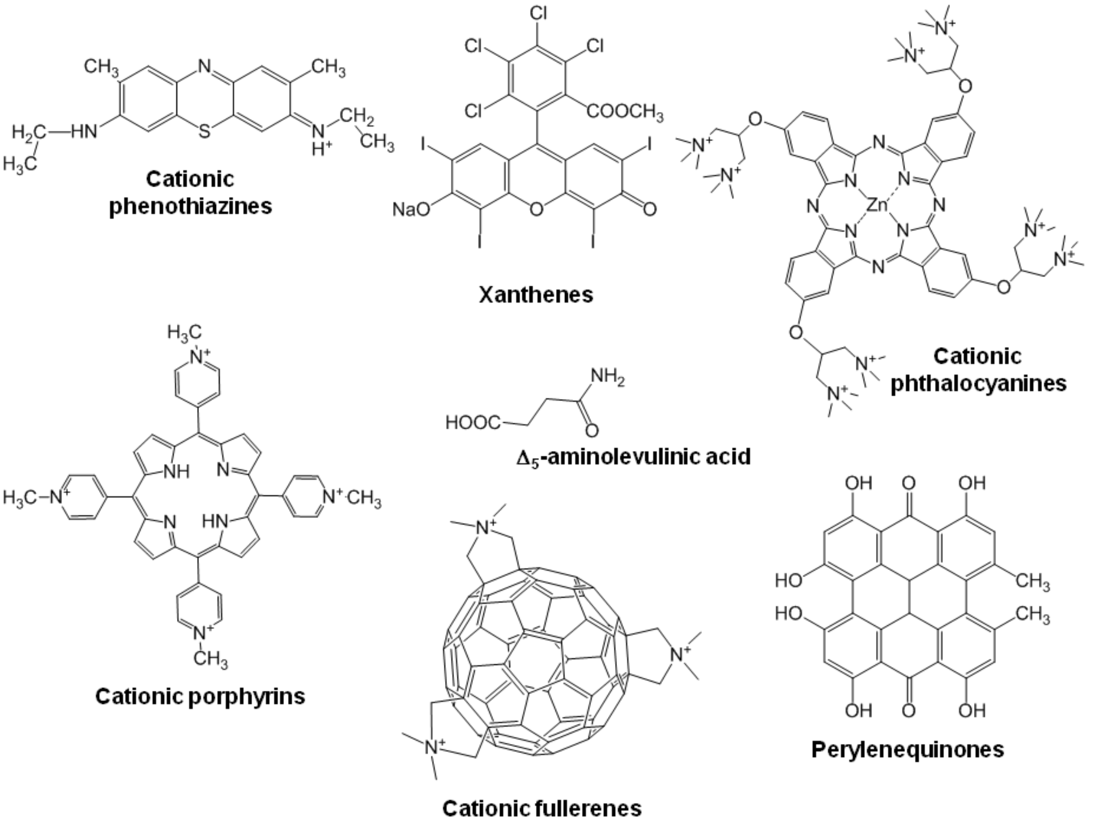
Cationic phenothiazines
Xanthenes
Cationic phthalocyanines
Cationic porphyrins
Δ5-aminolevulinic acid
Cationic fullerenes
Perylenequinones

Fig. 7: Examples of PS used in antimicrobial photodynamic therapy.

As seen above, gram-positive and gram-negative bacteria differ in the composition of their cell wall. This difference gives rise to a different response to antimicrobial agents depending on the kind of bacteria. Gram-positive bacteria can easily take up molecules such as neutral or anionic PS used for PDT and can be easily photoinactivated by them

[37]. In the case of gram-negative bacteria, photoinactivation is not so easy since they are relatively impermeable to neutral or anionic drugs due to their highly negatively charged surface. Notwithstanding, it was proved that many of these PS were effective against gram-negative bacteria if they were supplied with an agent able to disrupt the cell wall of the bacterium sufficiently to allow the access of the drug that can then cause lethal damage to the cell when it is exposed to light. Thus, disrupting agents such as polymixin B nonapeptide [38,39], oligomers of lysine [38,39] and ethylenediaminetetraacetic acid (EDTA) [40] were used.

However, it is desirable for clinical applications to avoid the coadministration of a disrupting agent, so an alternative strategy was preferred. A work carried out simultaneously by Merchat *et al.* [41], Minnock *et al.* [42], and Wilson *et al.* [43] showed that PS positively charged at physiological pH were active against both gram-positive and gram-negative bacteria, and consequently avoided the coadministration of the disrupting agent. Thus, cationic phenothiazines, porphyrins, phthalocyanines and even fullerenes containing quaternary groups have been synthesized [44-48].

Despite the potential and the wide range of these cationic PSs, some other strategies may overcome the lower affinity of typical PDT photosensitisers against gram-negative bacteria.

Another different strategy was performed by attaching covalently non-cationic PS to higher structures which provide the high affinity against bacterial cells, e.g. polymers with basic amino groups, such as polylysine or polyethylenimine [18,49-51], or even nanoparticles [52] or biomolecules [53]. The covalent attachment would preclude the coadministration of a second species, but keeping the disrupting effect produced by these molecules intact. The main advantages of these conjugates are that (1) they increase the specificity for microbial over human cells [54], and (2) PSs that were not accessible due to their low solubility in water can be used as the solubility is provided by the higher structure [52]. However, the targeting against specific regions in microbial cell, *i.e.*, the increase in the specificity and resulting decrease in the number of target sites in the microbial cell, could potentially promote development of resistance against APDT [54].

Active-targeted photosensitisers can increase the selectivity for bacterial cells, but the ideal selectivity would be realized if a photosensitiser is efficiently and exclusively confined in the pathogenic cells. In relation to that, it is worthy to be note that very recently, the first genetically-encoded PS has been reported, namely a phototoxic homolog of the green fluorescence protein (GFP) designed to produce ROS upon irradiation with green light [55]. Further studies carried out by Serebrovskaya *et al.* [56] concluded that $^1O_2$ was not involved in the cytotoxic effect of a conjugate between an antibody and that GFP-homolog. Since then, many other GFP-analogues have been synthesized and studied. Jimenez-Banzo *et al.* [57] reported the singlet oxygen quantum yield (Φ_Δ) value of the GFP-chromophore in its anionic form, namely $\Phi_\Delta = 0.004 \pm 0.001$. In addition, for the first time, the time-resolved $^1O_2$ phosphorescence at 1270 nm upon photosensitisation by a GFP-mutant was reported, demonstrating a clear shielding effect from oxygen of the GFP β-can. Although in its initial steps of research, genetically-encoded PS would open new perspectives for photodynamic therapy.

1.3.3. Selectivity

An important observation about cationic antimicrobial PSs concerns their selectivity for microbial cells compared to host mammalian cells [58]. It is thought that cationic molecules are only slowly taken up by host cells by the process of endocytosis, while their uptake into bacteria is relatively rapid. If illumination is performed at short intervals after PS application (minutes) then PDT damage to host tissue will be minimized.

There have been relatively few *in vitro* studies demonstrating selective killing of microbes under conditions in which mammalian cells were unharmed. Soukos *et al*. showed that *Streptococcus sanguis* was killed by toluidine blue and red light using parameters that spared human gingival keratinocytes and fibroblasts [59]. Zeina *et al*. used human keratinocytes that resisted killing by methylene blue-mediated PDT under conditions that killed several cutaneous microbial species [60]. Soncin *et al*. reported that certain cationic Zn-phthalocyanines, combined with a short incubation time (5 min) and relatively low light fluences, killed both wild-type and methicillin-resistant *S. aureus*, while human fibroblasts and keratinocytes were unharmed [61]. Maisch *et al.* reported, with porphyrin-based PSs, the effective killing of different MRSA strains via reactive oxygen species without harming fibroblasts or keratinocytes cells at the same concentrations [46].

1.3.4. Mechanisms of bacterial inactivation

Notwithstanding the vast progress made over the last few years, the mechanistic details of how APDT affects microbial cells are not fully understood.

As regards the uptake pathways of anionic and cationic PS, George *et al.* [62] reported that the uptake of anionic PSs by bacterial cells may be mediated through a combination of electrostatic charge interaction and by protein transporters, while the uptake of cationic PSs is mediated by electrostatic interactions and “self promoted” uptake pathways.

In relation to the mechanism of photodynamic inactivation, Jori *et al.* [25] proposed two alternative pathways of cationic PS for gram-positive and gram-negative bacteria (Fig. 8).

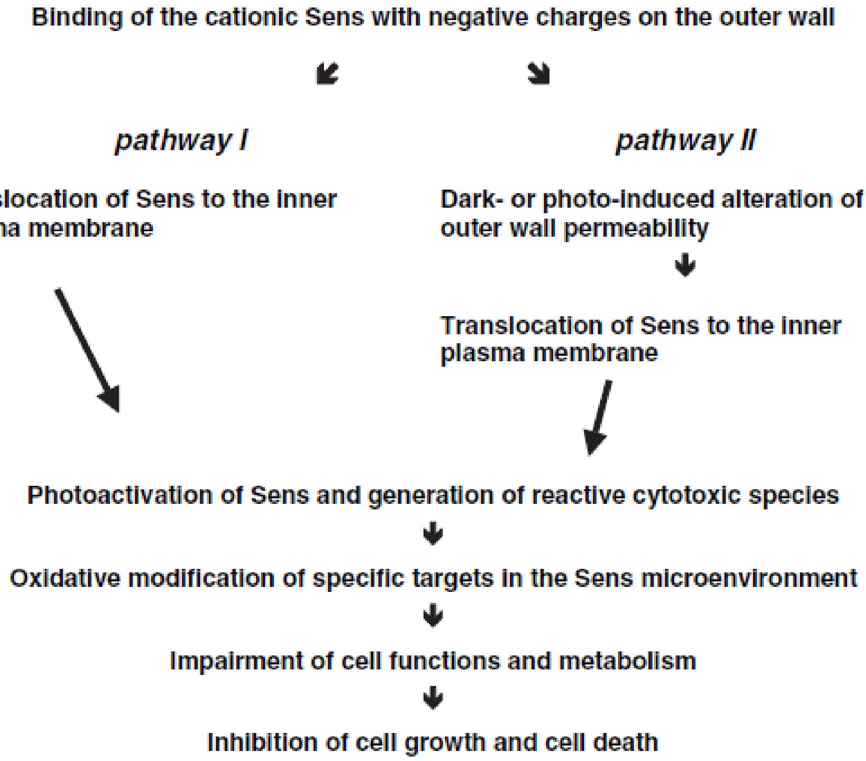
Binding of the cationic Sens with negative charges on the outer wall
pathway I
pathway II
Translocation of Sens to the inner plasma membrane
Dark- or photo-induced alteration of outer wall permeability
Translocation of Sens to the inner plasma membrane
Photoactivation of Sens and generation of reactive cytotoxic species
Oxidative modification of specific targets in the Sens microenvironment
Impairment of cell functions and metabolism
Inhibition of cell growth and cell death

Fig. 8: Scheme illustrating the essential steps involved in the process of photosensitiser binding to microbial cells and subsequent photoinactivation. Pathway I is operative for gram-positive bacteria; pathway II is operative for gram-negative bacteria. From [25].

An important goal in the investigation of photosensitisation processes in antimicrobial PDT is elucidation of the mechanism of action of a selected PS to determine whether a specific reaction proceeds *via* a type I or a type II pathway.

On one hand, some mechanistic studies involved type I mechanisms (*via* electron transfer and radicals) in APDT of bacteria. Martin and Logsdon investigated a set of thiazine, xanthene, acridine and phenazine dyes and their phototoxicity towards *E. coli* [63], concluding that oxygen radicals were primarily responsible for the oxygen-dependent toxicity of the dyes examined. Strong *et al*. compared two structurally different PS immunoconjugates targeted against *P. aeruginosa* that had different photophysical properties [64]. One had a lower singlet oxygen quantum yield, yet was more efficient in APDT, this was explained by hydroxyl radical generation due to the chemical structure of the conjugate.

On the other hand, other mechanistic studies have implicated type II mechanisms (*via* energy transfer and $^1O_2$). Maisch *et al.* [46] studied the inactivation mechanism of several cationic porphyrins against different *S. aureus* and *E. coli* strains, concluding that the killing was mediated predominantly by $^1O_2$. Phototoxicity efficacy was not affected when mannitol was used as a type I scavenger, but was modified when either 1,4-diazabicyclo-(2,2,2)octane (DABCO) or sodium azide was used as type II scavenger. A similar conclusion was reported by Ergaieg *et al.* using *Enterococcus hirae* and *E. coli* as gram-positive and negative bacteria, respectively. Their conclusion was that bacterial inactivation by TMPyP photosensitisation predominantly involved type II reactions mediated by the formation of $^1O_2$, but participation of other active oxygen species could not however be neglected [65].

As regards the cytotoxic damage, two basic mechanisms have been proposed to explain the lethal effect caused to bacteria after APDT treatment [37]:

a) *Damage to DNA*. DNA modification, breaks in both single- and double-stranded DNA and photomodification or disappearance of the plasmid supercoiled fraction of the cytoplasm have been detected in both kinds of bacteria upon PDI using structurally different types of sensitisers [66-69]. Guanine residues were found to be the most easily oxidized [70].
b) *Damage to the cytoplasmic membrane* followed by a leakage of cellular contents or inactivation of membrane transport systems and enzymes [67,69].

These mechanisms achieving cellular damage necessary for the success of APDT lead to cell lysis and, consequently, to its death.

1.4. OBJECTIVES

The main goal of this thesis is to study the details of antimicrobial photodynamic therapy by gaining insight into three different questions: (1) does it work?, (2) how does it work?, and (3) what can we do to improve it?. This is divided in the following specific objectives:

- Assess the potential of phenotiazinium dyes and a new tricationic porphycene against multidrug-resistant microbial cells *in vitro* and *in vivo,* on infected mouse burns.

- Mechanistic study of the production and fate of $^1O_2$ photosensitised by model porphyrin, phthalocyanine and phenothiazinium photosensitisers of the different families used in APDT in a gram-negative bacterium such as *Escherichia coli*.

- Investigate the ability of a red fluorescent protein to produce ROS and its potential as a genetically-encoded photosensitiser for CALI application.

- Investigate the plasmonic effect of silver island films on the $^1O_2$ luminescence produced by photosensitisers and its implications in $^1O_2$-detection and APDT.

1.5. REFERENCES

1. Singh MP and Greenstein M. Antibacterial leads from microbial natural products discovery. *Curr Opin Drug Discov Devel* **2000**; 3: 167-176.

2. Kollef MH and Fraser VJ. Antibiotic resistance in the intensive care unit. *Ann Intern Med* **2001**; 134: 298-314.

3. Alanis AJ. Resistance to antibiotics: Are we in the post-antibiotic era? *Arch Med Res* **2005**; 36: 697-705.

4. Hancock REW. The end of an era? *Nat Rev Drug Discovery* **2007**; 6: 28.

5. Levy SB. From tragedy the antibiotic era is born. In: Levy SB eds. The antibiotic paradox: How the misuse of antibiotics destroys their curative powers. Cambridge: Perseus Publishing. **2002**: 1-14.

6. Jones KE, Patel NG, Levy MA, Storeygard A, Balk D, Gittleman JL, and Daszak P. Global trends in emerging infectious diseases. *Nature* **2008**; 451: 990-9U4.

7. Blignaut E, Molepo J, Pujol C, Soll DR, and Pfaller MA. Clade-related amphotericin B resistance among south african *Candida albicans* isolates. *Diagn Microbiol Infect Dis* **2005**; 53: 29-31.

8. Pujol C, Pfaller MA, and Soll DR. Flucytosine resistance is restricted to a single genetic clade of Candida albicans. *Antimicrob Agents Chemother* **2004**; 48: 262-266.

9. Denning DW. Can we prevent azole resistance in fungi. *Lancet* **1995**; 346: 454-455.

10. Yang BH, Peng MY, Hou SJ, Sun JR, Lee SY, and Lu JJ. Fluconazole-resistant *Kodamaea ohmeri* fungemia associated with cellulitis: case report and review of the literature. *Int J Infect Dis* **2009**; 13.

11. Cerveny KE, DePaola A, Duckworth DH, and Gulig PA. Phage therapy of local and systemic disease caused by *Vibrio vulnificus* in iron-dextran-treated mice. *Infect Immun* **2002**; 70: 6251-6262.

12. Sajjan US, Tran LT, Sole N, Rovaldi C, Akiyama A, Friden PM, Forstner JF, and Rothstein DM. P-113D, an antimicrobial peptide active against *Pseudomonas aeruginosa*, retains activity in the presence of sputum from cystic fibrosis patients. *Antimicrob Agents Chemother* **2001**; 45: 3437-3444.

13. Tew GN, Scott RW, Klein ML, and Degrado WF. De novo design of antimicrobial polymers, foldamers, and small molecules: From discovery to practical applications. *Acc Chem Res* **2010**; 43: 30-39.

14. Wainwright M. Photodynamic antimicrobial chemotherapy (PACT). *J Antimicrob Chemother* **1998**; 42: 13-28.

15. Raab O. Über die wirkung fluoreszienrender stoffe auf infusorien. *Z Biol* **1900**; 39: 524-546.

16. Maisch T. A new strategy to destroy antibiotic resistant microorganisms: antimicrobial photodynamic treatment. *Mini-Rev Med Chem* **2009**; 9: 974-983.

17. Tang HM, Hamblin MR, and Yow CM. A comparative *in vitro* photoinactivation study of clinical isolates of multidrug-resistant pathogens. *J Infect Chemother* **2007**; 13: 87-91.

18. Lauro FM, Pretto P, Covolo L, Jori G, and Bertoloni G. Photoinactivation of bacterial strains involved in periodontal diseases sensitized by porphycene-polylysine conjugates. *Photochem Photobiol Sci* **2002**; 1: 468-470.

19. Tavares A, Carvalho CMB, Faustino MA, Neves MGPM, Tome JPC, Tome AC, Cavaleiro JAS, Cunha A, Gomes NCM, Alves E, and Almeida A. Antimicrobial photodynamic therapy: study of bacterial recovery viability and potential development of resistance after treatment. *Mar Drugs* **2010**; 8: 91-105.

20. Giuliani F, Martinelli M, Cocchi A, Arbia D, Fantetti L, and Roncucci G. *In vitro* resistance selection studies of RLP068/Cl, a new Zn(II) phthalocyanine suitable for antimicrobial photodynamic therapy. *Antimicrob Agents Chemother* **2010**; 54: 637-642.

21. Gilbert A and Baggott J. Essentials of molecular photochemistry, CRC Press, **1991**.

22. Braslavsky SE, Houk KN, and Verhoeven JW. Glossary of terms used in photochemistry, **1996**.

23. Foote CS, Valentine JS, Greenberg A, and Liebman JFe. Active oxygen in biochemistry, Blackie academic and professional, **1995**.

24. Dai T, Huang YY, and Hamblin MR. Photodynamic therapy for localized infections--state of the art. *Photodiagn Photodyn Ther* **2009**; 6: 170-188.

25. Jori G, Fabris C, Soncin M, Ferro S, Coppellotti O, Dei D, Fantetti L, Chiti G, and Roncucci G. Photodynamic therapy in the treatment of microbial infections: Basic principles and perspective applications. *Lasers Surg Med* **2006**; 38: 468-481.

26. Teichert MC, Jones JW, Usacheva MN, and Biel MA. Treatment of oral candidiasis with methylene blue-mediated photodynamic therapy in an immunodeficient murine model. *Oral Surg Oral Med Oral Pathol Oral Radiol Endodon* **2002**; 93: 155-160.

27. Calzavara-Pinton PG, Venturini M, Capezzera R, Sala R, and Zane C. Photodynamic therapy of interdigital mycoses of the feet with topical application of 5-aminolevulinic acid. *Photodermatol Photoimmunol Photomed* **2004**; 20: 144-147.

28. Gardlo K, Horska Z, Enk CD, Rauch L, Megahed M, Ruzicka T, and Fritsch C. Treatment of cutaneous leishmaniasis by photodynamic therapy. *J Am Acad Dermatol* **2003**; 48: 893-896.

29. Sohl S, Kauer F, Paasch U, and Simon JC. Photodynamic treatment of cutaneous leishmaniasis. *J Dtsch Dermatol Ges* **2007**; 5: 128-130.

30. Gonzalez U, Pinart M, Reveiz L, and Alvar J. Interventions for old world cutaneous leishmaniasis. *Cochrane Database Syst Rev* **2008**; CD005067.

31. Wainwright M. Photoinactivation of viruses. *Photochem Photobiol Sci* **2004**; 3: 406-411.

32. Mohr H, Knuver-Hopf J, Gravemann U, Redecker-Klein A, and Muller TH. West Nile virus in plasma is highly sensitive to methylene blue-light treatment. *Transfusion* **2004**; 44: 886-890.

33. Mohr H, Bachmann B, KleinStruckmeier A, and Lambrecht B. Virus inactivation of blood products by phenothiazine dyes and light. *Photochem Photobiol* **1997**; 65: 441-445.

34. Hancock REW. The bacterial outer membrane as a drug barrier. *Trends Microbiol* **1997**; 5: 37-42.

35. Allison RR, Downie GH, Cuenca R, Hu XH, Childs CJH, and Sibata CH. Photosensitizers in clinical PDT. *Photodiagn Photodyn Ther* **2004**; 1: 27-42.

36. Lang K, Mosinger J, and Wagnerova DM. Photophysical properties of porphyrinoid sensitizers non-covalently bound to host molecules; models for photodynamic therapy. *Coord Chem Rev* **2004**; 248: 321-350.

37. Hamblin MR and Hasan T. Photodynamic therapy: a new antimicrobial approach to infectious disease? *Photochem Photobiol Sci* **2004**; 3: 436-450.

38. Malik Z, Ladan H, and Nitzan Y. Photodynamic inactivation of gram-negative bacteria - Problems and possible solutions. *J Photochem Photobiol B:Biol* **1992**; 14: 262-266.

39. Vaara M and Vaara T. Polycations as outer membrane-disorganizing agents. *Antimicrob Agents Chemother* **1983**; 24: 114-122.

40. Bertoloni G, Rossi F, Valduga G, Jori G, and Vanlier J. Photosensitizing activity of water-soluble and lipid-soluble phthalocyanines on *Escherichia coli*. *FEMS Microbiol Lett* **1990**; 71: 149-155.

41. Merchat M, Bertolini G, Giacomini P, Villanueva A, and Jori G. Meso-substituted cationic porphyrins as efficient photosensitizers of gram-positive and gram-negative bacteria. *J Photochem Photobiol B:Biol* **1996**; 32: 153-157.

42. Minnock A, Vernon DI, Schofield J, Griffiths J, Parish JH, and Brown SB. Photoinactivation of bacteria. Use of a cationic water-soluble zinc phthalocyanine to photoinactivate both gram-negative and gram-positive bacteria. *J Photochem Photobiol B:Biol* **1996**; 32: 159-164.

43. Wilson M, Burns T, Pratten J, and Pearson GJ. Bacteria in supragingival plaque samples can be killed by low-power laser-light in the presence of a photosensitizer. *J Appl Bacteriol* **1995**; 78: 569-574.

44. Lazzeri D, Rovera M, Pascual L, and Durantini EN. Photodynamic studies and photoinactivation of *Escherichia coli* using meso-substituted cationic porphyrin derivatives with asymmetric charge distribution. *Photochem Photobiol* **2004**; 80: 286-293.

45. Segalla A, Borsarelli CD, Braslavsky SE, Spikes JD, Roncucci G, Dei D, Chiti G, Jori G, and Reddi E. Photophysical, photochemical and antibacterial photosensitizing properties of a novel octacationic Zn(II)-phthalocyanine. *Photochem Photobiol Sci* **2002**; 1: 641-648.

46. Maisch T, Bosl C, Szeimies RM, Lehn N, and Abels C. Photodynamic effects of novel XF porphyrin derivatives on prokaryotic and eukaryotic cells. *Antimicrob Agents Chemother* **2005**; 49: 1542-1552.

47. Kussovski V, Mantareva V, Angelov I, Orozova P, Wohrle D, Schnurpfeil G, Borisova E, and Avramov L. Photodynamic inactivation of *Aeromonas hydrophila* by cationic phthalocyanines with different hydrophobicity. *FEMS Microbiol Lett* **2009**; 294: 133-140.

48. Tegos GP, Demidova TN, Arcila-Lopez D, Lee H, Wharton T, Gali H, and Hamblin MR. Cationic fullerenes are effective and selective antimicrobial photosensitizers. *Chem Biol* **2005**; 12: 1127-1135.

49. Hamblin MR, O'Donnell DA, Murthy N, Rajagopalan K, Michaud N, Sherwood ME, and Hasan T. Polycationic photosensitizer conjugates: effects of chain length and Gram classification on the photodynamic inactivation of bacteria. *J Antimicrob Chemother* **2002**; 49: 941-951.

50. Soukos NS, Ximenez-Fyvie LA, Hamblin MR, Socransky SS, and Hasan T. Targeted antimicrobial photochemotherapy. *Antimicrob Agents Chemother* **1998**; 42: 2595-2601.

51. Tegos GP, Anbe M, Yang CM, Demidova TN, Satti M, Mroz P, Janjua S, Gad F, and Hamblin MR. Protease-stable polycationic photosensitizer conjugates between polyethyleneimine and chlorin(e6) for broad-spectrum antimicrobial photoinactivation. *Antimicrob Agents Chemother* **2006**; 50: 1402-1410.

52. Guo YY, Rogelj S, and Zhang P. Rose bengal-decorated silica nanoparticles as photosensitizers for inactivation of gram-positive bacteria. *Nanotechnol* **2010**; 21.

53. Friedberg JS, Tompkins RG, Rakestraw SL, Warren SW, Fischman AJ, and Yarmush ML. Antibody-Targeted Photolysis - Bacteriocidal effects of Sn (IV) chlorin e6- dextran-monoclonal antibody conjugates. *Ann NY Acad Sci* **1991**; 618: 383-393.

54. Garland MJ, Cassidy CM, Woolfson D, and Donnelly RF. Designing photosensitizers for photodynamic therapy: strategies, challenges and promising developments. *Fut Med Chem* **2009**; 1: 667-691.

55. Bulina ME, Chudakov DM, Britanova OV, Yanushevich YG, Staroverov DB, Chepurnykh TV, Merzlyak EM, Shkrob MA, Lukyanov S, and Lukyanov KA. A genetically encoded photosensitizer. *Nat Biotechnol* **2006**; 24: 95-99.

56. Serebrovskaya EO, Edelweiss EF, Stremovskiy OA, Lukyanov KA, Chudakov DM, and Deyev SM. Targeting cancer cells by using an antireceptor antibody-photosensitizer fusion protein. *Proc Natl Acad Sci USA* **2009**; 106: 9221-9225.

57. Jimenez-Banzo A, Nonell S, Hofkens J, and Flors C. Singlet oxygen photosensitization by EGFP and its chromophore HBDI. *Biophys J* **2008**; 94: 168-172.

58. Demidova TN and Hamblin MR. Photodynamic therapy targeted to pathogens. *Int J Immunopathol Pharmacol* **2004**; 17: 245-254.

59. Soukos NS, Wilson M, Burns T, and Speight PM. Photodynamic effects of toluidine blue on human oral keratinocytes and fibroblasts and *Streptococcus sanguis* evaluated in vitro. *Lasers Surg Med* **1996**; 18: 253-259.

60. Zeina B, Greenman J, Purcell WM, and Das B. Killing of cutaneous microbial species by photodynamic therapy. *Br J Dermatol* **2001**; 144: 274-278.

61. Soncin M, Fabris C, Busetti A, Dei D, Nistri D, Roncucci G, and Jori G. Approaches to selectivity in the Zn(II)-phthalocyanine-photosensitized inactivation of wild-type and antibiotic-resistant *Staphylococcus aureus*. *Photochem Photobiol Sci* **2002**; 1: 815-819.

62. George S, Hamblin MR, and Kishen A. Uptake pathways of anionic and cationic photosensitizers into bacteria. *Photochem Photobiol Sci* **2009**; 8: 788-795.

63. Martin JP and Logsdon N. The role of oxygen radicals in dye-mediated photodynamic effects in *Escherichia coli*-B. *J Biol Chem* **1987**; 262: 7213-7219.

64. Strong L, Yarmush DM, and Yarmush ML. Antibody-targeted photolysis - photophysical, biochemical, and pharmacokinetic properties of antibacterial conjugates. *Biochem Eng VIII* **1994**; 745: 297-320.

65. Ergaieg K, Chevanne M, Cillard J, and Seux R. Involvement of both type I and type II mechanisms in gram-positive and gram-negative bacteria photosensitization by a meso-substituted cationic porphyrin. *Sol Energy* **2008**; 82: 1107-1117.

66. Nitzan Y, Gutterman M, Malik Z, and Ehrenberg B. Inactivation of gram-negative bacteria by photosensitized porphyrins. *Photochem Photobiol* **1992**; 55: 89-96.

67. Malik Z, Hanania J, and Nitzan Y. Bactericidal effects of photoactivated porphyrins - An alternative approach to antimicrobial drugs. *J Photochem Photobiol B:Biol* **1990**; 5: 281-293.

68. Bertoloni G, Lauro FM, Cortella G, and Merchat M. Photosensitizing activity of hematoporphyrin on *Staphylococcus aureus* cells. *Biochim Biophys Acta, Gen Subj* **2000**; 1475: 169-174.

69. Valduga G, Bertoloni G, Reddi E, and Jori G. Effect of extracellularly generated singlet oxygen on gram-positive and gram-negative bacteria. *J Photochem Photobiol B:Biol* **1993**; 21: 81-86.

70. Hass BS and Webb RB. Photodynamic effects of dyes on bacteria .3. Mutagenesis by acridine-orange and 500-nm monochromatic light in strains of *Escherichia coli* that differ in repair capability. *Mutat Res* **1979**; 60: 1-11.

Chapter 2

General Techniques and Methods

This chapter describes the common photophysical techniques and specific methods used for the determination of photophysical properties in the light-induced reaction processes involved in this work. Specific details will be described in the experimental section of each chapter.

2.1. STEADY-STATE OPTICAL TECHNIQUES

2.1.1. Absorption and Transmittance.

Spectra were recorded in a Varian Cary 4E spectrophotometer periodically calibrated with a holmiun oxide filter. Transmittance measurements were recorded in a Varian Cary 4E spectrophotometer equipped with a 110 mm diameter integrating sphere and a high performance R928 photomultiplier tube. Integrating spheres have the ability to collect most reflected or transmitted radiation from turbid, translucent or opaque samples, removing any directional preferences and presenting an integrated signal to the detector.

Method

- **Photosensitisers absorption in cell suspensions**

Suspensions of the same amount of cells with and without photosensitiser were used in all cases as sample and baseline, respectively.

2.1.2. Emission.

Emission and excitation spectra were recorded in a Jobin-Ybon Spex Fluoromax-2 spectrofluorometer, ensuring that the absorbance of the sample was less than 0.05 in the overlap region between absorption and emission to avoid inner filter effects in the measurement of fluorescence.

Methods

- **Fluorescence quantum yield (Φ_F)**

The fluorescence quantum yield is defined as the number of photons emitted by the sample per absorbed photon. The fluorescence intensity integrated over the entire emission spectrum was measured as a function of the sample absorption factor ($1-10^{-A}$) for the sample and a suitable reference (*i.e.* with a similar emission spectrum as the sample), excited at the same wavelength. The quantum yields (Φ_F) were determined using *Eq. 1.*

$$\Phi_F \quad (sample) = \frac{\overline{F}_{sample} \cdot n_{sample}^2}{\overline{F}_{ref} \cdot n_{ref}^2} \cdot \Phi_F(ref) \qquad (1)$$

where F_i is the integrated fluorescence *vs* the absorption factor and n_i is the refractive index of the solvent used in each case.

- **Quantum yield of $O_2(a^1\Delta_g)$ formation (Φ_Δ) using fluorescent probes**

The quantum yield of singlet oxygen photosensitisation is defined as the number of photosensitized $^1O_2$ molecules per absorbed photon. The quantum yield of singlet oxygen production (Φ_Δ) was determined by comparison of the fluorescence intensity of a $^1O_2$ fluorescent probe (FP) upon light exposure of optically-matched solutions of the sample and reference photosensitisers under the same conditions, namely with the same amount of probe and in the same solvent mixture, upon irradiation at the same wavelength. Specifically, the fluorescence of the probe was measured at different irradiation times for both sample and reference and the slopes of the corresponding intensity vs irradiation time plots were determined. The Φ_Δ values were then calculated with *Eq. 2*:

$$\Phi_\Delta(\text{sample}) = \frac{\text{Slope}_{\text{sample}}}{\text{Slope}_{\text{ref}}} \cdot \Phi_\Delta(\text{ref}) \qquad (2)$$

2.2. TIME-RESOLVED OPTICAL TECHNIQUES

The time-resolved techniques used in this work involve the observation, through absorption or emission, of excited states or other reaction intermediates generated upon pulsed-laser irradiation of a sample. The formation of a large concentration of transient species upon absorption of light produces a change in the intensity of an analyzing beam (in the case of absorption spectroscopy) or in the intensity that emerges from the sample (in the case of emission spectroscopy), which the system is able to monitor with time resolution.

2.2.1 UV-VIS nanosecond laser flash photolysis

Transient absorption experiments in the UV-VIS region were carried out using a home-built nanosecond laser flash photolysis system. In this instrument, the 2nd harmonic (532 nm) and the 3rd harmonic (355 nm) of a Continuum Surelite I-10 Nd:YAG laser was directed into the sample to irradiate the sample (10 Hz, 5 ns pulsewidth, 1-10 mJ per pulse). Changes in the sample absorbance were detected using a Hamamatsu R928 photomultiplier to monitor the intensity variations of an analyzing beam produced by a 75 W short arc Xe lamp (USHIO) and spectral discrimination was obtained using a PTI 101 monochromator. The signal was fed to a Lecroy Wavesurfer 454 oscilloscope for digitizing and averaging (typically 10 shots) and finally transferred by an GPIB interface (National Instruments) to a PC computer for data storage and analysis. A Si photodiode (Laser-Optotronic BPX 65) capturing a reflection of the laser beam was used to trigger the oscilloscope. The energy of the laser pulse was varied by neutral density filters and measured with a pyroelectric energy meter (RJP 735 and RJP) from Laser Precisition Corp. The system was controlled by the home-developed LKS sofware (LabWindows, National Instruments).

A schematic representation of our setup is depicted in Fig. 1:

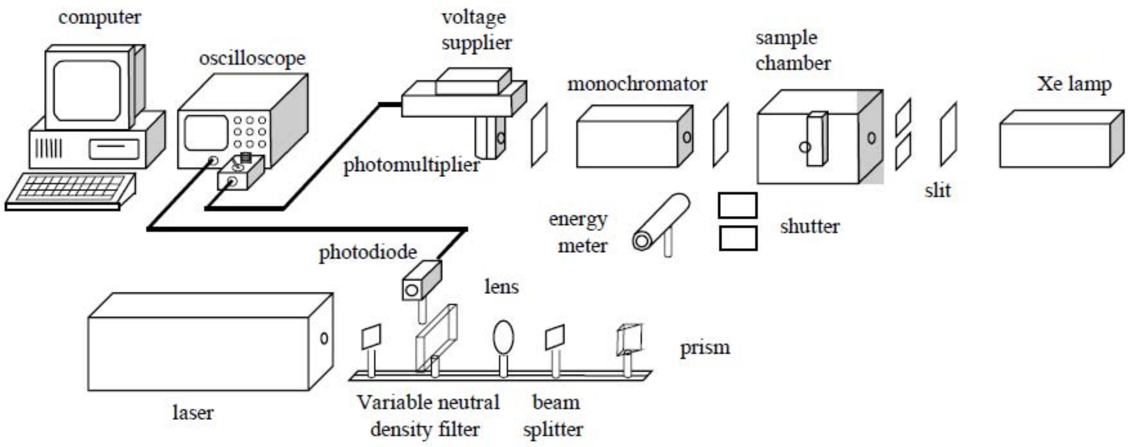

Fig. 1: Experimental setup for nanosecond UV-VIS laser flash photolysis.

2.2.2. Time-Correlated Single Photon Counting (TCSPC)

Time-Correlated Single Photon Counting is the most commonly used technique for singlet state lifetime determination. It is based on the detection of single photons of a periodical light signal, the measurement of the detection times of the individual photons and the reconstruction of the waveform from the individual time measurements. TCSPC technique makes use of the fact that for low-level, high-repetition-rate pulses, the produced light intensity is so low that the probability of detecting one photon in one signal period is less than one. Therefore, is not necessary to provide for the possibility of detecting several photons in one signal period. It is sufficient to record the photons, measure their time in the signal period, and build up a histogram of the photon times.

The principle is shown in Fig. 2:

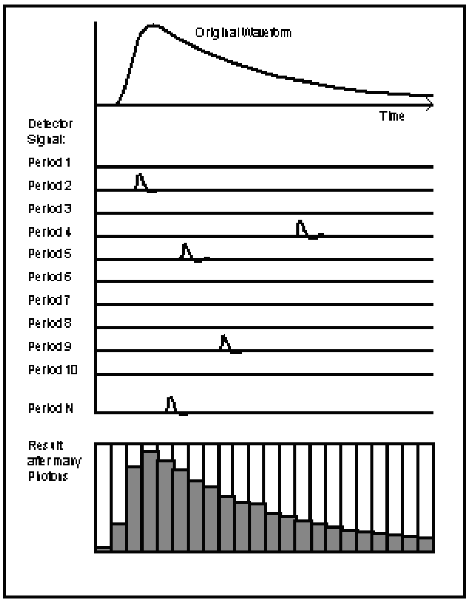

Fig. 2: Schematic representation of the TCSPC technique. From [2].

In most cases, the lifetime of the sample to be measured is on the same time scale as the response function of the system. In these cases, the actual decay may be obtained by deconvolution of the measured signal using an *instrumental response function* (IRF) generated from a light scattering sample.

TCSPC experiments were carried out using a PicoQuant Fluotime 200 fluorescence lifetime system. Excitation was achieved by means of picosecond diode lasers or LEDs (PicoQuant, 10 MHz repetition rate) and the counting frequency was always below 1 %. Singlet state lifetimes were determined using the PicoQuant FluoFit data analysis software.

Methods

- **Singlet state decay kinetics (τ_S)**

A solution of the sample in the proper solvent was prepared ensuring that the absorbance of the sample was less than 0.05 in the overlap region between absorption and emission to avoid inner filter effects. The deconvolution of the TCSPC fluorescence signal with the instrument response function (IRF) signal –reference sample (ludox in water) that directs a small fraction of the excitation light into the detection path– yields the singlet lifetime.

2.2.3. Time-resolved NIR phosphorescence detection (TRPD)

This technique is commonly used for directly and specifically monitoring the formation and decay of singlet oxygen ($^1O_2$ or $O_2(a^1\Delta_g)$), the measurement of its lifetime (τ_Δ) and its quantum yield of formation (Φ_Δ) [3]. It is based on the detection of the weak $O_2(a^1\Delta_g)$ phosphorescence, centred at 1270 nm.

The singlet oxygen spectrophotometer used is based on the Picoquant Fluotime 200 fluorescence lifetime system which has been subjected to the following modifications: (1) A diode-pumped solid-state Q-switched Nd:YAG laser (CryLas, FTQ355-QS) is used for excitation. This laser works at 10 kHz repetition rate, producing *ca.* 1 ns pulsewidth laser pulses at either 355 nm (5 mW, 0.5 μJ per pulse) or at 532 nm (12 mW, 1.2 μJ per pulse). (2) The original single-grating monochromator was replaced by a dual grating one, which allows extending its dispersion range from 200 to 2000 nm. A flip mirror is used to direct the dispersed light beam either to the visible or to near-IR detector ports. (3) A TE-cooled Hamamatsu near-IR photomultiplier (model H9170-45), sensitive from 950 to 1400 nm, is used to detect the weak $O_2(a^1\Delta_g)$ phosphorescence. (4) The output of the PMT is sent to a mutichannel scaler (Becker and Hickl, model MSA300 or Picoquant, NanoHarp 250MSC). In order to block NIR background radiation from the excitation source, either a KG-5 filter (CVI Laser Corporation, Alburquerque, USA) or a 1064 nm rugate notch filter (Edmund Optics, UK) is placed at the exit port of the laser. Likewise, a cold mirror (Edmund Scientific, Barrington, USA) is placed at the entry port of the dual grating monocromator to prevent any visible radiation form reaching the detector. Data was processed using PicoQuant's FluoFit 4.0 software.

Methods

- **Photosensitiser's triplet lifetime (τ_T) and $O_2(a^1\Delta_g)$ lifetime (τ_Δ)**

Singlet oxygen lifetime was obtained by fitting *Eq. 3* to the signal detected at 1270 nm,

$$S(t) = S(0) \cdot \frac{\tau_\Delta}{\tau_T - \tau_\Delta} \cdot \left(e^{-t/\tau_T} - e^{-t/\tau_\Delta} \right) \qquad (3)$$

where *S(0)* is the zero-time amplitude of the signal and τ_T and τ_Δ are the actual lifetimes of the photosensitiser triplet state and singlet oxygen, respectively.

Photosensitiser's triplet lifetime was determined, if possible, by fitting *Eq. 4* to the signal obtained at a wavelength where the triplet state of the photosensitiser emits,

$$[^3PS]_t = K_1 \cdot e^{-t/\tau_T} \qquad (4)$$

where K_1 reflects the concentration of triplet excited-states of the photosensitiser and τ_T is the actual lifetime of the photosensitiser triplet state.

- **Quantum yield of $O_2(a^1\Delta_g)$ formation (Φ_Δ)**

The pre-exponential factor *S(0)*, which is proportional to Φ_Δ, was determined by fitting *Eq. 3* to the time-resolved phosphorescence intensity at 1270 nm. The quantum yields of $^1O_2$ production were determined from the comparison of *S(0)* to that produced by an optically matched reference in the same solvent and at the same excitation wavelength and intensity (*Eq. 5*) [3].

$$\Phi_\Delta\ (sample) = \frac{S(0)_{sample}}{S(0)_{ref}} \cdot \Phi_\Delta(ref) \qquad (5)$$

- **Lifetime quenching.**

Stern-Volmer analysis was used to calculate reaction rate constants (k_q) from time-resolved data, by means of *Eq. 5*:

$$\frac{1}{\tau} = \frac{1}{\tau_0} + k_q [Q] \qquad (5)$$

where τ and τ_0 are the lifetimes of the reacting species in the presence and absence of a quencher Q, respectively.

2.2.4. Bioluminescence imaging

The bioluminescence imaging system (Hamamatsu Photonics KK, Bridgewater, NJ) has been described elsewhere in detail [1]. Briefly, an ICCD photon-counting camera (Model C2400-30H; Hamamatsu Photonics, Bridgewater, NJ) was used. The camera was mounted in a light-tight specimen chamber, fitted with a light-emitting diode, a set-up that allowed for a background gray-scale image of the entire mouse to be captured. By accumulating many images containing binary photon information (an integration time of 2 minutes was used), a pseudo-color luminescence image was generated. Superimposition of this image onto the gray-scale background image yielded information on the location and intensity in terms of photon number. The camera was also connected to a computer system through an image processor (Argus-50, Hamamatsu Photonics). Argus-50 control program (Hamamatsu Photonics) was used to acquire images and to process the image data collected.

A gray-scale background image was made, followed by a photon count of the same region. This entire photon count was quantified as relative luminescence units (RLUs) and was displayed in a false color scale ranging from pink (most intense) to blue (least intense).

2.3. MICROBIOLOGICAL TECHNIQUES

2.3.1. Microbial strains

The microbial strains used for the photodynamic inactivation experiments in *Chapters 3 and 4* were *Staphylococcus aureus* 8325-4 (Novick, 1967), methicilin-resistant *Staphylococcus aureus* Xen 31 (Caliper Life Sciences) *and Enterococcus faecalis* ATCC 29212 as Gram-positive bacteria*; Acinetobacter baumanii* ATCC 51393*, A. baumannii* ATCC BAA 747 transduced with the lux CDABE operon [4], *Escherichia coli* ATCC 53868, *Proteus mirabilis* ATCC 51393 and *Pseudomonas aeruginosa* ATCC 19660 as Gram-negative bacteria; and *Candida albicans* ATCC 18804 and *Candida krusei* (ATCC 6258) as yeasts.

E. coli CECT101 was used for the steady-state and the time-resolved optical measurements of *Chapter 5 and 6*.

2.3.2. Culture conditions

Bacterial cells were aerobically grown overnight at 37ºC in brain-heart infusion (BHI) or luria-bertani (LB) broth. Bacteria were then subcultivated in new medium at 37ºC in an orbital shaking incubator to an attenuance value of 0.5 at 600 nm or 0.35 at 660 nm, corresponding to *ca.* 10^8 colony forming unit (CFU)·mL^{-1}. The cell suspensions were then centrifuged (5 min, 3000 rpm) and resuspended with sterile phosphate buffered saline (PBS) at pH 7.4 at the same concentration.

Bacterial luminescent strains were stored and grown in the presence of the appropriate amount of antibiotics in the media, namely 250 µg/mL of carbenicillin for *A. baumanii* and 200 µg/mL of kanamycin for MRSA.

C. albicans was grown overnight at 30ºC in Yeast Peptone Dextrose (YPD) broth, centrifuged (5 min, 3500 rpm) and resuspended with sterile PBS at pH 7.4 up to *ca.* 10^7 CFU·mL^{-1} for phototoxicity experiments. *C. krusei* was grown overnight at 35ºC in Sabouraud broth (Merck), and then subcultivated in new Sabouraud medium at 35ºC in an orbital shaking incubator at 130 rpm to an Abs_{600} = 0.7, corresponding to *ca.* 10^7 CFU/mL. The suspensions were then centrifuged (5 min, 3500 rpm) and resuspended with sterile PBS at pH 7.4 at the same concentration for phototoxicity experiments.

2.3.3. Photosensitiser binding and quantification

Despite the words binding and uptake are commonly used interchangeably, binding of a photosensitiser is more generic terminology involving the PS located anywhere outside and/or inside the cell, while uptake implies the internalisation of the molecule.

The amount of photosensitiser bound to bacterial cells was determined by fluorescence spectroscopy using standard procedures [5,6].

Method

Bacterial suspensions were incubated in the dark at room temperature with different concentrations of PS and contact times (5 min to 20 hours) under gentle stirring. Afterwards, the cells were washed by centrifugation (10 min, 3000 rpm, 3 times) to remove any excess of PS. After the last centrifugation, a solution of 1% sodium dodecyl sulphate (SDS) in 0.1 M NaOH was added to the pellets and shaken for a minimum of 24 h. The extent of bound PS was then assessed by comparison of the fluorescence of this solution to that of standard solutions of known concentration under the same conditions. The fluorescence intensity values obtained for each sample were normalized by the total number of cells in the suspension to correct for variations between samples. Each experiment was repeated three times.

2.3.4. Spectroscopic measurements in cell suspensions

Spectroscopic measurements were recorded on the systems previously described. Cell suspension samples were prepared using the following method.

Method

Bacterial suspensions were incubated in the dark with the desired amount of PS for a given period of time. The cells were then washed three times with PBS and resuspended in PBS or deuterated (D)-PBS to a final concentration of ~ 5×10^8 $\mathrm{CFU \cdot mL^{-1}}$.

For time-resolved phosphorescence measurements, 3 mL of the bacterial suspensions were irradiated with 3 million laser pulses at 532 nm. The suspensions were gently stirred during the measurements.

2.3.5. Spheroplasts formation

A spheroplast is a bacterial cell from which the cell wall has been almost completely removed. The samples were prepared by means of the following protocol described by Segalla *et al.* [7].

Method

Spheroplasts were obtained by resuspending *E. coli* cells in Tris-HCl 0.05 M buffer at pH = 6.8 containing 0.01 M EDTA, 0.3 M sucrose and lysozyme (1 mg mL^{-1}) under stirring. After 1 h incubation at 37 ºC, tubes were centrifuged twice at 2000 rpm for 10 min. The pellet was then resuspended in PBS solution at pH 7.4.

PS-loaded spheroplasts were obtained by first incubating whole *E. coli* cells with PS and then subjecting them to the above procedure.

2.3.6. Photodynamic inactivation experiments *in vitro*

The light source used in the inactivation experiments was selected in order to provide the highest possible overlay between the irradiation range and the absorption spectrum of the PSs.

Method

Cell suspensions in PBS were incubated in the dark at room temperature for 30 min with the appropriated amount of PS in PBS. Centrifugation (3 min, 12000 rpm) of 1 mL aliquots was used to remove the excess of PS that was not taken up by the bacteria when experiments required it.

Then, 1 mL aliquots of the bacterial suspensions were placed in 24-well plates. The wells were illuminated from the top of the plates by use of the selected light, an optical fiber, and a lens (to form a 2-cm diameter spot).

At the time points when the requisite fluences had been delivered, 200 μL aliquots were taken from each well (the suspensions were thoroughly mixed before sampling to avoid the settlement of bacteria).

Light alone controls without PS were performed for all experimental conditions in order to rule out any inactivation effect due to the light.

For determination of CFUs, the aliquots were serially diluted, streaked on nutrient agar plates and incubated in the dark for 18 h at 37ºC (bacterial cells and *C. krusei*) or for 36 h at 30ºC (*C. albicans*). Experiments were carried out in triplicate for each condition.

2.3.7. *In vivo* burn infection model

Adult female BALB/c mice (Charles River Laboratories, Wilmington, MA), 6-8 week old and weighing 17-21 g, were used in the *in vivo* studies. The animals were housed one per cage and maintained on a 12-hour light/dark cycle with access to food and water *ad libitum*. All animal procedures were approved by the Subcommittee on Research Animal Care (IACUC) of Massachusetts General Hospital and met the guidelines of National Institutes of Health.

Method

Burn infections were performed by means of the protocol used by Dai *et al.* fully described elsewhere (Fig. 3) [4]. Briefly, mice were anesthetized by intraperitoneal (IP) injections of ketamine/xylazine cocktail. Then, burns were created by applying two pre-heated (≈95°C) brass blocks (Small Parts, Inc., Miami, FL) to the opposing sides of an elevated skin-fold on the dorsal surface of mice [8] for 10 seconds (non-lethal, full-thickness, third-degree burns). The combined brass block area was 15 mm × 10 mm giving an area of 150 mm^2, corresponding to a 4% of total body surface area (TBSA) [9]. Immediately after the creation of burns the mice were resuscitated with IP injections of 0.5 mL sterile saline (Phoenix Scientific Inc, St. Joseph, MO) to prevent dehydration. Then, a bacterial suspension containing 10^8 cells in 50 µL sterile PBS was inoculated onto the surface of each burn with a pipette tip and then was smeared onto the burn surface with an inoculating loop. The mice were imaged with the luminescence camera immediately after applying the bacteria to ensure that the bacterial inoculum applied to each burn was consistent.

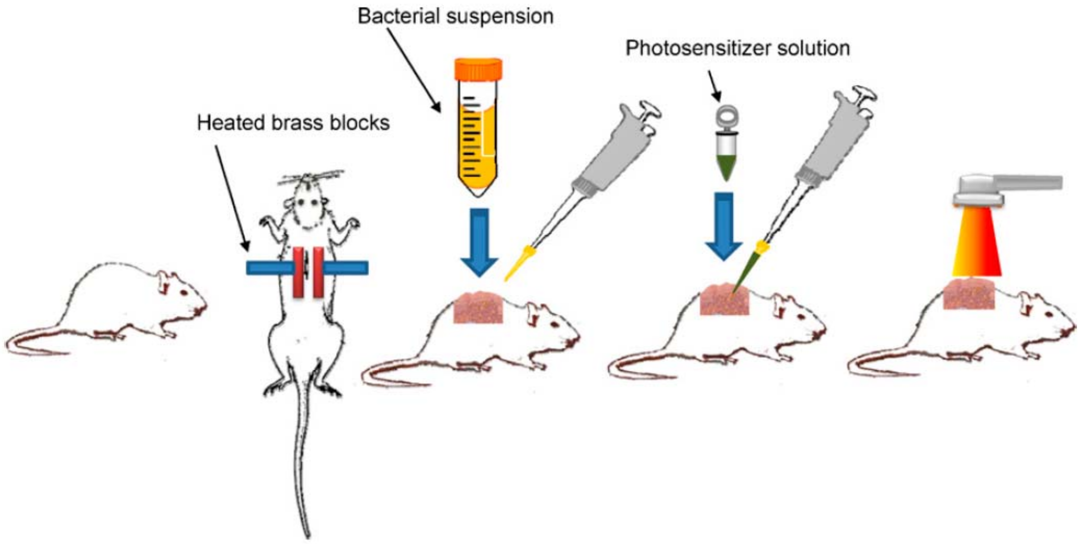

Fig. 3: Schematic depiction of the steps involved in performing antimicrobial PDT on a burn infection in mice. From [10].

2.3.8. Photodynamic inactivation experiments *in vivo*

The *in vivo* inactivation experiments were performed using the burn infection model described above (Fig. 3).

Method

Thirty minutes after application of the bacteria to the burns, the PS solution was applied to the PDT treated burns and also to dark controls. Thirty minutes after the addition, to allow the PS to bind to and/or penetrate the bacteria, the mice were again imaged using luminescence camera to quantify any dark toxicity to the bacteria. Mice were then illuminated with light delivered by a non-coherent light source. The light fluence rate was routinely measured using a LaserMate^{TM} power meter (Coherent, Portland, OR), and the fluence rate used was 100 $mW\cdot cm^{-2}$. Mice were given total light doses in aliquots with luminescence imaging taking place after each aliquot of light. Immediately after PDT, the mice were resuscitated with a second IP injection of 0.5 mL sterile saline to prevent dehydration.

2.3.9. Mouse follow-up

The regrowth of microbial infections after PDT treatment was controlled by means of the following procedure.

Method

Once a day, the mice were anesthetized by IP injection of the ketamine/xylazine cocktail prior to imaging and then placed on an adjustable stage in the specimen chamber, and the wounds were positioned directly under the camera. The bacterial luminescence from the mouse burns was recorded daily until the bioluminescence disappeared or the animals were determined to be moribund and euthanized.

2.4. REFERENCES

1. Hamblin MR, O'Donnell DA, Murthy N, Contag CH, and Hasan T. Rapid control of wound infections by targeted photodynamic therapy monitored by *in vivo* bioluminescence imaging. *Photochem Photobiol* **2002**; 75: 51-57.

2. Becker W. Advanced time-correlated single photon counting techniques, Springer, Germany, **2005**.

3. Nonell S and Braslavsky SE. Time-resolved singlet oxygen detection. In: Packer L, Sies H (Eds.), eds. Singlet oxygen, UV-A, and Ozone. Methods in enzymology, vol. 319. San Diego: Academic Press. **2000**: 37-49.

4. Dai TH, Tegos GP, Lu ZS, Huang LY, Zhiyentayev T, Franklin MJ, Baer DG, and Hamblin MR. Photodynamic therapy for *Acinetobacter baumannii* burn infections in mice. *Antimicrob Agents Chemother* **2009**; 53: 3929-3934.

5. Hamblin MR, O'Donnell DA, Murthy N, Rajagopalan K, Michaud N, Sherwood ME, and Hasan T. Polycationic photosensitizer conjugates: effects of chain length and gram classification on the photodynamic inactivation of bacteria. *J Antimicrob Chemother* **2002**; 49: 941-951.

6. Demidova TN and Hamblin MR. Effect of cell-photo sensitizer binding and cell density on microbial photoinactivation. *Antimicrob Agents Chemother* **2005**; 49: 2329-2335.

7. Segalla A, Borsarelli CD, Braslavsky SE, Spikes JD, Roncucci G, Dei D, Chiti G, Jori G, and Reddi E. Photophysical, photochemical and antibacterial photosensitizing properties of a novel octacationic Zn(II)-phthalocyanine. *Photochem Photobiol Sci* **2002**; 1: 641-648.

8. Stevens EJ, Ryan CM, Friedberg JS, Barnhill RL, Yarmush ML, and Tompkins RG. A quantitative model of invasive Pseudomonas infection in burn injury. *J Burn Care Rehabil* **1994**; 15: 232-235.

9. Gilpin DA. Calculation of a new Meeh constant and experimental determination of burn size. *Burns* **1996**; 22: 607-611.

10. Dai T, Huang YY, and Hamblin MR. Photodynamic therapy for localized infections--state of the art. *Photodiagn Photodyn Ther* **2009**; 6: 170-188.

Chapter 3

Photodynamic inactivation of *Acinetobacter baumannii* using phenothiazinium dyes

Phenothiazinium dyes have been reported to be effective photosensitisers inactivating a wide range of microorganisms *in vitro* after illumination with red light. However, their application *in vivo* has not extensively been explored. This study evaluates the bactericidal activity of phenothiazinium dyes against multidrug-resistant *Acinetobacter baumanii* both *in vitro* and *in vivo*.

The work described in this chapter is adapted from Xavier Ragàs, Tianhong Dai, George P Tegos, Montserrat Agut, Santi Nonell, and Michael R. Hamblin in *Lasers Surg Med* 2010, 42, 384-390 and was performed in Massachusetts General Hospital, Harvard Medical School.

3.1. INTRODUCTION

The use of photodynamic therapy (PDT) [1] to treat localized infections generally involves the topical application of a photosensitiser (PS) into the infected tissue, followed by illumination with visible or near-infrared light [2,3]. In the presence of oxygen, light induces the formation of reactive oxygen species by energy or electron transfer from the PS excited state, that are able to oxidize biomolecules and, thereby, kill cells [4]. The selectivity of the PS for bacteria over host tissue can be obtained by the appropriate chemical design [5-7] to ensure that the molecule will preferentially bind to bacterial cells rather than mammalian cells [8]. Three different classes of compounds have been used as photosensitisers to inactivate bacteria: 1) phenothiazinium salts [9] 2) tetrapyrroles such as phthalocyanines [10] and porphyrins with cationic charges [11], and 3) conjugates between tetrapyrroles with cationic polymers [12-14].

Phenothiazinium-based PS have been widely used against a range of microorganisms, demonstrating the efficacy of PDT to inactivate resistant forms of bacteria which are not easily killed by antibiotics such as methicillin [15] or vancomycin [16]. The substitution pattern of the phenothiazinium core has been varied to introduce important changes in the photochemical properties, like maximal absorption wavelength [15], or the lipophilicity [17], which affects the PS uptake and the location where the photodamage will be produced.

Phoenix *et al.* [18] observed that, for inactivation of a gram-negative species, *Escherichia coli,* dimethylmethylene blue (DMMB) was the most phototoxic phenothiazinium dye, while Wainwright *et al.* demonstrated that the inactivation of *Pseudomonas aeruginosa* was most efficient with toluidine blue O (TBO) that had the lowest minimal lethal concentration [7]. Indeed, it has been observed that even for different strains of the same species, the minimum lethal concentration of a dye may vary [15] indicating that minor changes in the bacterial wall could produce differences in the affinity of a dye for bacterial cells.

However, neither *in vitro* nor *in vivo* studies have been done using phenothiazinium-based PS for inactivating *Acinetobacter baumannii*, a gram-negative pathogenic bacterium that has recently attracted much attention due to its remarkable acquisition of multidrug resistance [19,20]. Indeed, a pandrug resistant *A. baumannii* strain with a tremendous ability to develop synergistic resistance mechanisms and, subsequently, very persistent chronic infections, has been found [21-23]. Thus, it is interesting to test the efficacy of PDT and phenothiazines against such new and hazardous pathogen.

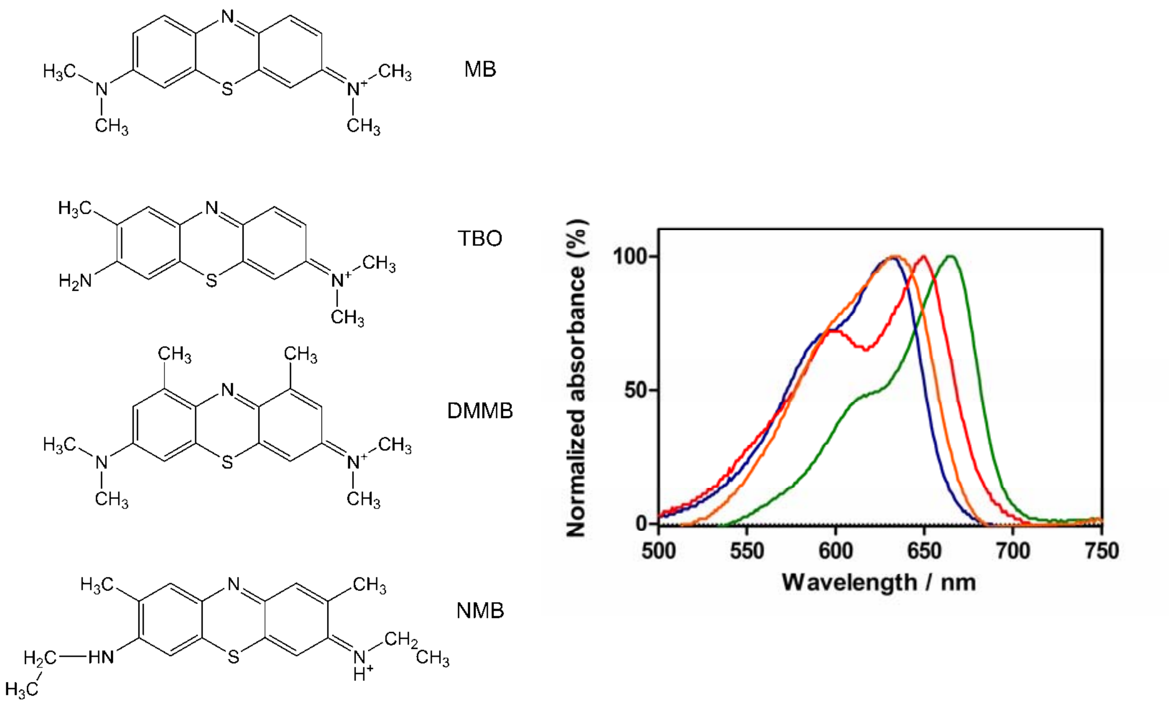

Fig. 1: Chemical structures and absorption spectra of the four phenothiazinium dyes: methylene blue (MB; green), toluidine blue O (TBO; orange), dimethylmethylene blue (DMMB; red) and new methylene blue N (NMB; blue). Counter-ions are not shown.

In this study we first performed *in vitro* studies using four different phenothiazinium dyes (Fig. 1) against a multidrug-resistant bioluminescent strain of *A. baumannii* in order to select the most phototoxic dye. Subsequently, we applied this selected PS and performed an *in vivo* experiment using mouse burns infected with bioluminescent *A. baumannii.*

3.2. EXPERIMENTAL SECTION

Photosensitisers and light sources

Toluidine blue O (TBO), methylene blue (MB), new methylene blue N (in the form of zinc chloride double salt; NMB), and 1,9-dimethylmethylene blue chloride (DMMB) were purchased from Sigma (St. Louis, MO, USA). These PS were dissolved in distilled water to give stock solutions with a dye concentration of 1 mM. All PS stock solutions were stored at 4°C in the dark for no more than 2 weeks, and immediately before experiments, were diluted in PBS without Ca^{2+} or Mg^{2+}. Red light at 635±15 nm or 652±15 nm was delivered using a noncoherent light source with interchangeable fiber bundles (LumaCare, Newport Beach, CA). The range given corresponds to the full width at half maximum.

Statistical methods

To compare the dose response curves obtained using bioluminescence assay with colony formation assay, the slopes between neighboring points were calculated and compared for statistical significance using a Student's *t* test.

The time courses of bacterial luminescence of the burn, were calculated by the use of numerical integration [24]. Differences in the areas under the curves between all the groups were compared for statistical significance by 1-factor ANOVA. *P* values of < 0.05 were considered significant.

3.3. RESULTS

In vitro experiments

Suspensions of a bioluminescent *A. baumanii* strain (10^8 CFU·mL^{-1}) in PBS were incubated in the dark at room temperature for 30 min with 0.1-20 μM of the PS in PBS. Centrifugation (3 min, 12000 rpm) was used to remove the excess of PS that was not taken up by the bacteria when experiments required it.

The cells were illuminated by means of either 635 nm light for TBO and NMB or 652 nm light for MB and DMMB. Under these conditions, all PSs absorbed comparable amounts of incident photons, thereby allowing the assessment of their relative efficiencies. Fluences ranged from 0 to 30 J·cm^{-2}, using a fluence rate of 125 mW·cm^{-2}. Fig. 2A shows the dye-concentration responses of *A. baumannii* survival with respects to all the phenothiazinium dyes. As observed, after 22.5 J·cm^{-2} irradiation with a dye concentration of only 2 μM, NMB was able to reduce the bacterial viability up to 6-log. DMMB, MB and TBO could only achieve a reduction of *A. baumannii* between 2 and 3-log under the same conditions.

Dye-concentration response after removing the excess of PS was also performed (Fig. 2B), observing that higher dye concentrations were needed to induce the same reduction to the bacterial viability compared with the concentrations needed without the removal of the excess PS. In that case, both NMB and DMMB were able to completely eliminate *A. baumannii* using a 10 μM concentration and 22.5 J·cm^{-2} light irradiation. However, neither 20 μM of MB nor TBO could produce such an effect, inducing only a 3-log reduction of bacterial viability in both cases.

Light-dose response curves were performed as well using a 10 μM concentration of the dyes (Fig. 2C). Both NMB and DMMB reduced 6-log of *A. baumannii* after 15 J·cm^{-2} irradiation without removing the PS, while 30 J·cm^{-2} irradiation was needed for MB and TBO to produce the same effect. After removing the PS, only NMB and DMMB were able to inactivate 6-log of bacteria after 30 and 22.5 J·cm^{-2} light had been delivered, respectively. Only 3-log reduction was obtained for MB and TBO after 30 J·cm^{-2} in the 1-wash curves.

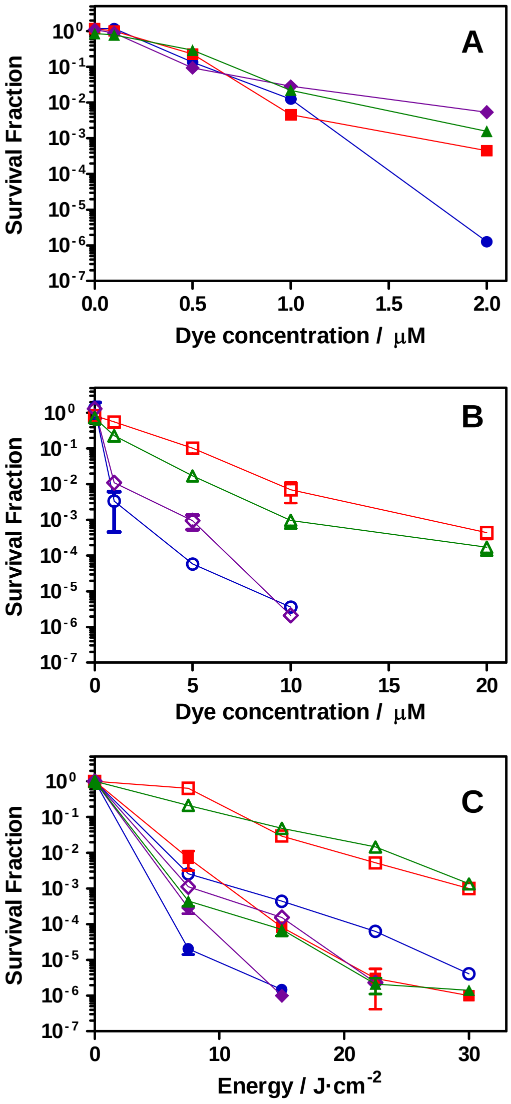

Fig. 2: *In vitro* photodynamic inactivation of *A. baumannii* with methylene blue (MB; squares), toluidine blue (TBO; triangles), dimethylmethylene blue (DMMB; diamonds) and new methylene blue N (NMB; circles), removing the PS from the solution (open symbols) and without removing it (filled symbols). The irradiation wavelength was 635 nm for TBO and NMB, and 652 nm for MB and DMMB. (**A, B**) Dye-dose response curves upon irradiation with 22.5 J·cm^{-2}. (**C**) Energy-dose response with a dye-dose of 10 µM. Error bars are SEM and in some cases are smaller than the diameter of the symbols.

Correlation between bacterial luminescence and CFU

Light-dose response curves were performed using a 0.5 µM and 1 µM concentration of NMB against *A. baumanii*. The survival fraction of bacteria was measured both by a colony formation assay and with the bioluminescence emitted by those bacteria. Bacterial luminescence was measured on aliquots of bacterial suspensions by means of a luminescence plate reader. As observed in Fig. 3, the trend with 0.5 µM of NMB was the same for both bioluminescence and CFU·mL^{-1} providing a *p* value of 0.65.

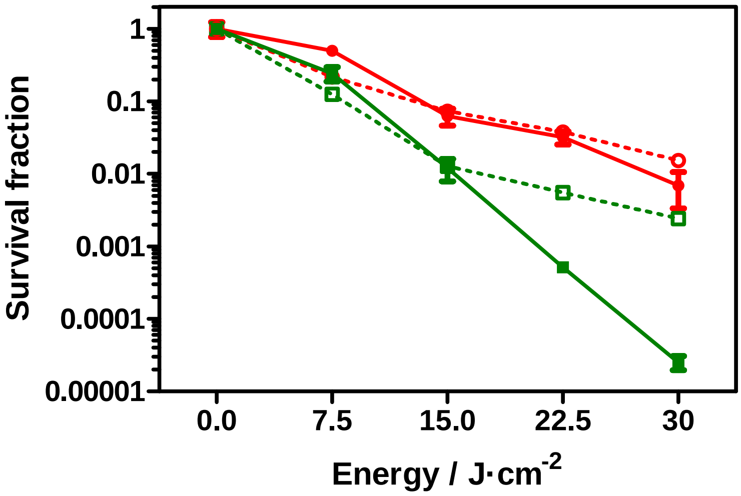

Fig. 3: Light-dose response of *A. baumannii* with 0.5 μM (circles) and 1 μM (squares) of new methylene blue N followed using a colony formation assay (solid line) and bacterial bioluminescence (dotted line).

With 1 μM concentration of NMB, similar survival fractions where observed using both methods after 7.5 and 15 J·cm^{-2} irradiation (p = 0.97), while clear differences were observed after 22.5 and 30 J·cm^{-2} irradiation (p = 0.02).

In vivo PDT treatment

Thirty minutes after application of the bacteria to the burns, NMB solution was applied. Three different aliquots of the PS were added. Initially, 50 μL of the PS solution was added to the burn and then two more additional aliquots of 20 μL were added during PDT after 84 and 240 J·cm^{-2} had been delivered. Mice were illuminated with 635±15 nm light to total light doses of up to 360 J·cm^{-2}.

Fig. 4A shows the successive bioluminescence images obtained from three representative mouse burns infected with *A. baumannii.* The PDT burn was treated with 800 μM of NMB and 635 nm light up to 360 J·cm^{-2}, the dark control with the same amount of NMB and no light, while the light control received 635 nm light up to 360 J·cm^{-2}.

The light-dose responses of normalized bioluminescence of the different mouse groups are shown in Fig. 4B. PDT induced a reduction of *ca.* 3.2-logs of the bioluminescence while only 0.8 and 0.4-logs reduction were observed for the dark controls and the light controls, respectively.

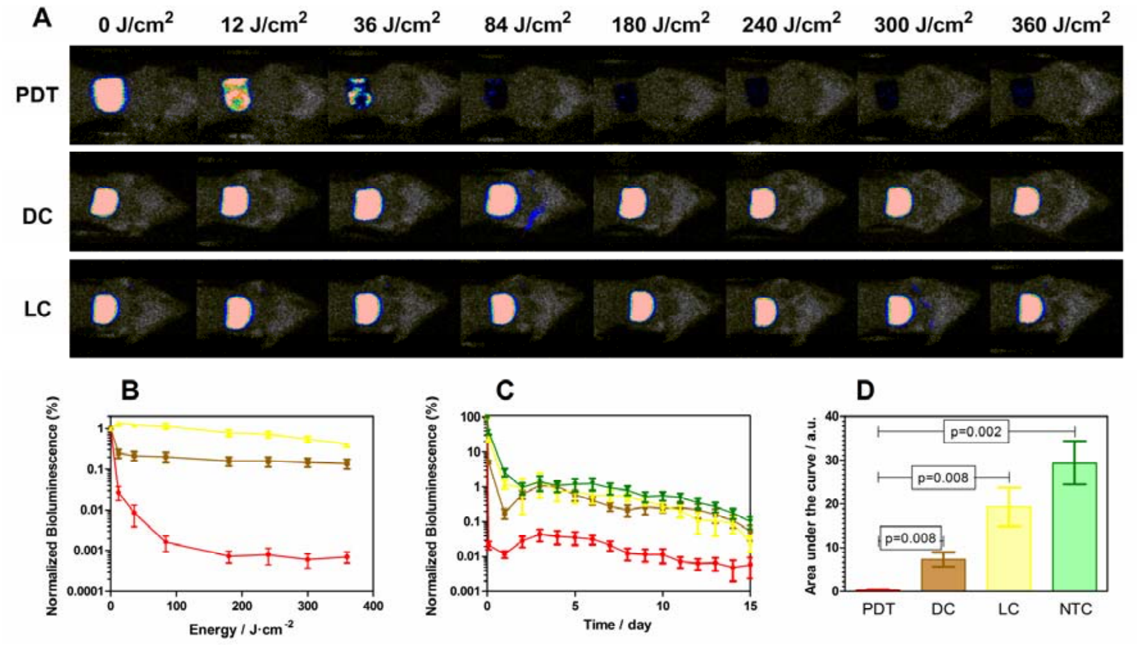

Fig. 4: (**A**) Dose response of bacterial luminescence from burns infected with luminescent *A. baumannii* and treated with 800μM new methylene blue N, NMB, and light (PDT), with 800 μM of NMB only (DC), and with light (LC) only. (**B**) Light-dose response curves of the normalized bioluminescence for mice treated with photodynamic therapy (red), mice treated only with NMB (brown), mice treated only with light (yellow). (**C**) Time course of normalized bacterial luminescence values and (**D**) areas under the curves of the infected burns in mice treated with photodynamic therapy (red; PDT), mice treated only with NMB (brown; DC), mice treated only with light (yellow; LC) and non treated mice (green; NTC).

Fig. 4C shows the time courses of the mean bacterial luminescence from day 0 to day 15 for the PDT treated group, the dark control group, the light control group and a non-treated control group where neither light nor PS was applied. Six mice were used for each group. As shown in the graph, all the controls exhibited a similar time course of bioluminescence signal from day 2 until day 15, with a decrease of the signal at day 1 after the infection followed by an increase at day 2 observed in the PS alone dark control.

The areas under the bioluminescence-time curves of each mouse group are represented in Fig. 4D. Analysis using an ANOVA 1-factor test showed statistically significant differences among the areas under the curves of all tested groups. ($p < 0.001$). Student's *t* tests were performed to compare the areas under the curves between each control and the PDT-treated group, obtaining statistically significant differences between all the controls and the PDT-treated group ($p < 0.008$).

3.4. DISCUSSION

Phenothiazinium dyes have been commonly reported as lethal photosensitisers for both gram-negative and gram-positive bacteria [18]. Four different phenothiazinium dyes were tested in this study in order to select the most phototoxic dye against *A. baumannii* for the *in vivo* experiments. NMB was found to be the most active with and without removing the excess of PS from the solution, showing in the last case very similar results to those observed with DMMB. The results can be rationalized by the different lipophilicity of the dyes. It is known that the log*P* values for MB and TBO are similar (-0.1 and -0.21, respectively) and lower than the ones for NMB and DMMB (1.2 and 1.01, respectively) [25]. Thus, MB and TBO should be more easily removed upon centrifugation than NMB and DMMB, as observed in our experiments.

It is clear that the photobactericidal effect of the dyes is affected by the initial interaction between dyes and bacteria and, subsequently, by the location of the dye and its strength of binding to the bacterial cell surface. Tegos and Hamblin [26] demonstrated that phenothiazinium dyes are substrates of microbial multidrug resistance pumps (MDRs). They used different wild-type, MDR-deficient and MDR-overexpressing bacterial strains, observing a higher inactivation for the MDR-deficient mutants and a higher resistance for the MDR-overexpressing mutants, relative to the wild-type strains. Since in our experiments we used a wild-type multidrug-resistant strain of *A. baumanii*, that will certainly possess MDRs, pumping out the PS from the outer structure of the gram-negative bacteria might contribute to the results obtained.

In addition, it has previously been shown that many phenothiazinium dyes, such as MB [27], TBO [27,28] and DMMB [29], interact with the bacterial lipopolysaccharides (LPS) that compose most of the outer structure of gram-negative bacteria. If DMMB and NMB interact with the LPS of the bacterial cell surface leading to either a stronger binding or to a deeper location within the bacterial cell wall than MB and TBO, this would lead either to a higher amount of ROS formed or to a higher proximity of the ROS formed to the cell wall critical targets. Consequently, this would explain the higher photobactericidal effect after removing the excess of PS observed for DMMB and NMB than the killing observed for MB and TBO at the same concentrations.

According to the results for both the dye-concentration and light-dose response curves *in vitro*, we decided to perform the *in vivo* experiments with NMB as PS. As the detection method of the survival fraction *in vivo* was the bioluminescence exhibited by *A. baumanii*, correlation between a colony formation assay and bioluminescence had to be demonstrated. It has been previously shown that *A. baumannii* CFUs quantified using serial dilutions of bacterial suspensions correlate linearly with the bioluminescence emitted by those bacteria [30]. In the present study, we confirmed that the bacterial bioluminescence reduction, measured in real time during PDT, correlated with the corresponding CFU reduction measured after serial dilution and colony formation as no statistical significant difference between both detection methods was observed with a 0.5 μM. However, the difference observed with 1 μM concentration of NMB can be rationalized as a result of the lower sensitivity exhibited by the bioluminescence detection method, *i.e.*, because the dynamic range for the reduction in bioluminescence signal is *ca.* 3-log reduction.

These results allowed us to use the bioluminescence signal exhibited by *A. baumannii* for the infected burn in the *in vivo* experiments. However, they demonstrate that higher light doses must be given to the infection, even after complete elimination of the bioluminescence signal, to assure the inactivation of the remaining bacteria during the PDT treatment in order to avoid a regrowth of the infection.

As for the *in vivo* experiments, it is interesting that there is no report on the use of NMB as PS in an *in vivo* infection model. Regarding other phenothiazinium dyes, these have not been extensively used *in vivo* to treat infections. TBO has been used in rats by Qin *et al.* [31] and Kömerik *et al.* [32] in order to treat periodontitis by reducing the total bacterial flora or inactivating inoculated *Porphyromonas gingivalis*. Wong *et al.* [33] used TBO as well in order to treat wounds infected with *Vibrio vulnificus* in a mouse model, obtaining a 50% survival fraction of the PDT treated mice. MB has also been used in some *in vivo* experiments. Teichert *et al.* [34] used PDT with MB to treat oral candidiasis in an immunosuppressed murine model. Also Zolfaghari *et al.* [35] used MB as PS against methicillin-resistant *Staphylococcus aureus* in two different wound models obtaining a 1.4 and a 1.15-log reduction in the number of viable bacteria recovered from the wounds.

In our experiments with *A. baumanii*, a complete elimination of the bioluminescence signal was observed after a light dose of 180 $J \cdot cm^{-2}$ in the presence of NMB. After that, in order to inactivate the remaining bacteria that were not detectable by bioluminescence imaging and, subsequently, avoid the recurrence of infection, an additional 200 $J \cdot cm^{-2}$ of light was given to each mouse. It is known that phenothiazinium dyes can be photobleached after long exposures to red light, and the photobleaching can be magnified in the presence of either biomolecules [36] or bacteria [37]. In order to replace the PS destroyed by photobleaching, two additional aliquots of 20 μL of NMB were subsequently added during the irradiation process -after

180 J·cm^{-2} and after 300 J·cm^{-2}. These results are consistent with those obtained by Dai *et al.* using a conjugate between polyethylenimine and chlorin(e6) as PS and the same mouse model [30], where a 3.6-log reduction of the bacterial luminescence was observed.

Additionally, a key feature of a successful antimicrobial PS is that the damage inflicted to the bacterial cells *in vivo* is so extensive that regrowth of the microbial pathogens is effectively prevented [38]. In our case, the mean bioluminescence of the PDT treated mice was 1.5 to 2 logs lower than the mean bioluminescence of all three control groups at every time point over the two week period, demonstrating the absence of a significant regrowth of the infection, and therefore the effectiveness of the PDT treatment. As regards the decrease in the signal at day 1 for the dark control, this was presumably due to significant dark toxicity of the NMB to the bacteria.

3.5. CONCLUSIONS

We have demonstrated that new methylene blue is the most powerful phenothiazinium dye tested for inactivating multi-drug resistant *A. baumannii* and is able to reduce more than 6-log the survival fraction of bacteria after an irradiation of 30 $J \cdot cm^{-2}$ of red light with a dye concentration of 10 μM or 2 μM with and without removing the excess of PS respectively.

In addition, we have shown that bacterial luminescence can be used as a real time marker to monitor the survival fraction of bacteria during the initial 3-logs reduction of bacterial viability. There is no statistically significant difference between the light-dose responses quantified by the bacterial luminescence of the *A. baumannii* strain and a colony formation assay.

Moreover, we have obtained more than 3-log reduction in the bacterial luminescence from the mouse burns infected with *A. baumannii*, and demonstrated that there is a statistically significant difference between the areas under the bioluminescence-time curves for the normalized bioluminescence between all the controls and the PDT treated mice.

In conclusion, new methylene blue is an effective antimicrobial photosensitiser for treating *A. baumannii* burn infections *in vivo*. As methylene blue and toluidine blue are already photosensitisers in clinical practice, and based on the efficacy pattern obtained in this study, it may be interesting to clinically test NMB as a potential photosensitiser in a wide range of localized infections.

3.6. REFERENCES

1. Bonnett R. Chemical aspects of photodynamic therapy, Gordon and Breach Science Publishers, Amsterdam, **2000**.

2. Demidova TN and Hamblin MR. Photodynamic therapy targeted to pathogens. *Int J Immunopathol Pharmacol* **2004**; 17: 245-254.

3. Hamblin MR and Hasan T. Photodynamic therapy: a new antimicrobial approach to infectious disease? *Photochem Photobiol Sci* **2004**; 3: 436-450.

4. Mroz P. and Hamblin MR. Advances in photodynamic therapy: basic, translational and clinical, Artech House, Norwood, MA, **2008**.

5. Minnock A, Vernon DI, Schofield J, Griffiths J, Parish JH, and Brown SB. Photoinactivation of bacteria. Use of a cationic water-soluble zinc phthalocyanine to photoinactivate both gram-negative and gram-positive bacteria. *J Photochem Photobiol B:Biol* **1996**; 32: 159-164.

6. Merchat M, Bertolini G, Giacomini P, Villanueva A, and Jori G. Meso-substituted cationic porphyrins as efficient photosensitizers of gram-positive and gram-negative bacteria. *J Photochem Photobiol B:Biol* **1996**; 32: 153-157.

7. Wainwright M, Phoenix DA, Marland J, Wareing DRA, and Bolton FJ. A study of photobactericidal activity in the phenothiazinium series. *FEMS Immunol Med Microbiol* **1997**; 19: 75-80.

8. Maisch T, Bosl C, Szeimies RM, Lehn N, and Abels C. Photodynamic effects of novel XF porphyrin derivatives on prokaryotic and eukaryotic cells. *Antimicrob Agents Chemother* **2005**; 49: 1542-1552.

9. Romanova NA, Brovko LY, Moore L, Pometun E, Savitsky AP, Ugarova NN, and Griffiths MW. Assessment of photodynamic destruction of *Escherichia coli* O157 : H7 and *Listeria monocytogenes* by using ATP bioluminescence. *Appl Environ Microbiol* **2003**; 69: 6393-6398.

10. Bertoloni G, Rossi F, Valduga G, Jori G, Ali H, and Vanlier JE. Photosensitizing activity of water-soluble and lipid-soluble phthalocyanines on prokaryotic and eukaryotic microbial-cells. *Microbios* **1992**; 71: 33-46.

11. Nitzan Y, Gutterman M, Malik Z, and Ehrenberg B. Inactivation of gram-negative bacteria by photosensitized porphyrins. *Photochem Photobiol* **1992**; 55: 89-96.

12. Hamblin MR, O'Donnell DA, Murthy N, Rajagopalan K, Michaud N, Sherwood ME, and Hasan T. Polycationic photosensitizer conjugates: effects of chain length and Gram classification on the photodynamic inactivation of bacteria. *J Antimicrob Chemother* **2002**; 49: 941-951.

13. Tegos GP, Anbe M, Yang CM, Demidova TN, Satti M, Mroz P, Janjua S, Gad F, and Hamblin MR. Protease-stable polycationic photosensitizer conjugates between polyethyleneimine and chlorin(e6) for broad-spectrum antimicrobial photoinactivation. *Antimicrob Agents Chemother* **2006**; 50: 1402-1410.

14. Polo L, Segalla A, Bertoloni G, Jori G, Schaffner K, and Reddi E. Polylysine-porphycene conjugates as efficient photosensitizers for the inactivation of microbial pathogens. *J Photochem Photobiol B:Biol* **2000**; 59: 152-158.

15. Wainwright M, Phoenix DA, Laycock SL, Wareing DRA, and Wright PA. Photobactericidal activity of phenothiazinium dyes against methicillin-resistant strains of *Staphylococcus aureus*. *FEMS Microbiol Lett* **1998**; 160: 177-181.

16. Wainwright M, Phoenix DA, Gaskell M, and Marshall B. Photobactericidal activity of methylene blue derivatives against vancomycin-resistant *Enterococcus spp. J Antimicrob Chemother* **1999**; 44: 823-825.

17. Verma S, Sallum UW, Athar H, Rosenblum L, Foley JW, and Hasan T. Antimicrobial photodynamic efficacy of side-chain functionalized benzo[a]phenothiazinium Dyes. *Photochem Photobiol* **2009**; 85: 111-118.

18. Phoenix DA, Sayed Z, Hussain S, Harris F, and Wainwright M. The phototoxicity of phenothiazinium derivatives against *Escherichia coli* and *Staphylococcus aureus*. *FEMS Immunol Med Microbiol* **2003**; 39: 17-22.

19. Peleg AY. Optimizing therapy for *Acinetobacter baumannii*. *Sem in Resp Crit Care Med* **2007**; 28: 662-671.

20. Perez F, Endimiani A, and Bonomo RA. Why are we afraid of *Acinetobacter baumannii*? *Exp Rev Anti Infec Ther* **2008**; 6: 269-271.

21. Falagas ME and Bliziotis IA. Pandrug-resistant gram-negative bacteria: the dawn of the post-antibiotic era? *Int J Antimicrob Agents* **2007**; 29: 630-636.

22. Gootz TD and Marra A. Acinetobacter balumannii: an emerging multidrug-resistant threat. *Exp Rev Anti Infec Ther* **2008**; 6: 309-325.

23. Doi Y, Husain S, Potoski BA, McCurry KR, and Paterson DL. Extensively drug-resistant *Acinetobacter baumannii*. *Emerg Infect Dis* **2009**; 15: 980-982.

24. Davis PJ and Rabinowitz P. Methods of numerical integration, Academic Press, Inc.; New York, NY, **1975**.

25. Phoenix DA and Harris F. Phenothiazinium-based photosensitizers: antibacterials of the future? *Trends in Molec Med* **2003**; 9: 283-285.

26. Tegos GP and Hamblin MR. Phenothiazinium antimicrobial photosensitizers are substrates of bacterial multidrug resistance pumps. *Antimicrob Agents Chemother* **2006**; 50: 196-203.

27. Usacheva MN, Teichert MC, and Biel MA. The interaction of lipopolysaccharides with phenothiazine dyes. *Lasers Surg Med* **2003**; 33: 311-319.

28. Komerik N, Wilson M, and Poole S. The effect of photodynamic action on two virulence factors of gram-negative bacteria. *Photochem Photobiol* **2000**; 72: 676-680.

29. Keler T and Nowotny A. Metachromatic assay for the quantitative-determination of bacterial-endotoxins. *Anal Biochem* **1986**; 156: 189-193.

30. Dai TH, Tegos GP, Lu ZS, Huang LY, Zhiyentayev T, Franklin MJ, Baer DG, and Hamblin MR. Photodynamic therapy for *Acinetobacter baumannii* burn infections in mice. *Antimicrob Agents Chemother* **2009**; 53: 3929-3934.

31. Qin YL, Luan XL, Bi LJ, Sheng YQ, Zhou CN, and Zhang ZG. Comparison of toluidine blue-mediated photodynamic therapy and conventional scaling treatment for periodontitis in rats. *J Periodontal Res* **2008**; 43: 162-167.

32. Komerik N, Nakanishi H, MacRobert AJ, Henderson B, Speight P, and Wilson M. *In vivo* killing of *Porphyromonas gingivalis* by toluidine blue-mediated photosensitization in an animal model. *Antimicrob Agents Chemother* **2003**; 47: 932-940.

33. Wong TW, Wang YY, Sheu HM, and Chuang YC. Bactericidal effiects of toluidine blue-mediated photodynamic action on *Vibrio vulnificus*. *Antimicrob Agents Chemother* **2005**; 49: 895-902.

34. Teichert MC, Jones JW, Usacheva MN, and Biel MA. Treatment of oral candidiasis with methylene blue-mediated photodynamic therapy in an immunodeficient murine model. *Oral Surg Oral Med Oral Pathol Oral Radiol Endodon* **2002**; 93: 155-160.

35. Zolfaghari PS, Packer S, Singer M, Nair SP, Bennett J, Street C, and Wilson M. *In vivo* killing of *Staphylococcus aureus* using a light-activated antimicrobial agent. *BMC Microbiol* **2009**; 9: 27.

36. Zhang LZ and Tang GQ. The binding properties of photosensitizer methylene blue to herring sperm DNA: a spectroscopic study. *J Photochem Photobiol B:Biol* **2004**; 74: 119-125.

37. Usacheva MN, Teichert MC, Sievert CE, and Biel MA. Effect of Ca^{2+} on the photobactericidal efficacy of methylene blue and toluidine blue against gram-negative bacteria and the dye affinity for lipopolysaccharides. *Lasers Surg Med* **2006**; 38: 946-954.

38. Jori G, Fabris C, Soncin M, Ferro S, Coppellotti O, Dei D, Fantetti L, Chiti G, and Roncucci G. Photodynamic therapy in the treatment of microbial infections: Basic principles and perspective applications. *Lasers Surg Med* **2006**; 38: 468-481.

Chapter 4

A tricationic porphycene as potential photosensitiser in antimicrobial photodynamic therapy

Structures of typical photosensitisers in antimicrobial photodynamic therapy are based on porphyrins, phthalocyanines and phenothiazinium salts with cationic charges at physiological pH values. However, derivatives of the porphycene macrocycle (a porphyrin isomer) have barely been investigated as antimicrobial agents. In this chapter, we describe the basic photochemical properties of the first aryl tricationic water-soluble porphycene and assess its potential *in vitro* and *in vivo* as an APDT photosensitiser.

The work described in this chapter was partially performed in Massachusetts General Hospital, Harvard Medical School in Prof. Michael R. Hamblin laboratory and is adapted from X. Ragàs, D. Sánchez-García, R. Ruiz-González, T. Dai, M. Agut, M. R. Hamblin, and S. Nonell, *J Med Chem* 2010, accepted.

4.1. INTRODUCTION

Antimicrobial photodynamic therapy (APDT) [1] is being actively studied as a possible alternative to antibiotic treatment for localized infections [2,3]. The basic principles are well understood: in essence, the interaction between light and photoactive drugs, usually called photosensitisers (PSs), forms reactive oxygen species (ROS) created through either electron transfer (type I) or energy transfer (type II) reactions [4]. These ROS will react with many cellular components that will induce oxidative processes leading to cell death [5-7].

PSs belonging to a variety of chemical structures have been used to inactivate microbial cells, most of them were porphyrin-based [8], phthalocyanine-based [9] and phenothiazinium-based [10]. Porphycene, a structural porphyrin isomer, is endowed with favorable photophysics that allows it to act as a photodynamic agent [11], but has barely been used in the field of APDT. The only two studies using polylysine-porphycene conjugates [12,13] showed promising results but that research was not pursued, likely due to the lengthy and complex synthesis of this kind of macrocycles. The recent discovery in our laboratory of a straightforward, four-step synthesis of porphycenes [14] provides an opportunity for the assessment of the potential of these compounds in APDT.

The use of outer wall-disrupting agents, such as EDTA [15] or cationic polypeptide polymixin B [8,16], and the conjugation of the PS with polymers [17], nanoparticles [18], or biomolecules [19], provides a higher affinity of the PSs against microbial cells. Nevertheless, the discovery that positively charged PSs at physiological pH values promote the photoinactivation of microbial cells [20-22] has stimulated the development of new synthetic routes to develop new useful cationic PSs for APDT.

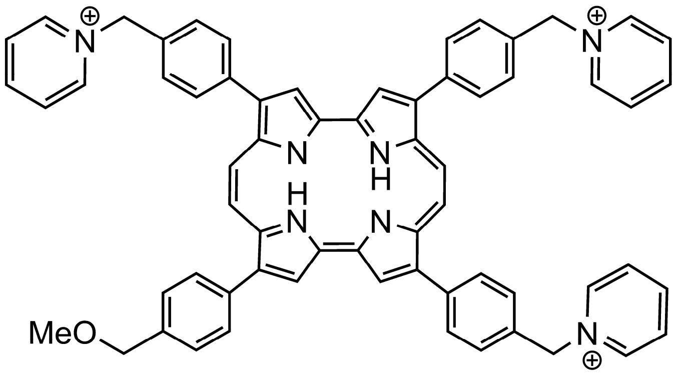

Fig. 1: Molecular structure of 2,7,12-tris(*p*-(*p*-(pyridilmethyl)phenyl)–17-(*p*-(metoximethyl)phenyl) porphycene (Py$_3$MeO-TBPo).

In addition, Caminos *et al.* showed that, in porphyrins with cationic (A) and non-cationic (B) groups, the photosensitized inactivation of *E. coli* cellular suspensions with those compounds follows the order: $A_3B^{3+} > A_4^{4+} >> ABAB^{2+} > AB_3^{+}$ [23].

In this chapter, we present the photochemical characterization of the first aryl cationic water-soluble porphycene (Fig.1; see *Annex*) as well as the results of a study designed to evaluate *in vitro* the broad-spectrum antimicrobial efficacy of this novel light-activated PS against a panel of prototypical human pathogenic microbes. Besides, its potential *in vivo* application to infection using a 3rd degree mouse burn model infected with a drug-resistant bacterial strain, methicillin-resistant *Staphylococcus aureus* (MRSA), is also evaluated.

4.2. EXPERIMENTAL SECTION

Chemicals and light source

Py_3MeO-TBPo was synthesized as described in the *Annex*. Photochemical measurements were performed in MeOH of spectrophotometric grade, purchased in Solvents Documentation Synthesis (SDS, Peypin, France), and water of Milli-Q purity. Dimethylacetamide (DMA) was provided by Sigma (St. Louis, MO, USA). Brain heart infusion (BHI) medium and yeast peptone dextrose medium (YPD) were provided by Fisher Scientific (Pittsburgh, PA, USA). Red light at 652±15 nm was delivered using a noncoherent light source with interchangeable fiber bundles (LumaCare, Newport Beach, CA). Red light at 635±10 nm was delivered using a Sorisa Photocare LED light source.

Statistics

Survival fractions are expressed as means ± standard error of the mean (SEM) of three independent experiments. Differences between the killing curves were evaluated by means of paired Student's *t* test. Differences between three or more means were compared by a one-way ANOVA. p values of < 0.05 were considered as significant.

4.3. RESULTS

Physical and photophysical properties

The photophysical properties of Py_3MeO-TBPo are summarized in Table 1. As observed in Fig. 2, Py_3MeO-TBPo shows the typical porphycene absorption spectrum in MeOH, with three bands in the red range of the spectrum and absorption coefficients in the 50.000 M^{-1} cm^{-1} range. The spectrum in water loses much of the structure, indicating not surprisingly that aggregation is occurring in aqueous media despite the three positive charges. The extent of aggregation can be controlled by changing the ionic strength of the solution, *i.e.*, the compound is substantially more aggregated in PBS than in pure water.

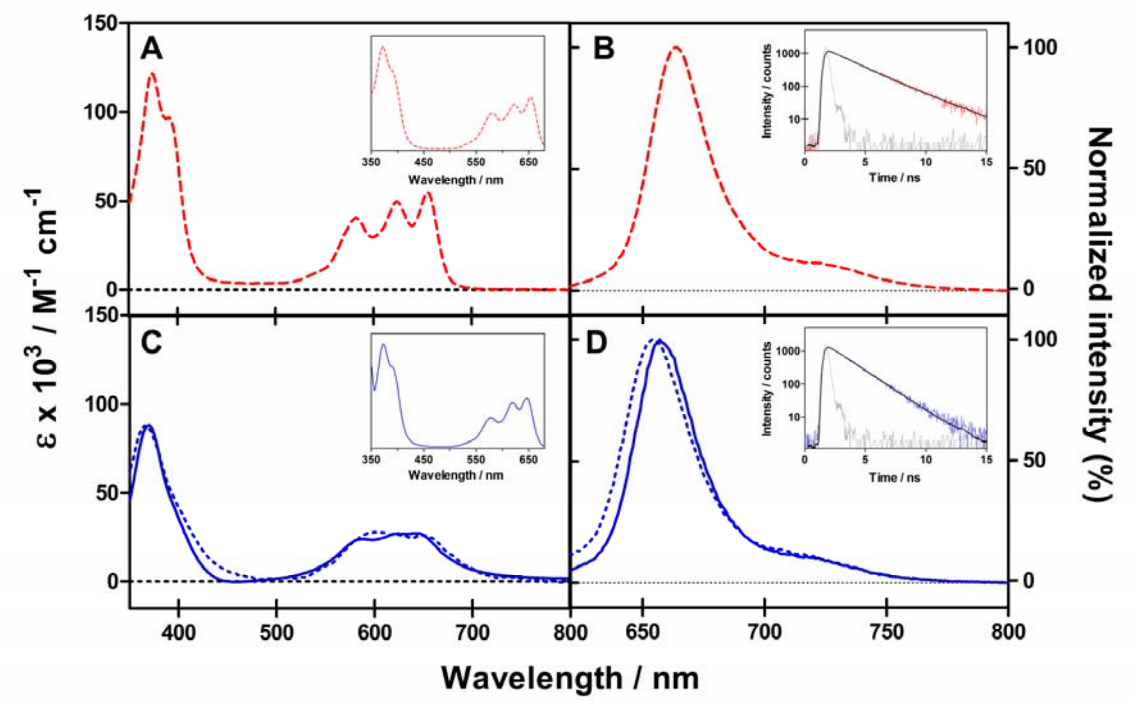

Fig. 2: (A,C) Absorption and **(B,D)** fluorescence spectrum of porphycene 3 in (A,B) MeOH and (C,D) water and PBS (solid and dotted line, respectively). Insets: (A,C) Excitation spectrum of the fluorescence at 661 nm. (B,D) Time-resolved fluorescence of Py_3MeO-TBPo. Signal, fit and instrument response function at 661 nm upon excitation at 375 nm.

However, both in water and in MeOH, the fluorescence spectra match the typical fluorescence spectrum of porphycenes where a main band and a weaker shoulder at lower energies are observed that are the mirror image of the $S_1 \leftarrow S_0$ absorption transition [11]. Interestingly, the excitation spectrum matches in all cases the absorption spectrum of the monomer, indicating that the aggregates are not emissive.

The fluorescence quantum yield, Φ_F, was determined by comparing the integrated fluorescence intensity of the porphycene to that of an optically-matched solution of cresyl violet in MeOH as reference ($\Phi_F = 0.54$) [24]. A value of Φ_F. = 0.075 ± 0.005 was found in MeOH, while in water the results showed a marked dependence on the excitation wavelength, reflecting the fraction of monomers that were excited at each wavelength. The fluorescence decay was monoexponential in both solvents (Fig. 3), with lifetime 1.8 ± 0.1 ns in water and 2.6 ± 0.1 ns in MeOH.

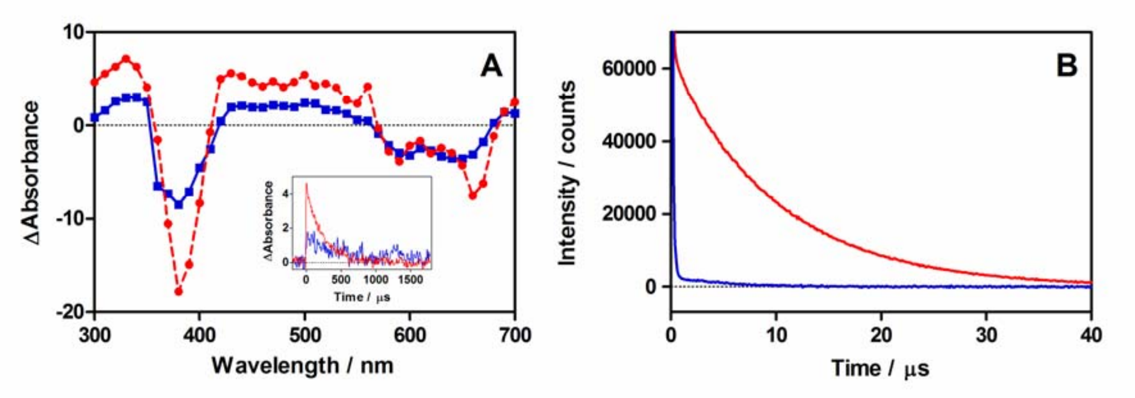

Fig. 3: (A) Transient absorption spectrum of the triplet excited state of porphycence **3** in water (blue) and MeOH (red). Inset: Transient absorbance at 420 nm upon excitation at 355 nm. **(B)** Singlet oxygen phosphorescence kinetics at 1270 nm of an aqueous solution (blue) and MeOH solution (red) of Py$_3$MeO-TBPo.

Transient absorption spectra of Py$_3$MeO-TBPo in argon atmosphere are shown in Fig. 3. Again, they present a shape similar to that of the triplet-minus-singlet spectrum of TPPo, confirming that only the monomeric species can undergo intersystem crossing [25]. The decays at 420 nm showed a triplet lifetime of 330 µs in water and 152 µs in MeOH (Fig. 3A Inset), with rate constants of oxygen quenching (k_q) of 1.5 x 10^9 $M^{-1} \cdot s^{-1}$ and 3.5 x 10^9 $M^{-1} \cdot s^{-1}$, respectively.

The singlet oxygen ($^1O_2$) production quantum yield, Φ_Δ, was determined by means of its phosphorescence at 1270 nm (Fig. 3B), comparing the intensity of the $^1O_2$ signal shown by the porphycene to that of optically-matched solutions of reference PSs [26]. Using *m*-THPP and TMPyP as standards (Φ_Δ^{ref} = 0.69 and 0.74, respectively) [27,28], Φ_Δ values of 0.004 ± 0.001 and 0.19 ± 0.01 were determined in water and MeOH respectively, upon excitation at 532 nm. While in MeOH the Φ_Δ values were independent of the excitation wavelength, we obtained $\Phi_\Delta = 0.03 \pm 0.01$ in water upon excitation at 355 nm using sulfonated phenalenone as standard ($\Phi_\Delta^{ref} \sim 1$) [29]. It can thus be concluded that the photophysical properties of **3** in MeOH are very similar to those of typical tetraphenylporphycenes [11], while in aqueous media aggregation strongly prevents its photosensitizing ability. This finding is fully in line with the results of several decades of research on related tetrapyrrole macrocycles.

In vitro photoinactivation of bacteria

All bacterial species were tested in a porphycene-concentration (Fig. 4) and energy-dose (Fig. 5) dependent manner with and without removing the excess of PS. No significant statistical difference was obtained in any case when the excess of Py_3MeO-TBPo was eliminated ($p > 0.26$), which implies that the porphycene displays strong binding to the bacterial cells..

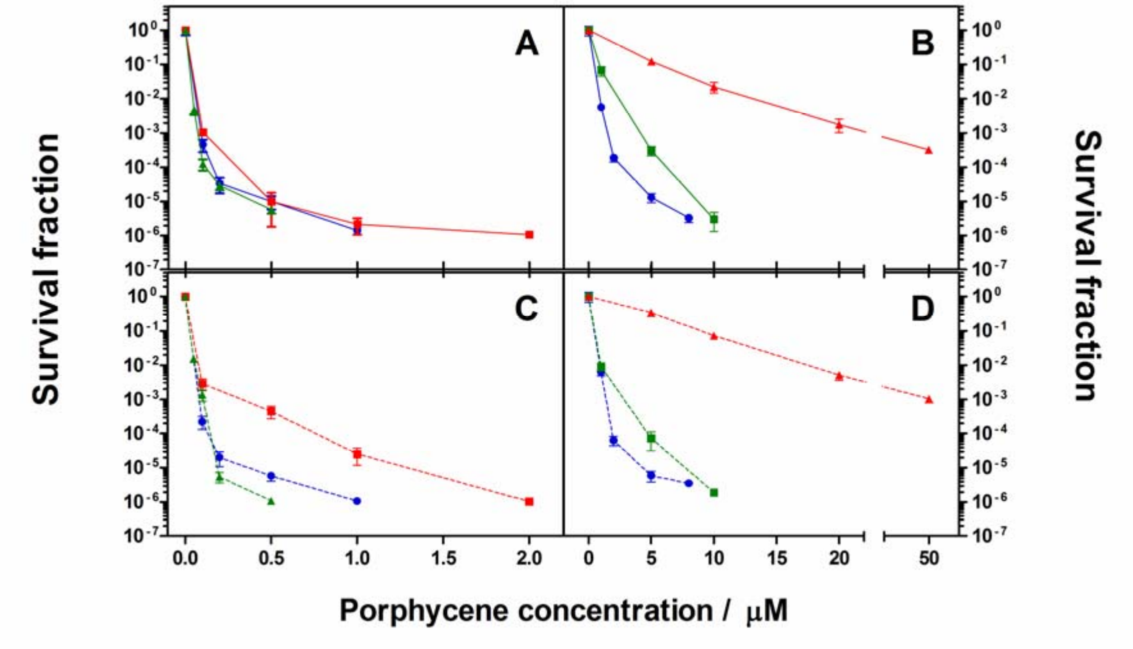

Fig. 4: Bacterial photoinactivation with Py_3MeO-TBPo. **(A,C)** Survival curves of MRSA (squares), *S. aureus* (circles), *E. faecalis* (triangles) with (dashed line) and without (solid line) removing the excess of photosensitiser (PS) from the solution after 30 J·cm^{-2} of 652-nm light. **(B,D)** Survival curves of *A. baumanii* (circles), *E. coli* (squares), *P. mirabilis* (triangles) with (dashed line) and without (solid line) removing the excess of PS from the solution after 60 J·cm^{-2} (*E. coli*) and 100 J·cm^{-2} (*A. baumanii* and *P. mirabilis*) of 652-nm light.

All gram-positive species were completely eliminated (no colonies observed) by PDT using Py_3MeO-TBPo. *E. faecalis* was the most sensitive species against Py_3MeO-

TBPo-PDT showing 6-$\log_{10}$ reduction in bacterial viability with a 0.5 μM porphycene concentration and an energy dose of 30 J·cm^{-2}. A porphycene concentration of 1 μM or 2 μM proved adequate to produce a similar effect for *S. aureus* and MRSA, respectively, upon irradiation with 15 J·cm^{-2}.

Gram-negative species could be similarly inactivated, although higher concentrations and light doses were needed. For instance, 8 μM concentration of Py$_3$MeO-TBPo and 100 J·cm^{-2} were needed to induce a 6-$\log_{10}$ reduction in the bacterial viability for *A. baumanii,* while 10 μM and 60 J·cm^{-2} were needed in the case of *E. coli*. Only a 3-$\log_{10}$ reduction in the survival fraction was achieved for *P. mirabillis* even at 50 μM and 100 J·cm^{-2}, and no relevant inactivation (< 1-$\log_{10}$ reduction in the survival fraction) could be observed for *P. aeruginosa* even at 100 μM porphycene concentration and a light dose of 100 J·cm^{-2}.

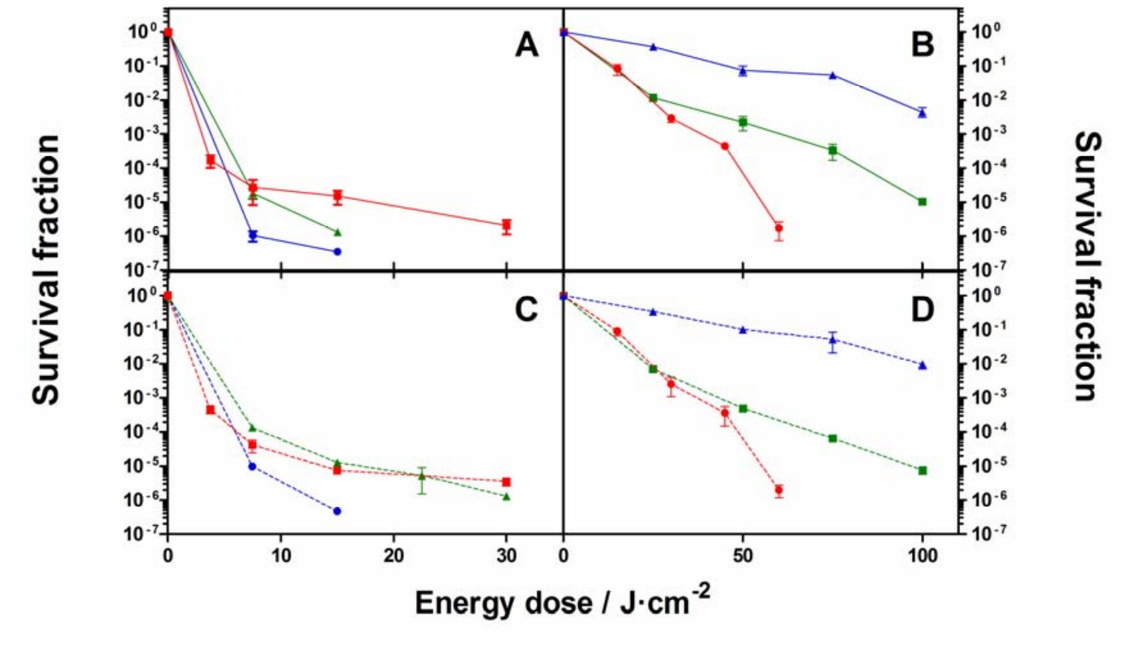

Fig. 5: Light-dose response inactivation curves of bacteria upon irradiation with light of 652-nm at 125 mW·cm^{-2}. **(A,C)** Survival curves of MRSA (triangles), *S. aureus* (circles), *E. faecalis* (squares) with (dashed line) and without (solid line) removing the excess of PS from the solution with a bulk concentration of Py$_3$MeO-TBPo of 0.5 μM (*E. faecalis*) and 1 μM (MRSA and *S. aureus*). **(B,D)** Survival curves of *A. baumanii* (squares), *E. coli* (circles), *P. mirabilis* (triangles) with (dashed line) and without (solid line) removing the excess of PS from the solution with a bulk concentration of 5 μM (*A. baumanii* and *E. coli*) and 20 μM (*P. mirabilis*). Error bars show the standard error of the mean of 3 different experiments.

In vitro photoinactivation of yeasts

Candida species are generally used in APDT as representative models of fungal cells as they grow as single cell suspensions. Both species were completely eliminated by

Py_3MeO-TBPo in a concentration (Fig. 6A) and light-dose dependent manner (Fig. 6B), irrespective of the removal or not of the porphycene excess from the solution. As observed in figure, while 50 μM concentration of Py_3MeO-TBPo and 30 $J\cdot cm^{-2}$ were needed to obtain a 5-$\log_{10}$ reduction in the cell viability of *C. albicans*, only 10 μM concentration and 15 $J\cdot cm^{-2}$ proved necessary to produce the same reduction in the cell viability of *C. krusei*. Removing the excess of PS did not produce any significant difference ($p > 0.75$).

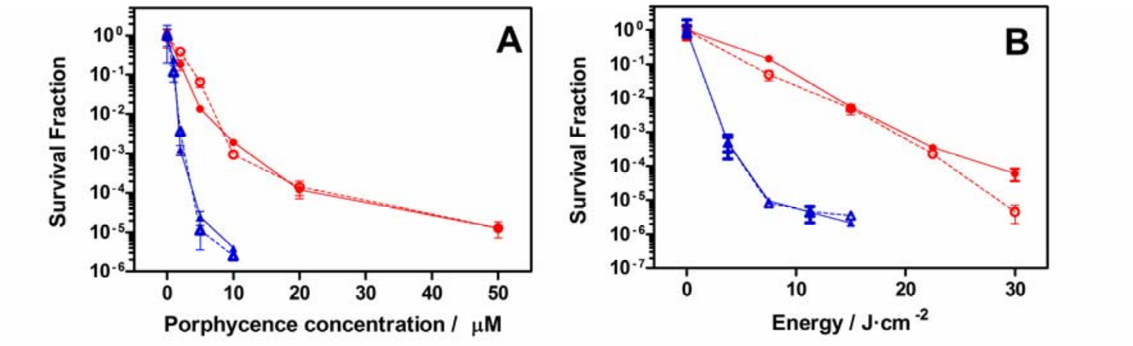

Fig. 6: Yeast photoinactivation with Py_3MeO-TBPo. Survival curves with (dashed line) and without (solid line) removing the excess of photosensitiser (PS) from the solution. **(A)** Drug-dose response of *C. albicans* (circles) after 30 $J\cdot cm^{-2}$ of 652-nm light and *C. krusei* (triangles) after 15 $J\cdot cm^{-2}$ of 635-nm light. **(B)** Light-dose response of *C. albicans* and C. *krusei* with a bulk concentration of Py_3MeO-TBPo of 20 μM and 10 μM, respectively.

In vivo photoinactivation of MRSA in infected burns

Bioluminescent MRSA (Xen31) has a stably integrated lux operon that has been optimized for expression in Gram-positive bacteria [30] and leads to spontaneous light emission at 37ºC in the absence of any exogenously added substrate. It has been previously demonstrated that MRSA CFUs quantified using serial dilutions of bacterial suspensions correlate linearly with the bioluminescence emitted by those bacteria.

Fig. 7A shows the successive bioluminescence images obtained from four representative mouse burns infected with MRSA [30].

The burn treated with PDT received 100 μM of Py_3MeO-TBPo and 652 nm light up to 180 $J\cdot cm^{-2}$, the dark control burn received the same amount of porphycene and no light; while the light alone burn received 652 nm light up to 180 $J\cdot cm^{-2}$ and no porphycene. A non-treated control burn, received neither PS nor light. A complete elimination of the bioluminescence signal was observed in the PDT treated burn after a light dose of 180 $J\cdot cm^{-2}$ in the presence of Py_3MeO-TBPo.

The light-dose responses of normalized mean bioluminescence values ($n = 5$) of the different mouse groups are shown in Fig. 8B. PDT induced a reduction of *ca.* 2.6-$\log_{10}$ of the bioluminescence while less than 0.3-$\log_{10}$ reduction was observed for all the control groups. The statistical analysis at each energy-dose by 1-factor ANOVA test showed significant differences among all the control groups and the PDT-treated group ($p < 0.001$).

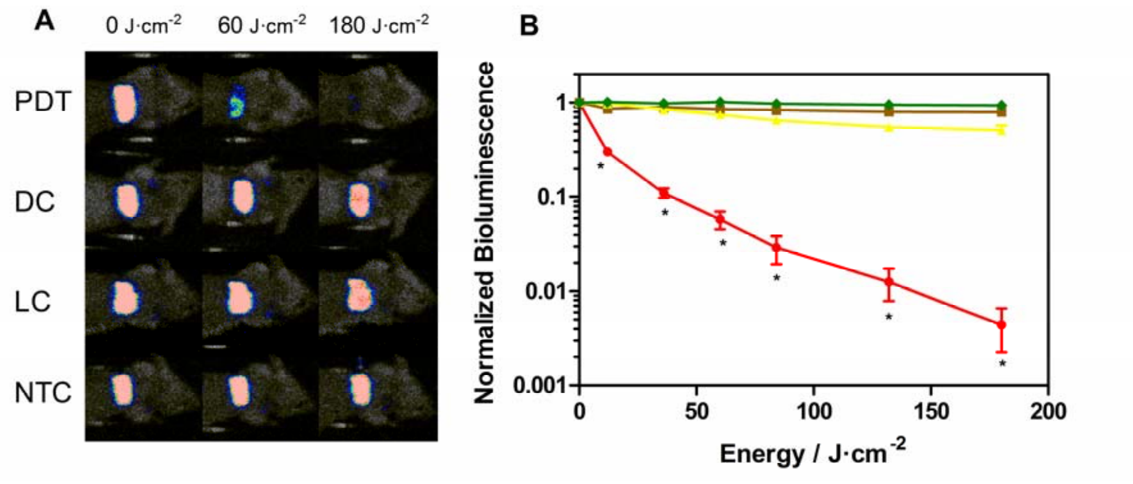

Fig. 7: *In vivo* MRSA photoinactivation with Py_3MeO-TBPo. **(A)** Dose response of bacterial luminescence from burns infected with luminescent MRSA and treated with 100 μM of Py_3MeO-TBPo and 652 nm light (PDT), with 100 μM of Py_3MeO-TBPo only (DC), with light (LC) only, and without treatment (NTC). **(B)** Light-dose response curves of the normalized bioluminescence for mice treated with photodynamic therapy (red), mice treated only with Py_3MeO-TBPo (brown), mice treated only with light (yellow), and without treatment (green). Every point is an average of five independent mice. *, $p < 0.001$.

4.4. DISCUSSION

A potential PS for APDT must have appropriate photophysical properties, such as a large long wavelength absorption band and a high quantum yield for the generation of both long-lived triplet excited state and cytotoxic ROS species. It also has to be water soluble and must have a high affinity for microbial cells and a low affinity for host cells; characteristics that are strongly related to the presence of cationic charges in the molecular structure.

Table 1. Photophysical properties of the porphycene.

Solvent	λ_{abs} / nm	λ_f / nm	Φ_f [a]	τ_S / ns	τ_T / µs [b]	k_q / $M^{-1}s^{-1}$ [c]	Φ_Δ (λ_{ex} / nm)[d]
H_2O	644	656	0.005	1.8	330	1.5×10^9	0.03 (355) 0.004 (532)
MeOH	655	661	0.075	2.6	152	3.5×10^9	0.19

[a] Cresil violet was used as reference. [b] Lifetime of the decays at 420 nm in argon-saturated solutions. [c] Rate constant for triplet quenching by oxygen. Error bar 10%. [d] Singlet oxygen quantum yield in air-saturated solutions. Excitation wavelength in parentheses.

As observed in the absorption spectrum and despite the cationic charges, Py_3MeO-TBPo is soluble although aggregated in water, which deteriorates its photophysical properties. The differential behavior in aqueous and more lipophilic environments may be valuable for unmistakably ascertaining the localization of the porphycene bound to the cells by means of fluorescence microscopy. From the point of view of APDT applications, it can be expected that Py_3MeO-TBPo would be a good PS if binding to microbial cells prevents its aggregation. Conversely, any non-bound PS will be aggregated and thus will not be able to cause photodamage to surrounding tissue. The fact that the absorption spectrum of the aggregates shows lower absorption coefficients is also an advantage as these non-bound molecules will see their light-filtering ability reduced. The presence of aggregates can also be observed in the Φ_F and Φ_Δ values in water. For instance, as observed in Table 1, the Φ_Δ drops from 0.03 to 0.004 when changing the excitation wavelength. This change is due to the different absorption coefficient ratio monomer/aggregates at both wavelengths. At 355 nm, the ratio is higher, leading to a lower light-filtering effect, *i.e.*, to a higher Φ_Δ. The different trend observed in the lifetime values of the singlet (τ_S) and triplet (τ_T) excited states can be explained by two different factors. On one hand, the presence of aggregates in H_2O enables a new deactivation pathway by intermolecular interactions of the porphycene molecules, leading to a decrease in the τ_s value. Compared to TPPo (τ_T = 4.8 ns in toluene) [31], τ_s in MeOH is lower probably due to the higher freedom degree of the residues bound to the porphycene ring. On the other hand, the triplet excited state population is basically controlled by the oxygen concentration in the solutions ($k_q \sim 10^9$ $M^{-1}s^{-1}$). Thus, despite the measurements having been performed in argon-saturated solutions, the solubility of oxygen in H_2O is lower than in MeOH, *i.e.*, the remaining amount of oxygen molecules in the solutions is lower, leading then to a longer τ_T value. As regards k_q, the values are in the range of those observed in diffusional controlled quenching reactions, and the reduction observed in H_2O, relative to that in MeOH, is due to the higher viscosity of water.

Concerning the *in vitro* experiments of Gram-positive bacteria, it was observed that low concentrations of porphycene (< 2 μM), as well as low light doses (< 30 $J \cdot cm^{-2}$) were enough to completely eliminate all the strains. On the other hand, because of the generally higher resistance of Gram-negative species [16], higher light doses (> 60 $J \cdot cm^{-2}$) were needed in order to inactivate the Gram-negative bacterial strains tested with somewhat larger PS concentrations (< 10 μM). However, neither high concentrations of porphycene nor high light doses were able to completely eliminate *P. mirabilis* or significantly inactivate *P. aeruginosa*. As previously demonstrated by Tegos *et al.* [32], the number of cationic charges in the PS' structure strongly affects the ability to inactivate bacteria, suggesting that a porphycene with higher number of cationic charges in its structure might be able to inactivate such species.

Consistent with the photophysics results there are no significant differences between the inactivation curves recorded in the presence or absence of the excess PS ($p >$ 0.26), suggesting a high lipophilicity of the porphycene, *i.e.*, a high affinity against bacterial cells, which indicates that only the PS bound to the cells is involved in the photodynamic effect. Thus, according to the classification of PSs established by Deminova and Hamblin [17], the porphycene might be tightly bound to the microbial cell and might be able to penetrate into microorganisms, as happened when poly-L-lysine chlorin(e6) conjugate was used as PS.

As for the yeast studies, *Candida* species were selected as model to study the activity of porphycenes against fungal cells. Our data show that porphycenes can be used as a valuable alternative to typical anti-fungal PSs, as they are able to completely inactivate both *C. albicans* and *C. krusei* using lower light doses and lower porphycene concentrations than for currently-used PSs [17,33-35].

Despite the optimal properties of the porphycene *in vitro*, its value as PS must be further assessed from experiments *in vivo*. The test in burns infected with MRSA demonstrate that porphycenes can clearly produce statistically significant differences between the controls and the PDT-treated group ($p < 0.001$), reducing by 2.6-$\log_{10}$ units the bioluminescence of MRSA in an energy-dose dependent manner upon irradiation with 180 $J{\cdot}cm^{-2}$ and a porphycene concentration of 100 μM. These results compare favorably to those obtained by Dai *et al.* [36], where a 2.7-$\log_{10}$ reduction of the bioluminescence signal was obtained in a skin abrasion wound infected with MRSA by using a PS such as polyethylenimine-chlorin(e6) conjugate and 660-nm red light, and by Zolfaghari *et al.* [37], where 1.4-$\log_{10}$ and 1.15-$\log_{10}$ where obtained in excision and superficial scarified wounds treated with methylene blue and 670-nm red light, respectively.

4.5. CONCLUSIONS

The synthetic availability of cationic porphycenes, as well as their optimal physical and photophysical properties, suggests the porphycene-core macrocycle can be a potentially interesting antimicrobial PS. The demonstrated high photodynamic activity against a broad spectrum of microbial cells *in vitro* as well as an *in vivo* infection model, supports the further scrutiny of this family of compounds.

4.6. REFERENCES

1. Wainwright M. Photodynamic antimicrobial chemotherapy (PACT). *J Antimicrob Chemother* **1998**; 42: 13-28.

2. Wainwright M. Photoantimicrobials--so what's stopping us? *Photodiagn Photodyn Ther* **2009**; 6: 167-169.

3. Dai T, Huang YY, and Hamblin MR. Photodynamic therapy for localized infections--state of the art. *Photodiagn Photodyn Ther* **2009**; 6: 170-188.

4. Schweitzer C and Schmidt R. Physical mechanisms of generation and deactivation of singlet oxygen. *Chem Rev* **2003**; 103: 1685-1757.

5. Michaeli A and Feitelson J. Reactivity of singlet oxygen toward amino acids and peptides. *Photochem Photobiol* **1994**; 59(3): 284-289.

6. Stark G. Functional consequences of oxidative membrane damage. *J Membr Biol* **2005**; 205: 1-16.

7. Ravanat JL, Di Mascio P, Martinez GR, Medeiros MHG, and Cadet J. Singlet oxygen induces oxidation of cellular DNA. *J Biol Chem* **2000**; 275: 40601-40604.

8. Nitzan Y, Gutterman M, Malik Z, and Ehrenberg B. Inactivation of gram-negative bacteria by photosensitized porphyrins. *Photochem Photobiol* **1992**; 55: 89-96.

9. Bertoloni G, Rossi F, Valduga G, Jori G, Ali H, and Vanlier JE. Photosensitizing activity of water-soluble and lipid-soluble phthalocyanines on prokaryotic and eukaryotic microbial-cells. *Microbios* **1992**; 71: 33-46.

10. Romanova NA, Brovko LY, Moore L, Pometun E, Savitsky AP, Ugarova NN, and Griffiths MW. Assessment of photodynamic destruction of *Escherichia coli* O157 : H7 and *Listeria monocytogenes* by using ATP bioluminescence. *Appl Environ Microbiol* **2003**; 69: 6393-6398.

11. Stockert JC, Canete M, Juarranz A, Villanueva A, Horobin RW, Borrell J, Teixido J, and Nonell S. Porphycenes: Facts and prospects in photodynamic therapy of cancer. *Curr Med Chem* **2007**; 14: 997-1026.

12. Polo L, Segalla A, Bertoloni G, Jori G, Schaffner K, and Reddi E. Polylysine-porphycene conjugates as efficient photosensitizers for the inactivation of microbial pathogens. *J Photochem Photobiol B:Biol* **2000**; 59: 152-158.

13. Lauro FM, Pretto P, Covolo L, Jori G, and Bertoloni G. Photoinactivation of bacterial strains involved in periodontal diseases sensitized by porphycene-polylysine conjugates. *Photochem Photobiol Sci* **2002**; 1: 468-470.

14. Sanchez-Garcia D, Borrell JI, and Nonell S. One-pot synthesis of substituted 2,2 '-bipyrroles. A straightforward route to aryl porphycenes. *Org Lett* **2009**; 11: 77-79.

15. Bertoloni G, Rossi F, Valduga G, Jori G, and Vanlier J. Photosensitizing activity of water-soluble and lipid-soluble phthalocyanines on *Escherichia coli*. *FEMS Microbiol Lett* **1990**; 71: 149-155.

16. Malik Z, Ladan H, and Nitzan Y. Photodynamic inactivation of gram-negative bacteria -problems and possible solutions. *J Photochem Photobiol B:Biol* **1992**; 14: 262-266.

17. Demidova TN and Hamblin MR. Effect of cell-photo sensitizer binding and cell density on microbial photoinactivation. *Antimicrob Agents Chemother* **2005**; 49: 2329-2335.

18. Guo YY, Rogelj S, and Zhang P. Rose bengal-decorated silica nanoparticles as photosensitizers for inactivation of gram-positive bacteria. *Nanotechnol* **2010**; 21.

19. Friedberg JS, Tompkins RG, Rakestraw SL, Warren SW, Fischman AJ, and Yarmush ML. Antibody-targeted photolysis - bacteriocidal effects of Sn (IV) chlorin e6- Dextran-monoclonal antibody conjugates. *Ann NY Acad Sci* **1991**; 618: 383-393.

20. Minnock A, Vernon DI, Schofield J, Griffiths J, Parish JH, and Brown SB. Photoinactivation of bacteria. Use of a cationic water-soluble zinc phthalocyanine to photoinactivate both gram-negative and gram-positive bacteria. *J Photochem Photobiol B:Biol* **1996**; 32: 159-164.

21. Merchat M, Bertolini G, Giacomini P, Villanueva A, and Jori G. Meso-substituted cationic porphyrins as efficient photosensitizers of gram-positive and gram-negative bacteria. *J Photochem Photobiol B:Biol* **1996**; 32: 153-157.

22. Wainwright M, Phoenix DA, Marland J, Wareing DRA, and Bolton FJ. A study of photobactericidal activity in the phenothiazinium series. *FEMS Immunol Med Microbiol* **1997**; 19: 75-80.

23. Caminos DA, Spesia MB, and Durantini EN. Photodynamic inactivation of *Escherichia coli* by novel meso-substituted porphyrins by 4-(3-*N,N,N*-trimethylammoniumpropoxy)phenyl and 4-(trifluoromethyl)phenyl groups. *Photochem Photobiol Sci* **2006**; 5: 56-65.

24. Magde D, Brannon JH, Cremers TL, and Olmsted J. Absolute luminescence yield of cresyl violet - Standard for the red. *J Phys Chem* **1979**; 83: 696-699.

25. Rubio N, Borrell JI, Teixido J, Canete M, Juarranz A, Villanueva A, Stockert JC, and Nonell S. Photochemical production and characterisation of the radical ions of tetraphenylporphycenes. *Photochem Photobiol Sci* **2006**; 5: 376-380.

26. Nonell S and Braslavsky SE. Methods in Enzimology, Academic Press, **2000**.

27. Wilkinson F, Helman WP, and Ross AB. Quantum yields for the photosensitized formation of the lowest electronically excited singlet state of molecular oxygen in solution. *J Phys Chem Ref Data* **1993**; 22: 113-262.

28. Redmond RW and Gamlin JN. A compilation of singlet oxygen yields from biologically relevant molecules. *Photochem Photobiol* **1999**; 70: 391-475.

29. Nonell S, Gonzalez M, and Trull FR. 1*H*-Phenalen-1-one-2-sulfonic acid - An extremely efficient singlet molecular-oxygen sensitizer for aqueous-media. *Afinidad* **1993**; 50: 445-450.

30. Francis KP, Joh D, Bellinger-Kawahara C, Hawkinson MJ, Purchio TF, and Contag PR. Monitoring bioluminescent *Staphylococcus aureus* infections in living mice using a novel luxABCDE construct. *Infect Immun* **2000**; 68: 3594-3600.

31. Rubio N, Prat F, Bou N, Borrell JI, Teixido J, Villanueva A, Juarranz A, Canete M, Stockert JC, and Nonell S. A comparison between the photophysical and photosensitising properties of tetraphenyl porphycenes and porphyrins. *New J Chem* **2005**; 29: 378-384.

32. Tegos GP, Demidova TN, Arcila-Lopez D, Lee H, Wharton T, Gali H, and Hamblin MR. Cationic fullerenes are effective and selective antimicrobial photosensitizers. *Chem Biol* **2005**; 12: 1127-1135.

33. Foley JW, Song XZ, Demidova TN, Jilal F, and Hamblin MR. Synthesis and properties of benzo[a]phenoxazinium chalcogen analogues as novel broad-spectrum antimicrobial photosensitizers. *J Med Chem* **2006**; 49: 5291-5299.

34. Zeina B, Greenman J, Purcell WM, and Das B. Killing of cutaneous microbial species by photodynamic therapy. *Br J Dermatol* **2001**; 144: 274-278.

35. Codling CE, Maillard JY, and Russell AD. Aspects of the antimicrobial mechanisms of action of a polyquaternium and an amidoamine. *J Antimicrob Chemother* **2003**; 51: 1153-1158.

36. Dai T, Tegos GP, Zhiyentayev T, Mylonakis E, and Hamblin MR. Photodynamic therapy for methicillin-resistant *Staphylococcus aureus* infection in a mouse skin abrasion model. *Lasers Surg Med* **2010**; 42: 38-44.

37. Zolfaghari PS, Packer S, Singer M, Nair SP, Bennett J, Street C, and Wilson M. *In vivo* killing of *Staphylococcus aureus* using a light-activated antimicrobial agent. *BMC Microbiol* **2009**; 9: 27.

38. Jux N. *o*-(bromomethyl)-substituted tetraarylporphyrin building blocks. *Org Lett* **2000**; 2: 2129-2132.

39. Yamashita T, Uno T, and Ishikawa Y. Stabilization of guanine quadruplex DNA by the binding of porphyrins with cationic side arms. *Bioorg Med Chem* **2005**; 13: 2423-2430.

40. Ikawa Y, Moriyama S, Harada H, and Furuta H. Acid-base properties and DNA-binding of water soluble *N*-confused porphyrins with cationic side-arms. *Org Biomol Chem* **2008**; 6: 4157-4166.

4.7. Annex

Synthesis

The synthetic process followed to obtain the aryl cationic porphycene is shown in Fig. A1 and was performed by Ruben Ruiz and David Sánchez-García.

Porphycene **1** was available from earlier studies and was prepared using previously described procedures [14]. Then, the methoxy ethers of porphycene **1** were deprotected to the corresponding bromo derivative by means of the addition of a HBr solution to a dichloromethane solution of compound **1**. The procedure was adapted from that described by Jux [38]. Reaction of porphycene **2** with pyridine yielded the substitution of the bromide atom followed by precipitation of a dark solid corresponding to porphycene **3**, namely Py$_3$MeO-TBPo [39,40].

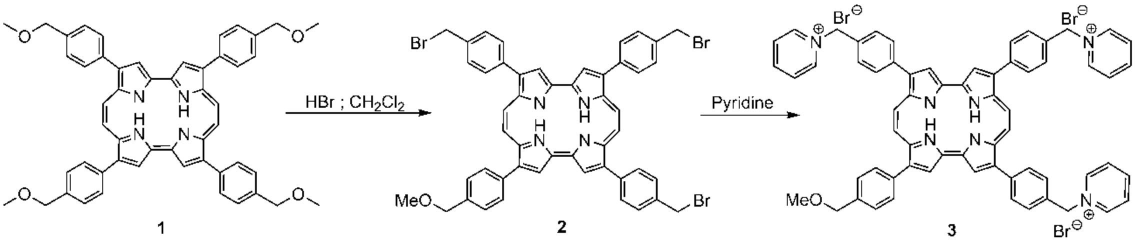

Fig. A1: Synthetic pathway used for the synthesis of the cationic porphycene.

Chapter 5

Singlet oxygen in *E. coli* : new insights for antimicrobial photodynamic therapy

Antimicrobial photodynamic therapy is an emerging treatment for bacterial infections that is becoming increasingly more attractive. However, there is a limited knowledge about the localization of the photoactive drug in the bacteria and about the details of production of the main cytotoxic species singlet oxygen. This chapter describes a combination of spectroscopic and time-resolved photophysical techniques that provide such information for a cationic porphyrin photosensitiser in gram-negative *Escherichia coli* bacteria.

The work described in this chapter is adapted from Xavier Ragàs, Montserrat Agut and Santi Nonell in *Free Rad Biol Med* 2010, 49, 770-776.

5.1. INTRODUCTION

Pathogenic microorganisms and viruses, including those resistant to antibiotics, e.g. MRSA, can be inactivated successfully *in vitro* and *in vivo* using antimicrobial photodynamic therapy (APDT), often referred to as photodynamic inactivation [1-8]. The fundamentals of APDT are now well understood: a photoactive drug, referred to as the photosensitiser (PS), is delivered to the microorganism and then is irradiated with *per se* harmless visible light. The photoexcited PS forms reactive oxygen species (ROS) [9] that react with substrates in the proximate environment of the PS, affecting the integrity and function of microbial cell walls, membranes, enzymes or nucleic acids [10-13]. The large variety of molecular targets and the ability to cause damage to the pathogen without PS internalisation, suggest that APDT is very unlikely to develop resistance [14]. As such it is being increasingly recognized as an attractive alternative to antibiotics [8,15].

Notwithstanding the vast progress made over the last few years, the mechanistic details of how APDT affects microbial cells are not fully understood. Of specific concern, little is known about the localization of the PS and hence about the site where the primary photodamage is produced. Fluorescence microscopy is a very useful technique to assess the localization of a PS in eukaryotic cells [16]. However, the resolution of current microscopes is not sufficient for prokaryotic cells, disenabling fluorescence microscopy as a useful tool for mechanistic understanding in APDT.

While free radicals may contribute to the photodamage observed, singlet oxygen ($^1O_2$) is regarded as the ROS that plays the major role in APDT with porphyrins [17]. Production of $^1O_2$ occurs by energy transfer from the electronic triplet excited-state of the PS (^{3}PS) to molecular oxygen [18]. The kinetics of this process are strongly affected by the environment, thereby allowing to distinguish among different cell sites [19,20]. Monitoring both ^{3}PS and $^1O_2$ through their time-resolved phosphorescence can thus overcome the limitations of fluorescence microscopy in prokaryotic cells.

There is one single report on the kinetics of $^1O_2$ in bacteria, namely that by Maisch *et al.* [21], who used porfimer sodium to photosensitise $^1O_2$ in bacterial suspensions. These authors explored the effects of oxygen and bacterial concentration on the $^1O_2$ phosphorescence kinetics. Unfortunately, their studies were restricted to *Staphylococcus aureus, a* gram-positive species. It is known that gram-negative bacteria are less susceptible to APDT [22] than their gram-positive counterparts, owing to the higher complexity of the cell wall [23]. It appears therefore of interest to gain insight into the mechanism of photodynamic inactivation of gram-negative bacteria as this could give clues for the design of more efficient photosensitisers for such pathogens.

This study reports on the kinetics of $^1O_2$ production and decay in *Escherichia coli,* a model for gram-negative bacteria, by monitoring the phosphorescence of both $^1O_2$ and its precursor ^3PS in bacterial suspensions. The tetracationic porphyrin 5,10,15,20-tetrakis(*N*-methyl-4-pyridyl)-21*H*,23*H*-porphine (TMPyP) was chosen as PS, building on the fact that cationic dyes are the most effective towards gram-negative bacteria [24,25]. The results obtained may explain why there is no need to internalize a photodynamic drug into the pathogen for its effective killing.

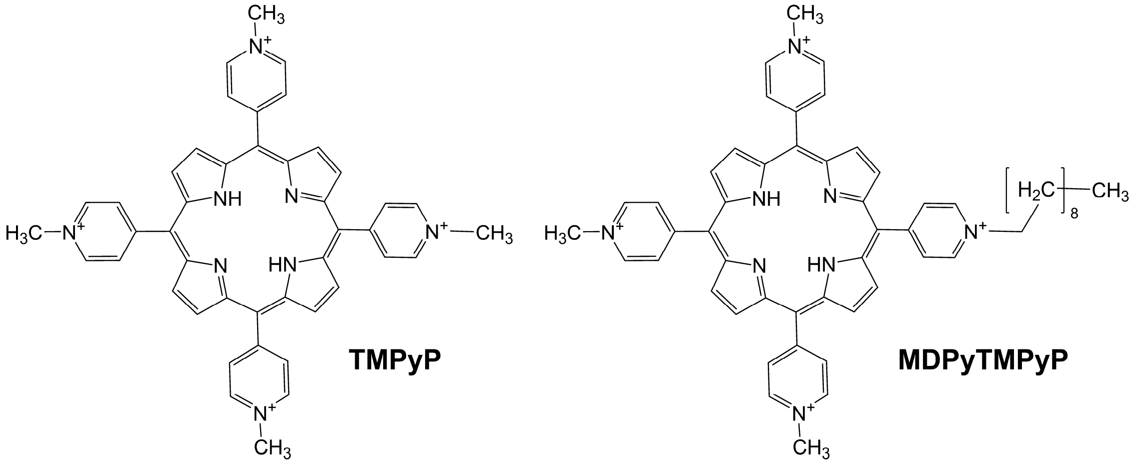

Fig. 1: Chemical structures of 5,10,15,20-tetrakis(*N*-methyl-4-pyridyl)-21*H*,23*H*-porphine (TMPyP) and 5-mono(*N*-decyl-4-pyridyl)-10,15,20-tri(*N*-methyl-4-pyridyl)-21*H*,23*H*-porphine (MDPyTMPyP).

5.2. EXPERIMENTAL SECTION

Chemicals

5,10,15,20-tetrakis(*N*-methyl-4-pyridyl)-21*H*,23*H*-porphine tetratosylate (TMPyP) and 5-mono(*N*-decyl-4-pyridyl)-10,15,20-tri(*N*-methyl-4-pyridyl)-21*H*,23*H*-porphine dihydrochloride tetrachloride (MDPyTMPyP) were supplied by Frontier Scientific (Logan, UT, USA) and had a minimal purity of 99% (Fig. 1). Deuterium oxide (99.9%) was purchased from Solvents Documentation Synthesis (SDS, Peypin, France). Bovine serum albumin (98%), lysozyme, sodium dodecyl sulphate (SDS), trizma, and Dubelcco’s phosphate buffered saline (PBS) were purchased from Sigma-Aldrich Co. (St. Louis, MO, USA). Saccharose and ethylenediamine tetraacetic acid (EDTA) were provided by Panreac S.A. (Barcelona, Spain).

Deuterated PBS (D-PBS) was prepared by dissolving PBS powder in deuterium oxide.

5.3. RESULTS

TMPyP binding to *E. coli*

The uptake of TMPyP was determined by measuring its fluorescence in cell lysates obtained by treatment with NaOH 0.1 M / 1 % SDS. The uptake of TMPyP increases up to a plateau value after *ca.* 18 h. The largest uptake was observed at 8 μM bulk concentration of TMPyP, resulting in *ca.* 5 x 10^5 TMPyP molecules per *E. coli* cell (Fig. 2). The next higher concentration tested (16 μM) lead to unacceptable dark toxicity, as assessed by colony-formation assays carried out before and after contact with the PS.

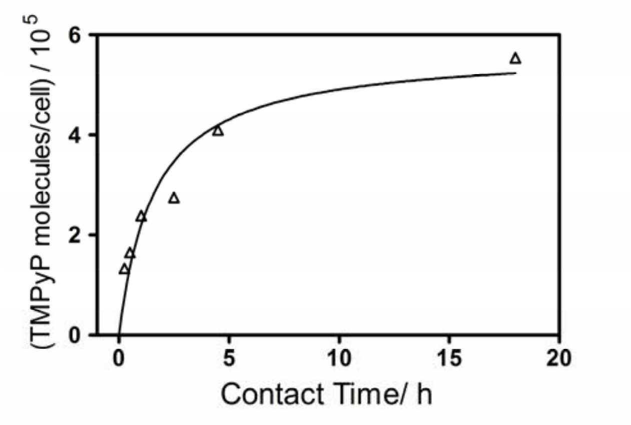

Fig. 2: TMPyP binding to *E.coli* expressed as molecules per cell, with a bulk concentration of 8 μM.

The new microenvironment experienced by TMPyP upon bacterial uptake lead to measurable changes in its photophysical properties. The absorption spectrum showed a bathochromic shift of 20 nm relative to that in the buffer (Fig. 3A). The fluorescence emission spectrum showed two well-resolved bands, in contrast with the single, structureless broad band found in the buffer (Fig. 3B). Two bands were also observed in the NaOH-SDS micellar media, corresponding to the Q(0-0) and Q(0-1) transitions.

Time-resolved fluorescence measurements provided additional insight on the effects of photosensitiser uptake. In buffered solution, the fluorescence, observed either at 655 or 714 nm, decayed monoexponentially with a lifetime of 4.6 ± 0.2 ns, in very good agreement with literature reports [26]. In contrast, the signals obtained in *E. coli* required two additional exponential terms with lifetimes 2.0 ± 0.5 and 10.5 ± 1 ns, 30% and 10% relative amplitudes respectively. A third set of experiments carried out on *E. coli* spheroplasts showed an intermediate behaviour, namely biexponential decay with lifetimes 2.3 ± 0.5 ns and 10.5 ± 1 ns, 60% and 40% relative amplitudes respectively (Fig. 4).

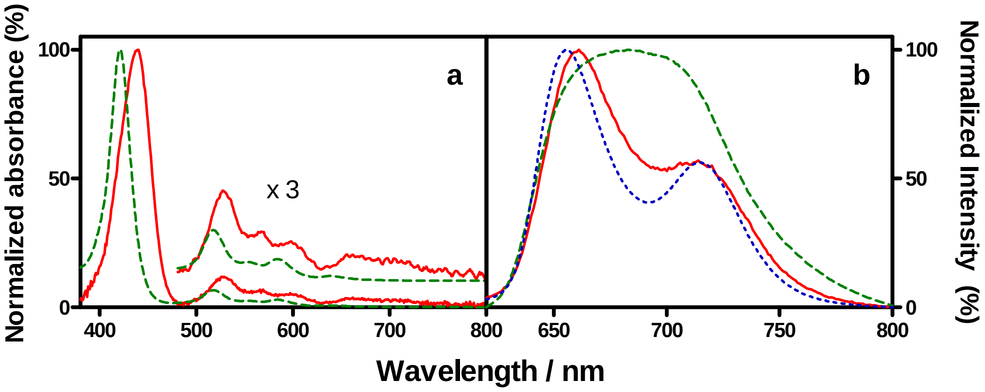

Fig. 3: Normalized (a) absorption and (b) fluorescence spectra of TMPyP in *E. coli* (solid line), PBS (dashed line), and NaOH 0.1 M / 1% SDS (dotted line).

Phosphorescence of $^1O_2$ and TMPyP in *E. coli* cells in PBS

Pulsed-laser irradiation of TMPyP-loaded *E. coli* cells suspended in phosphate buffer solution at pH 7.4 (PBS) produced clear time-resolved phosphorescence signals. At 1280 nm, where $^1O_2$ emits, the signals grew with a lifetime $^{1280}\tau_1^{PBS} = 2.5 \pm 1$ μs, and decayed biexponentially with lifetimes $^{1280}\tau_2^{PBS} = 3.5 \pm 1$ μs and $^{1280}\tau_3^{PBS} = 20 \pm 2$ μs, respectively (Fig. 5a). At 960 nm, where the phosphorescence of TMPyP is observed instead, the signal decayed with two exponential terms, $^{960}\tau_1^{PBS} = 2.5 \pm 1$ μs and $^{960}\tau_2^{PBS} = 20 \pm 3$ μs, respectively (Fig. 5b).

Effect of solvent deuteration

It is well known that the lifetime of $^1O_2$ is increased in deuterated solvents [18]. Irradiation of *E. coli* cells in deuterated PBS (D-PBS) produced differences in the phosphorescence signals relative to those in PBS. At 1280 nm, the signals grew biexponentially with lifetimes $^{1280}\tau_1^{D\text{-}PBS} = 2.5 \pm 1$ μs and $^{1280}\tau_2^{D\text{-}PBS} = 20 \pm 2$ μs, and decayed with a single exponential component with lifetime $^{1280}\tau_3^{D\text{-}PBS} = 66 \pm 4$ μs (Fig. 5c). At 960 nm, the phosphorescence of TMPyP showed the same kinetics as in PBS, namely $^{960}\tau_1^{D\text{-}PBS} = 2.5 \pm 1$μs and $^{960}\tau_2^{D\text{-}PBS} = 20 \pm 3$μs (Fig. 5d).

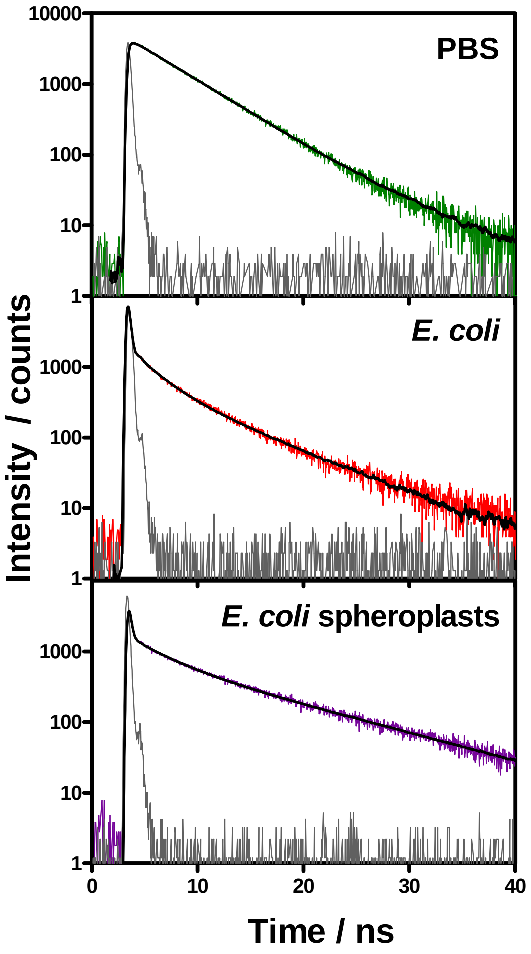

Fig. 4: Time-resolved fluorescence of TMPyP at 655 nm upon excitation at 405 nm. Signal, instrument response function, and fit in PBS at pH 7.4, *E. coli*, and *E. coli* spheroplasts.

Effect of bovine serum albumin

Bovine serum albumin (BSA) is an efficient $^1O_2$ quencher (quenching rate constant k_q = 5 x 10^8 M^{-1} s^{-1}) that, because of its large size (molecular weight of 65 kDa), cannot penetrate the cell and remains in the buffer [20]. Addition of 0.75 mM BSA to D-PBS suspensions of *E. coli* cells loaded with TMPyP induced significant changes to the $^1O_2$ kinetics. Thus, the rise and decay of the signal at 1280 nm became monoexponential, with lifetimes $^{1280}\tau_1^{BSA}$ = 3 ± 1 μs and $^{1280}\tau_2^{BSA}$ = 20 ± 3 μs, respectively (Fig. 5e). In contrast, the kinetics of TMPyP phosphorescence, monitored at 960 nm, were not affected by BSA, *i.e.,* the decay was still biexponential with lifetimes $^{960}\tau_1^{BSA}$ = 3 ± 1 μs and $^{960}\tau_2^{BSA}$ = 20 ± 3 μs (Fig. 5f).

Effect of cell wall: *E. coli* spheroplasts

In order to assess the role of the external structure of the cell wall, the phosphorescence of $^1O_2$ and TMPyP was measured in *E. coli* spheroplasts, *i.e.*, bacteria from which the cell wall has been almost completely removed.

In contrast to the observations made in whole cells, the signal of $^1O_2$ in D-PBS rose monoexponentially, with lifetime $^{1280}\tau_1^{\text{D-PBS}}$ = 20 ± 2 μs. Its decay matched that in whole cells, namely a single component with $^{1280}\tau_2^{\text{D-PBS}}$ = 69 ± 4 μs (Fig. 5g). The phosphorescence of TMPyP was observed to decay monoexponentially, with $^{960}\tau_1^{\text{D-PBS}}$ = 20 ± 2 μs (Fig. 5h).

When 0.75 mM BSA was added to the spheroplasts suspension, the growth of the $^1O_2$ signal was much faster ($^{1280}\tau_1^{\text{BSA}}$ = 2 ± 1 μs), while its decay, as well as that of TMPyP phosphorescence, remained unchanged ($^{1280}\tau_2^{\text{BSA}} = {}^{960}\tau_1^{\text{BSA}}$ = 22 ± 2 μs; Fig. 5i and 5j, respectively).

Effect of the sensitiser’s side chain length

Reddi *et al.* observed that increasing the length of a single *N*-alkyl substituent from 1 to 14 carbon atoms enhances the efficiency of *N*-substituted tetrapyridylporphyrin accumulation in *E. coli* and reduces its release during centrifugations [27]. Following this reference, we hypothesized that the longer chain in 5-mono(*N*-decyl-4-pyridyl)-10,15,20-tri(*N*-methyl-4-pyridyl)-21*H*,23*H*-porphine (MDPyTMPyP) would preclude its penetration into the cytosol of the cells. As such, a change of kinetics relative to TMPyP would provide additional insight on the localization of TMPyP. Accordingly, the phosphorescence of $^1O_2$ was recorded in *E. coli* cells loaded with MDPyTMPyP under the same concentration and contact time conditions as for the TMPyP experiments.

In agreement with our expectations, the signal in D-PBS at 1280 nm grew and decayed now with monoexponential kinetics, with lifetimes $^{1280}\tau_1^{\text{D-PBS}}$ = 3 ± 1 μs and $^{1280}\tau_2^{\text{D-PBS}}$ = 67 ± 3 μs, respectively (Fig. 5k). Unfortunately, we were not able to observe any phosphorescence of MDPyTMPyP at 960 nm.

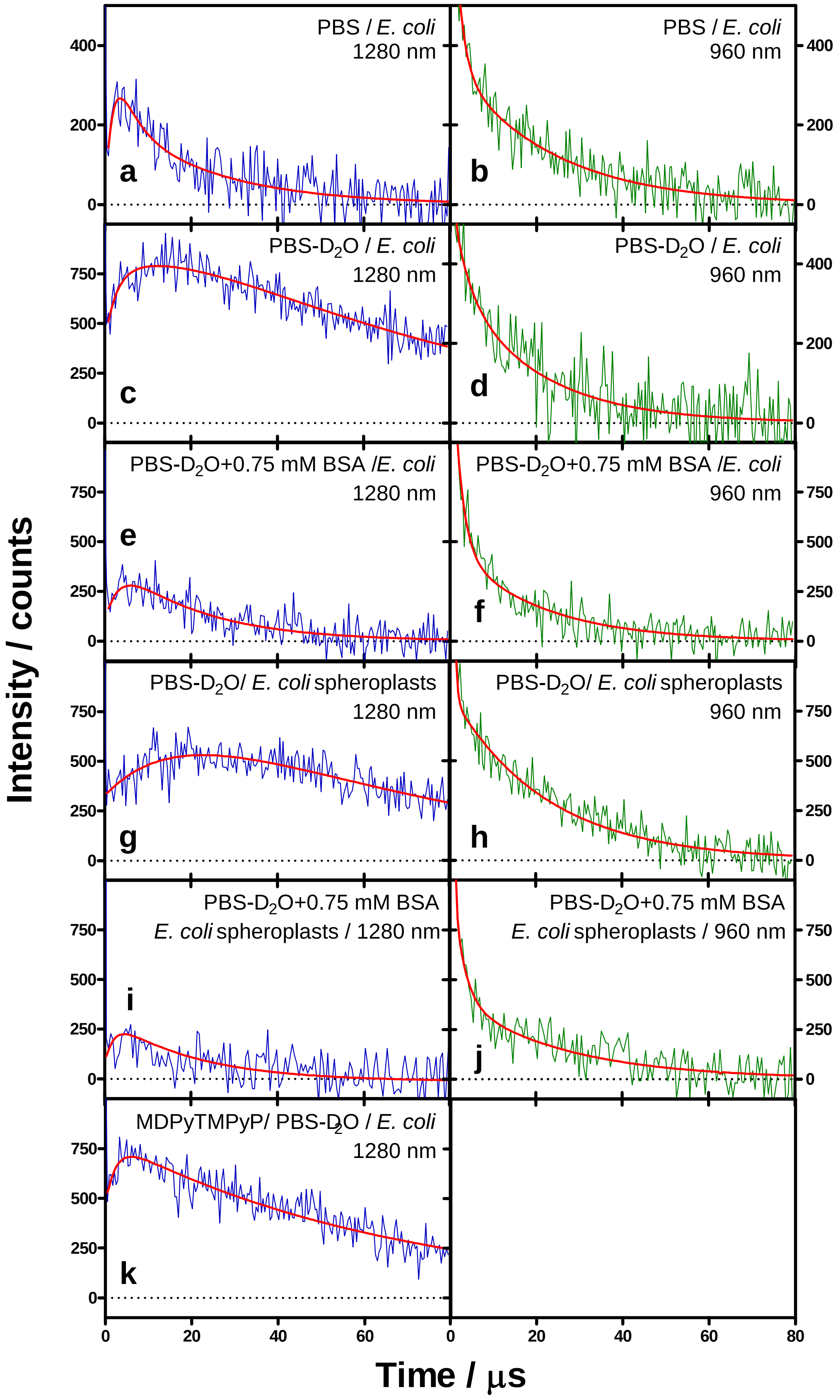

Fig. 5: Left panels: $^1O_2$ phosphorescence at 1280 nm. Right panels: TMPyP phosphorescence at 960 nm.

Control measurements in bacterial suspensions

Different controls have been performed in order to assure:

1) Origin of the luminescence signals: It was critical in our experiments to eliminate any photosensitiser molecule from the external aqueous buffer in order to ensure that the observed fluorescence or phosphorescence was produced by cell-bound molecules. The external aqueous solutions were routinely tested before and after the *in vitro* measurements.

2) Light dose: Irradiation during APDT may induce the release or relocalization of the PS from its initial binding site [23]. Also, the kinetics of $^1O_2$ formation and decay may change upon irradiation due to the photodynamic modification of cell components [28,29]. In order to prevent these effects, all the experiments were performed with the lowest possible amount of energy per bacterial cell (7 nJ/cell), well below the doses reported by Kuimova *et al*. [28] in eukaryotic cells (*ca.* 0.5 mJ/cell) and comparable to those used by Schlothauer *et al*. (2-40 nJ/cell) [29].

3) Identification of $^1O_2$ as the species responsible for the emission recorded at 1280 nm: Many controls have been carried out to demonstrate that we were indeed looking at $^1O_2$ photosensitized by TMPyP in the luminescence experiments with *E. coli*:
    - No signal could be detected in the absence of TMPyP.
    - No signal was observed at 1150 nm under any conditions, *i.e.*, the spectrum of the signal matched that of $^1O_2$ [18].
    - The phosphorescence disappeared when oxygen was excluded from the medium by flowing a stream of argon above the cell suspension for 1 hour.
    - The duration of the luminescence increased when H_2O was replaced by D_2O in the buffer.

5.4. DISCUSSION

The main goal of this study was to obtain insight into the mechanism of photodynamic inactivation of gram-negative bacteria.

Our first efforts were aimed at identifying the optimal conditions to obtain unambiguous time-resolved phosphorescence signals from viable bacterial cells. A concentration of 8 μM in the medium and a contact time of 18 h proved adequate to this respect. While such TMPyP concentration is in the range of those used to photoinactivate *E. coli* [30], the contact time is much longer than those typically used in APDT [31,32]. A contact time of 18 h was nevertheless chosen as it provided a higher drug uptake at such concentration, allowing us to minimize the light dose necessary to obtain proper luminescence signals (*vide supra*). This is an essential requirement as the kinetics of $^1O_2$ in cells changes with increasing light exposure. Specifically, as the light dose accumulates, the extent of reaction between singlet oxygen and cell components increases, which changes the cellular microenvironment and therefore the singlet oxygen kinetics [28,29]. Control experiments showed no significant dark toxicity under those conditions. The sensitiser load achieved with this procedure was about 5 x 10^5 TMPyP molecules per bacterial cell, within the typical range for APDT studies [33].

The localization of a PS determines where the ROS are produced and it is therefore important to establish it in order to understand the mechanism of APDT. Since fluorescence microscopy techniques lack the necessary resolution, an alternative approach had to be sought. Our results, based on spectroscopic and photophysical measurements, suggest a double localization of TMPyP in *E. coli* cells. First, the bathochromic shift in the absorption spectrum and the appearance of structure in the fluorescence spectrum upon binding to *E. coli* reveal a change in the TMPyP's microenvironment [26,34,35]. This conclusion is confirmed by time-resolved fluorescence measurements. While in PBS the fluorescence kinetics were monoexponential (lifetime 4.6 ns), three exponential terms were detected in *E. coli* cells (4.6, 2.0, and 10.5 ns), whereas only two were found in spheroplasts (2.3 and 10.5 ns). It is worth noting that in either case the supernatant obtained after centrifugations showed no signal, confirming that the fluorescence stems from cell-bound TMPyP molecules. Thus, it can safely be concluded that a fraction of TMPyP molecules is bound to the external structure of the cell wall, experiencing an aqueous-like environment (4.6 ns), and the rest has been internalized. It is well known that TMPyP readily binds to the nucleic acids, either intercalated between guanine-cytosine base pairs, or groove bound at adenine-thymine sites [36]. The fluorescence lifetime changes concomitantly to 1.7-2.5 ns (intercalation) [35] and 10-11 ns (groove binding)

[37], values close to those observed in this work. This seems to indicate that internalized TMPyP molecules are bound to the cytosolic nucleic acids. Salmon-Divon *et al.* [30] have demonstrated that TMPyP induces photodamage to *E. coli* nucleic acids in the order genomic-DNA > total RNA > plasmid-DNA.

The observed kinetics for ^{3}PS and $^1O_2$ can be interpreted in the light of these findings. In the first place, the dual localization of TMPyP is reflected in its triplet-state kinetics, as evidenced by the biexponential decay of its phosphorescence at 960 nm in intact cells. The shorter component decays with a lifetime of 2.5 μs, close to the value reported for TMPyP in air-saturated aqueous environments [38]. We assign it to TMPyP molecules bound to the cell wall in concurrence with the fluorescence results. Thus, external binding to *E. coli* does not shield TMPyP from oxygen and allows the production of $^1O_2$. The longer component (20 μs) is assigned in turn to TMPyP molecules bound to the nucleic acids groove, because nucleic acid-intercalated TMPyP molecules are subject to reductive electron-transfer quenching by guanine residues [26] and are therefore not expected to contribute to the observed phosphorescence. Hence, binding to the nucleic acids does not preclude the formation of the triplet state of TMPyP but shields it from dissolved oxygen, as evidenced by its 20-μs lifetime in air-saturated media. Consistent with this interpretation, the TMPyP phosphorescence decay in spheroplasts is monoexponential and its lifetime (20 μs) matches that of the internalized PS.

Likewise, the kinetics of $^1O_2$ phosphorescence at 1280 nm reflects both the dual localization of the PS and the environment of the nascent $^1O_2$. In order to facilitate the interpretation of the signals, it must be borne in mind that $^1O_2$ is formed by energy transfer from ^{3}PS to oxygen and therefore the kinetics of its formation match those of ^{3}PS decay (*Eq. 1*). This helps assigning which of the observed components corresponds to $^1O_2$ formation (= ^{3}PS decay) and which to its decay.

$$^3\mathrm{PS} + \mathrm{O_2} \xrightarrow{\tau_T} \mathrm{PS} + {}^1\mathrm{O_2} \xrightarrow{\tau_\Delta} \mathrm{Products} \qquad (1)$$

Eqs. 2 and *3* are readily derived from this simplified scheme:

$$[^3\mathrm{PS}]_t = K_1 \cdot e^{-t/\tau_T} \qquad (2)$$

$$[{}^1O_2]_t = K_2 \cdot \frac{\tau_\Delta}{\tau_T - \tau_\Delta}\left(e^{-t/\tau_T} - e^{-t/\tau_\Delta}\right), \qquad (3)$$

where τ_T and τ_Δ are the lifetimes of ^{3}PS and $^1O_2$, respectively; K_1 and K_2 reflect the concentration of ^{3}PS and $^1O_2$ formed by the laser pulse and their values depend on the laser energy used in each particular experiment. Thus, the phosphorescence of ^{3}PS is expected to decay monotonically while that of $^1O_2$ is expected to rise and decay. It is worth noting that due to the sign of the pre-exponential term in *Eq. 3*, the signals at 1280 nm rise with the shortest of the two lifetimes, τ_T or τ_Δ, and decay with the longest one [39].

In heterogeneous systems, it is often assumed that each site behaves independently, and therefore the observed phosphorescence is the sum of the signals from each site [40]. Assuming this to be valid in our case, we have assigned the observed lifetimes to τ_T and τ_Δ for all experiments. They are collected in table 1.

Analysis of the data in table 1 reveals that both populations of triplet TMPyP molecules are able to produce $^1O_2$, as evidenced by the biexponential growth of the signals in D-PBS suspensions of *E. coli* cells. This is confirmed by the results in spheroplasts and when TMPyP was replaced by MDPyTMPyP, conditions that selectively eliminate the components due to the external and internal PS populations, respectively.

The second observation is that $^1O_2$ decays with a single lifetime, irrespective of the site of formation. This suggests a fast equilibration between internal and external populations of $^1O_2$ prior to its decay [41]. The τ_Δ values are similar to those obtained in aqueous solution (3.5 μs in PBS and 67 μs D-PBS) [42], indicating that, for those $^1O_2$ molecules we can observe, the most important pathway for $^1O_2$ deactivation is through interactions with water, the reactive pathway contribution, leading to cell death [17], being of lesser importance. Of course, the possibility that another fraction of $^1O_2$ molecules reacts with or is quenched by cell components so fast that it does not contribute to the observed signal cannot be excluded.

Table 1: Triplet TMPyP and $^1O_2$ lifetimes (τ_T and τ_Δ, respectively) assigned from the phosphorescence signals observed at 960 nm and 1280 nm.

	960 nm	**1280 nm**
PBS	τ_T = 2.0 μs	τ_T = 2.0 μs τ_Δ = 3.5 μs
D-PBS	τ_T = 2.5 μs	τ_T = 2.5 μs τ_Δ = 64 μs
***E. coli* / PBS**	τ_{T1} = 2.5 μs; τ_{T2} = 20 μs	τ_{T1} = 2.5 μs; τ_{T2} = 20 μs τ_Δ = 3.5 μs
***E. coli* / D-PBS**	τ_{T1} = 2.5 μs; τ_{T2} = 20 μs	τ_{T1} = 2.5 μs; τ_{T2} = 20 μs τ_Δ = 66 μs
***E. coli* / D-PBS + BSA 0.75 mM**	τ_{T1} = 3.0 μs; τ_{T2} = 20 μs	τ_{T1} = 3.0 μs; τ_{T2} = 20 μs τ_Δ = 3.0 μs
***E. coli* spheroplasts / D-PBS**	τ_T = 20 μs	τ_T = 20 μs τ_Δ = 69 μs
***E. coli* spheroplasts / D-PBS + BSA 0.75 mM**	τ_T = 22 μs	τ_T = 22 μs τ_Δ = 2.0 μs
MDPyTMPyP / *E.coli* / D-PBS	–	τ_T = 3.0 μs τ_Δ = 69 μs

A consequence of the previous observation is that $^1O_2$ must be able to cross the cell wall. This is deduced from the BSA quenching experiments: in spheroplasts, the lifetime of $^1O_2$ produced inside the cell decreases when BSA is added to external aqueous buffer. Thus, $^1O_2$ can at least cross the inner membrane. In intact cells, $^1O_2$ is unequivocally produced both inside and outside. The facts that in this situation (1) there is a single decay lifetime for $^1O_2$ and that (2) in the presence of the external quencher BSA this lifetime decreases, imply that the inner population is able to cross the cell wall prior to its decay. Should this not be the case, we would see independent decay kinetics for the inner and outer populations. The relevance of this conclusion is that it provides direct evidence for the observation that the PS does not need to be internalized for inflicting photodamage on vital structures of the cell [43], strengthening the view that APDT is not likely to develop resistance in microorganisms, as the typical bacterial responses to antibiotics, e.g., enhanced drug metabolism, changes in the drug binding sites, efflux pumps, etc., cannot counteract the singlet oxygen mobility.

5.5. CONCLUSIONS

An overall mechanistic picture emerges from all observations reported above, namely that after an initial binding to *E. coli* cells driven by electrostatic interactions, TMPyP is partially internalized into the bacterium, where it binds to the nucleic acids (Fig. 6).

Likewise, exposure to visible light induces the formation of $^1O_2$ both inside and outside the cells. Our data demonstrate that $^1O_2$ can cross the cell wall and that the main deactivation mechanism for those molecules is by interactions with water.

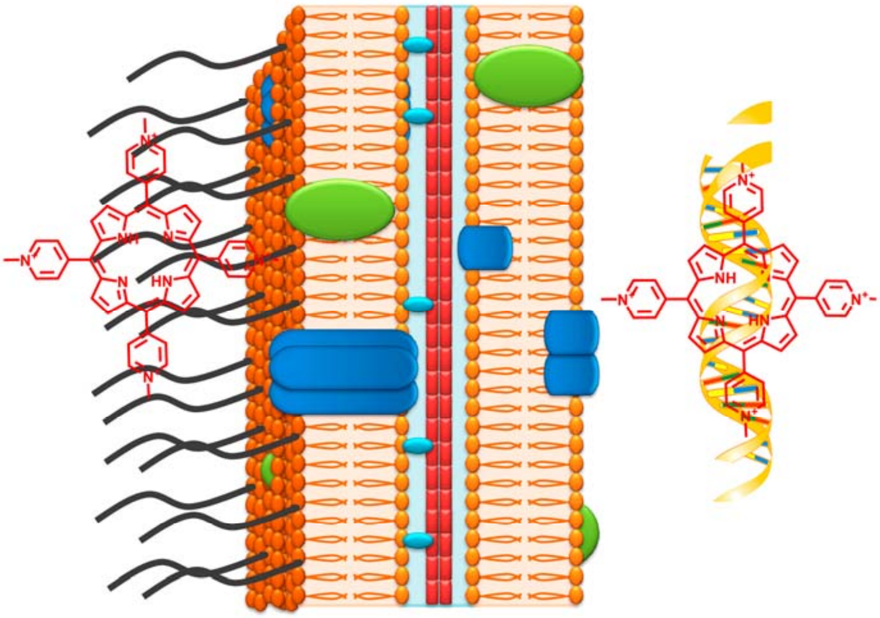

Fig. 6: Pictorial representation of the dual localization of TMPyP in *E. coli*.

5.6. REFERENCES

1. Lin LL, Hanson CV, Alter HJ, Jauvin V, Bernard KA, Murthy KK, Metzel P, and Corash L. Inactivation of viruses in platelet concentrates by photochemical treatment with amotosalen and long-wavelength ultraviolet light. *Transfusion* **2005**; 45: 580-590.

2. Teichert MC, Jones JW, Usacheva MN, and Biel MA. Treatment of oral candidiasis with methylene blue-mediated photodynamic therapy in an immunodeficient murine model. *Oral Surg Oral Med Oral Pathol Oral Radiol Endodon* **2002**; 93: 155-160.

3. Smetana Z, Ben-Hur E, Mendelson E, Salzberg S, Wagner P, and Malik Z. Herpes simplex virus proteins are damaged following photodynamic inactivation with phthalocyanines. *J Photochem Photobiol B:Biol* **1998**; 44: 77-83.

4. Gardlo K, Horska Z, Enk CD, Rauch L, Megahed M, Ruzicka T, and Fritsch C. Treatment of cutaneous leishmaniasis by photodynamic therapy. *J Am Acad Dermatol* **2003**; 48: 893-896.

5. Zheng X, Sallum UW, Verma S, Athar H, Evans CL, and Hasan T. Exploiting a bacterial drug-resistance mechanism: a light-activated construct for the destruction of MRSA. *Angew Chem Int Ed Engl* **2009**; 48: 2148-2151.

6. Tseng SP, Teng LJ, Chen CT, Lo TH, Hung WC, Chen HJ, Hsueh PR, and Tsai JC. Toluidine blue O photodynamic inactivation on multidrug-resistant *Pseudomonas aeruginosa*. *Lasers Surg Med* **2009**; 41: 391-397.

7. Grinholc M, Szramka B, Olender K, and Graczyk A. Bactericidal effect of photodynamic therapy against methicillin-resistant *Staphylococcus aureus* strain with the use of various porphyrin photosensitizers. *Acta Biochim Pol* **2007**; 54: 665-670.

8. Dai TH, Tegos GP, Lu ZS, Huang LY, Zhiyentayev T, Franklin MJ, Baer DG, and Hamblin MR. Photodynamic therapy for *Acinetobacter baumannii* burn infections in mice. *Antimicrob Agents Chemother* **2009**; 53: 3929-3934.

9. Bonnett R. Chemical Aspects of Photodynamic Therapy, Gordon and Breach Science Publishers, Amsterdam, **2000**.

10. Michaeli A and Feitelson J. Reactivity of singlet oxygen toward amino acids and peptides. *Photochem Photobiol* **1994**; 59: 284-289.

11. Stark G. Functional consequences of oxidative membrane damage. *J Membr Biol* **2005**; 205: 1-16.

12. Ravanat JL, Di Mascio P, Martinez GR, Medeiros MHG, and Cadet J. Singlet oxygen induces oxidation of cellular DNA. *J Biol Chem* **2000**; 275: 40601-40604.

13. Spesia MB, Caminos DA, Pons P, and Durantini EN. Mechanistic insight of the photodynamic inactivation of *Escherichia coli* by a tetracationic zinc(II) phthalocyanine derivative. *Photodiagn Photodyn Ther* **2009**; 6: 52-61.

14. Giuliani F, Martinelli M, Cocchi A, Arbia D, Fantetti L, and Roncucci G. *In vitro* resistance selection studies of RLP068/Cl, a new Zn(II)phthalocyanine suitable for antimicrobial photodynamic therapy (APDT). *Antimicrob Agents Chemother* **2010**; 54: 637-42.

15. Wainwright M. Photoantimicrobials--so what's stopping us? *Photodiagn Photodyn Ther* **2009**; 6: 167-169.

16. Stockert JC, Juarranz A, Villanueva A, Nonell S, Horobin RW, Soltermann AT, Durantini EN, Rivarola V, Colombo LL, Espada J, and Cañete M. Photodynamic therapy: selective uptake by photosensitising drugs into tumor cells. *Curr Top Pharmacol* **2004**; 8: 185-217.

17. Ergaieg K, Chevanne M, Cillard J, and Seux R. Involvement of both type I and type II mechanisms in gram-positive and gram-negative bacteria photosensitization by a meso-substituted cationic porphyrin. *Sol Energy* **2008**; 82: 1107-1117.

18. Schweitzer C and Schmidt R. Physical mechanisms of generation and deactivation of singlet oxygen. *Chem Rev* **2003**; 103: 1685-1757.

19. Jimenez-Banzo A, Sagrista ML, Mora M, and Nonell S. Kinetics of singlet oxygen photosensitization in human skin fibroblasts. *Free Rad Biol Med* **2008**; 44: 1926-1934.

20. Snyder JW, Skovsen E, Lambert JDC, and Ogilby PR. Subcellular, time-resolved studies of singlet oxygen in single cells. *J Am Chem Soc* **2005**; 127: 14558-14559.

21. Maisch T, Baier J, Franz B, Maier M, Landthaler M, Szeimies RM, and Baumler W. The role of singlet oxygen and oxygen concentration in photodynamic inactivation of bacteria. *Proc Nat Acad Sci USA* **2007**; 104: 7223-7228.

22. Hamblin MR and Hasan T. Photodynamic therapy: a new antimicrobial approach to infectious disease? *Photochem Photobiol Sci* **2004**; 3: 436-450.

23. Jori G, Fabris C, Soncin M, Ferro S, Coppellotti O, Dei D, Fantetti L, Chiti G, and Roncucci G. Photodynamic therapy in the treatment of microbial infections: Basic principles and perspective applications. *Lasers Surg Med* **2006**; 38: 468-481.

24. Wilson M and Yianni C. Killing of methicillin-resistant *Staphylococcus aureus* by low-power laser-light. *J Med Microbiol* **1995**; 42: 62-66.

25. Minnock A, Vernon DI, Schofield J, Griffiths J, Parish JH, and Brown SB. Photoinactivation of bacteria. Use of a cationic water-soluble zinc phthalocyanine to photoinactivate both gram-negative and gram-positive bacteria. *J Photochem Photobiol B:Biol* **1996**; 32: 159-164.

26. Chirvony VS. Primary photoprocesses in cationic 5,10,15,20-meso-tetrakis(4-*N*-methylpyridiniumyl)porphyrin and its transition metal complexes bound with nucleic acids. *J Porphyrins Phthalocyanines* **2003**; 7: 766-774.

27. Reddi E, Ceccon M, Valduga G, Jori G, Bommer JC, Elisei F, Latterini L, and Mazzucato U. Photophysical properties and antibacterial activity of meso-substituted cationic porphyrins. *Photochem Photobiol* **2002**; 75: 462-470.

28. Kuimova MK, Botchway SW, Parker AW, Balaz M, Collins HA, Anderson HL, Suhling K, and Ogilby PR. Imaging intracellular viscosity of a single cell during photoinduced cell death. *Nat Chem* **2009**; 1: 69-73.

29. Schlothauer J, Hackbarth S, and Roder B. A new benchmark for time-resolved detection of singlet oxygen luminescence - revealing the evolution of lifetime in living cells with low dose illumination. *Laser Phys Lett* **2009**; 6: 216-221.

30. Salmon-Divon M, Nitzan Y, and Malik Z. Mechanistic aspects of *Escherichia coli* photodynamic inactivation by cationic tetra-meso(*N*-methylpyridyl)porphine. *Photochem Photobiol Sci* **2004**; 3: 423-429.

31. Caminos DA, Spesia MB, and Durantini EN. Photodynamic inactivation of *Escherichia coli* by novel meso-substituted porphyrins by 4-(3-*N,N,N*-

trimethylammoniumpropoxy)phenyl and 4-(trifluoromethyl)phenyl groups. *Photochem Photobiol Sci* **2006**; 5: 56-65.

32. Hamblin MR, O'Donnell DA, Murthy N, Rajagopalan K, Michaud N, Sherwood ME, and Hasan T. Polycationic photosensitizer conjugates: effects of chain length and Gram classification on the photodynamic inactivation of bacteria. *J Antimicrob Chemother* **2002**; 49: 941-951.

33. Verma S, Sallum UW, Athar H, Rosenblum L, Foley JW, and Hasan T. Antimicrobial photodynamic efficacy of side-chain functionalized benzo[a]phenothiazinium dyes. *Photochem Photobiol* **2009**; 85: 111-118.

34. Lee S, Lee YA, Lee HM, Lee JY, Kim DH, and Kim SK. Rotation of periphery methylpyridine of meso-tetrakis(n-*N*-methylpyridiniumyl)porphyrin (n=2, 3, 4) and its selective binding to native and synthetic DNAs. *Biophys J* **2002**; 83: 371-381.

35. De Paoli VM, De Paoli SH, Borissevitch LE, and Tedesco AC. Fluorescence lifetime and quantum yield of $TMPyPH_2$ associated with micelles and DNA. *J Alloys Compd* **2002**; 344: 27-31.

36. Lang K, Mosinger J, and Wagnerova DM. Photophysical properties of porphyrinoid sensitizers non-covalently bound to host molecules; models for photodynamic therapy. *Coord Chem Rev* **2004**; 248: 321-350.

37. Vergeldt FJ, Koehorst RBM, Vanhoek A, and Schaafsma TJ. Intramolecular interactions in the ground and excited-state of tetrakis(*N*-methylpyridyl)porphyrins. *J Phys Chem* **1995**; 99: 4397-4405.

38. Kruk NN, Shishporenok SI, Korotky AA, Galievsky VA, Chirvony VS, and Turpin P-Y. Binding of the cationic 5,10,15,20-tetrakis(4-*N*-methylpyridyl)porphyrin at 5'CG3' and 5'GC3' sequences of hexadeoxyribonucleotides: triplet-triplet transient absorption, steady-state and time-resolved fluorescence and resonance Raman studies. *J Photochem Photobiol B:Biol* **1998**; 45: 67-74.

39. Parker JG and Stanbro WD. Dependence of photosensitized singlet oxygen production on porphyrin structure and solvent. In: Doiron DR, Gomer CJ (Eds.), Porphyrin localization and treatment of tumors. New York: Alan R. Liss. **1984**: 259-284.

40. Niedre M, Patterson MS, and Wilson BC. Direct near-infrared luminiscence detection of singlet oxygen generated by photodynamic therapy in cells *in vitro* and tissues *in vivo*. *Photochem Photobiol* **2002**; 75: 382-391.

41. Lee PC and Rodgers MAJ. Singlet molecular-oxygen in micellar systems: distribution equilibria between hydrophobic and hydrophilic compartments. *J Phys Chem* **1983**; 87: 4894-4898.

42. Rodgers MAJ. Solvent-induced deactivation of singlet oxygen: additivity relationships in nonaromatic solvents. *J Am Chem Soc* **1983**; 105: 6201-6205.

43. Dahl TA, Midden WR, and Hartman PE. Pure singlet oxygen cytotoxicity for bacteria. *Photochem Photobiol* **1987**; 46: 345-352.

Chapter 6

Mechanistic aspects of antimicrobial photodynamic therapy in *E. coli*: Photosensitiser-dependent singlet oxygen formation and decay.

Many different families of photosensitisers, with distinct physical and photochemical properties, have been used in antimicrobial photodynamic therapy. These differences can lead to different kinetics of singlet oxygen production and decay when the PS is taken up by bacterial cells. It is therefore intriguing to study the mechanism of those PSs against gram-negative bacteria to better understand the structure-activity relationship of the different families of PSs.

The work described in this chapter will be submitted for publication. Manuscript in preparation.

6.1. INTRODUCTION

Antimicrobial photodynamic therapy (APDT) [1] has been shown as a viable alternative to antibiotics against microbial pathogens, even those whom have developed resistance [2,3]. Briefly, the combination of a drug, usually called photosensitiser (PS), light and molecular oxygen leads to the production of reactive oxygen species (ROS), *via* electron or energy transfer (type I or type II reaction, respectively) from the triplet excited-state of the PS to molecular oxygen [4].

Many different PSs have been used over the years in APDT as antimicrobial agents [5,6]. Nowadays, the most typical ones are those cationic at physiological pH, such as phenothiazines, porphyrins and phthalocyanines [7-9]. These PSs exhibit a higher affinity than conventional PSs used in photodynamic therapy against microbial cells, especially against gram-negative bacteria, due to the negative net charge found in the microbial cell wall [10-12].

In the previous chapter we reported how, by means of a combination of spectroscopic and time-resolved photophysical techniques, it is possible to understand where the PS localizes and how singlet oxygen ($^1O_2$), one of the species that plays a major role in APDT [13], react with the nearest environment. In that case, tetra-*N*-methylpyridylporphyrin (TMPyP) was used as a model, demonstrating a double localization both inside and outside the cell, and the ability of $^1O_2$ to cross the cell wall and react with the external aqueous media [14].

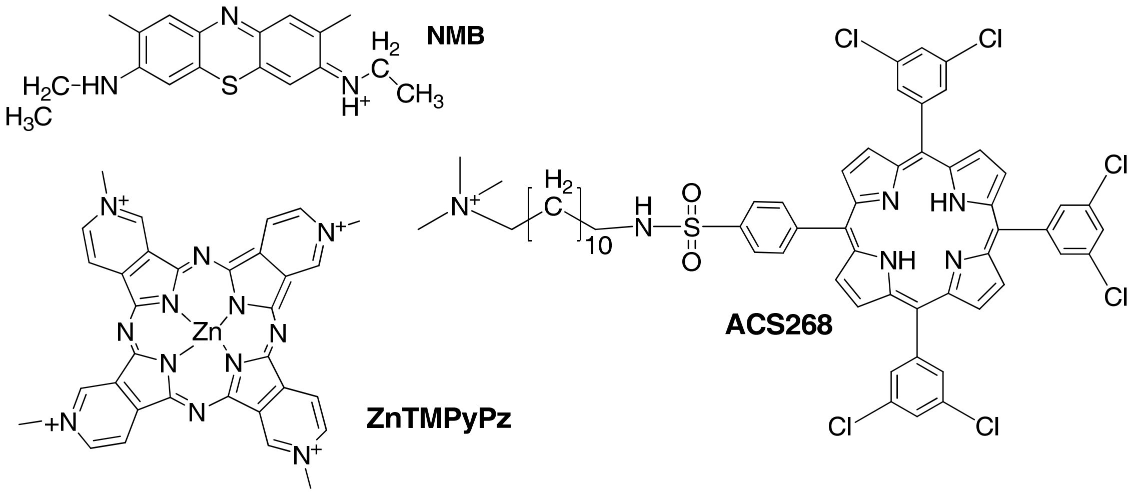

Fig. 1: Chemical structures of the photosensitisers used in the study.

Thus, in this paper we report the differences in the kinetics of $^1O_2$ production and decay in *Escherichia coli* upon photosensitisation with different cationic PSs chosen as representative members of the aforementioned families, *i.e.*, new methylene blue (NMB) as a phenothiazine, a hydrophobic porphyrin with a cationic alkyl chain (ACS268), and a tetracationic zinc(II) pyridoporphyrazine (ZnTMPyPz) (Fig. 1). These compounds are efficient antimicrobial photodynamic agents *in vitro* [15,16].

Notwithstanding the cationic charges, each PS possesses different physical and photophysical properties [6]. These variations should likely lead to a different PS localization and therefore, to a different microenvironment. It may be therefore insightful to study the details of $^1O_2$ photosensitisation by different PSs to better understand the structure-activity relationship of different families of PS.

6.2. EXPERIMENTAL SECTION

Chemicals

New methylene Blue (NMB) was supplied by Sigma-Aldrich Co. (St. Louis, MO, USA). Zinc-tetramethyltetrapyridino[3,4-b: 39,49-g: 30,40-l: 3-,4-q]porphyrazinium salt (ZnTMPyPz) was synthesised as described by Marti *et al.* [17].

5,10,15-tris(2,6-dichlorophenyl)-20-[*N*-(12-trimethyl ammonium chloride)-dodecyl-*p*-sulphonamidophenyl]porphyrin (ACS268) was synthesised by means of the procedure described in the *Annex*. Deuterium oxide (>99.9%) and dimethylformamide were purchased from Solvents Documentation Synthesis (Peypin, France). Bovine serum albumin (98%), lysozyme, sodium dodecyl sulphate (SDS), trizma, and Dubelcco's phosphate buffered saline (PBS) were purchased from Sigma-Aldrich Co. Saccarose and ethylendiamine tetraacetic acid (EDTA) were supplied by Panreac S.A. (Barcelona, Spain).

Deuterated PBS (D-PBS) was prepared by dissolving PBS powder in deuterium oxide.

Control experiments

Controls were performed to unmistakably ascertain the origin of the luminescence signals, the light doses and the identification of $^1O_2$ as the emissive species (see *results section, Chapter 5*) for all the experiments in bacterial suspensions and all the PSs.

6.3. RESULTS

PSs binding to *E. coli*

The uptake of NMB and ACS268 was studied by means of its fluorescence in cell lysates obtained by treatment with NaOH 0.1 M / 1 % sodium dodecyl sulphate (SDS). Bulk concentrations of 10 μM and 7.5 μM were used, respectively. While the uptake of ACS268 reaches a plateau value after only 1 h, the uptake of NMB requires *ca.* 20 h for completion (Fig. 2). For ZnTMPyPz we adopted the uptake conditions described by Dupouy *et al.* [18], namely 30 min contact time at 37 ºC and 10 μM bulk concentration.

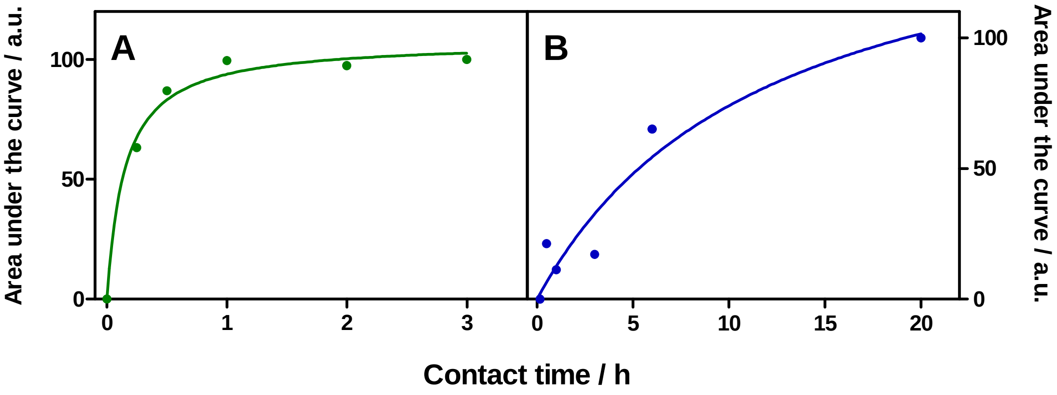

Fig. 2: Binding to *E. coli* of **(A)** NMB and **(B)** ACS268, with a bulk concentration of 10 μM and 7.5 μM, respectively.

It was critical in our experiments to eliminate any PS molecule from the external aqueous buffer in order to ensure that all the spectroscopic data was produced by cell-bound molecules. Therefore, to unmistakably assign the spectroscopic data, the external aqueous solutions were routinely tested before and after the *in vitro* measurements, providing no significant signal in all cases.

Thus, regarding the absorption and fluorescence emission of the PSs bound to *E. coli*, the absorption spectrum of NMB showed a bathochromic shift of 8 nm relative to that in the buffer (Fig. 3A), as well as a slight change in the monomer-dimer band ratio. However, no significant change was observed in the fluorescence emission spectrum (Fig. 3B). For ZnTMPyPz, the absorption spectra both in *E. coli* and buffer showed a similar structureless broad-band distinct from the spectrum obtained in DMF, where it is in a monomeric form (Fig. 3C). A 5 nm bathochromic shift was observed in the fluorescence spectrum relative to that in DMF (Fig. 3D). For ACS268, the absorption spectrum in *E. coli* showed a 7 nm bathochromic shift relative to that in buffer (Fig. 3E).

The fluorescence spectra in *E. coli* and buffer showed similar structures but with a 5 nm bathochromic shift (Fig. 3F).

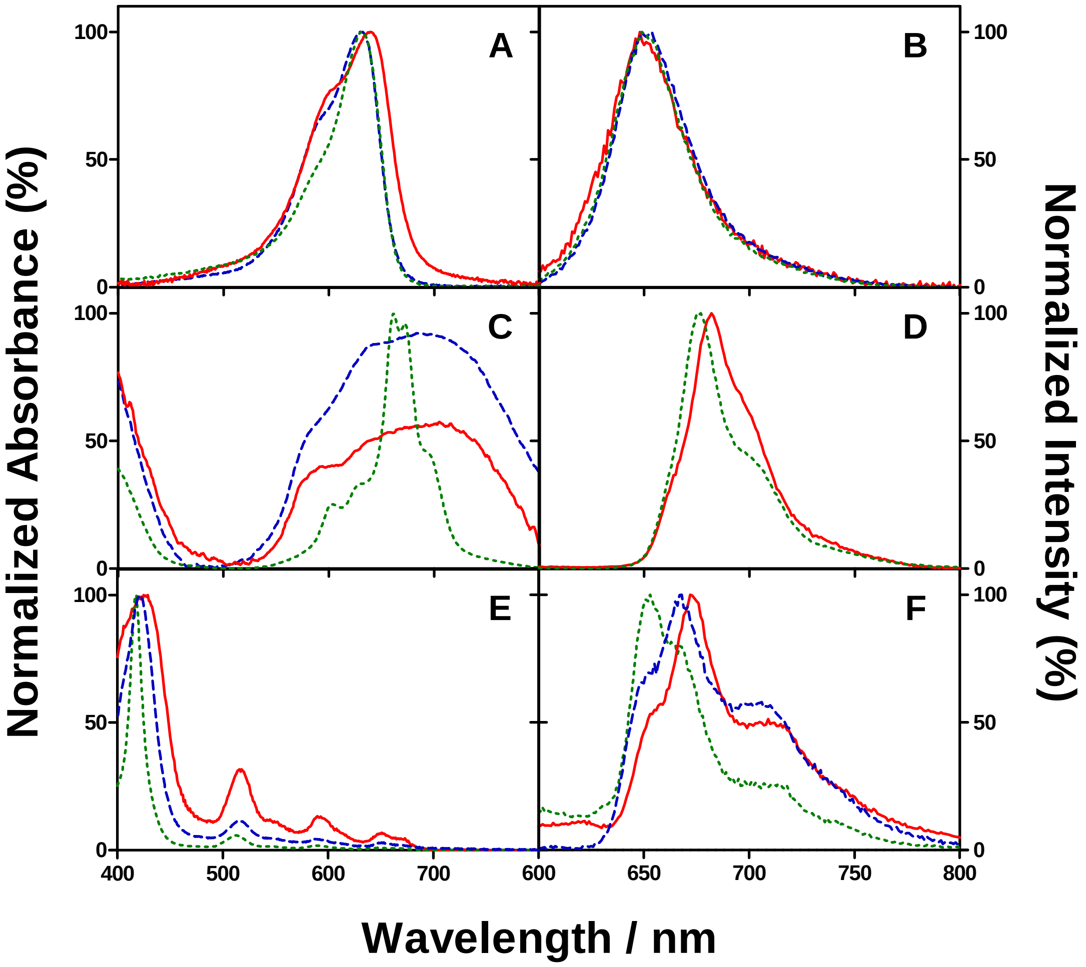

Fig. 3: (A,C,E) Absorption and **(B,D,F)** fluorescence spectra of: **(A,B)** New methylene blue in *E. coli* (solid line), PBS (dashed line), 1% SDS in 0.1 M NaOH (dotted line). **(C,D)** ZnTMPyPz in *E. coli* (solid line), PBS (dashed line), DMF (dotted line). **(E,F)** ACS268 in *E. coli* (solid line), PBS (dashed line), DMF (dotted line).

Time-resolved fluorescence measurements provided additional insight on the uptake of the PSs (Fig. 4). The fluorescence kinetics of NMB at 657 nm decayed monoexponentially with a lifetime of 0.5 ± 0.1 ns both in *E. coli* and in buffer. For ZnTMPyPz, the time-resolved fluorescence measurement in *E. coli* at 675 nm required only one exponential term with lifetime 2.8 ± 0.5 ns. An additional exponential term was necessary in buffer with a lifetime of 0.5 ± 0.1 ns, respectively. Time-resolved fluorescence of ACS268 was inconclusive as the kinetics in solution were too complex to extract any conclusion.

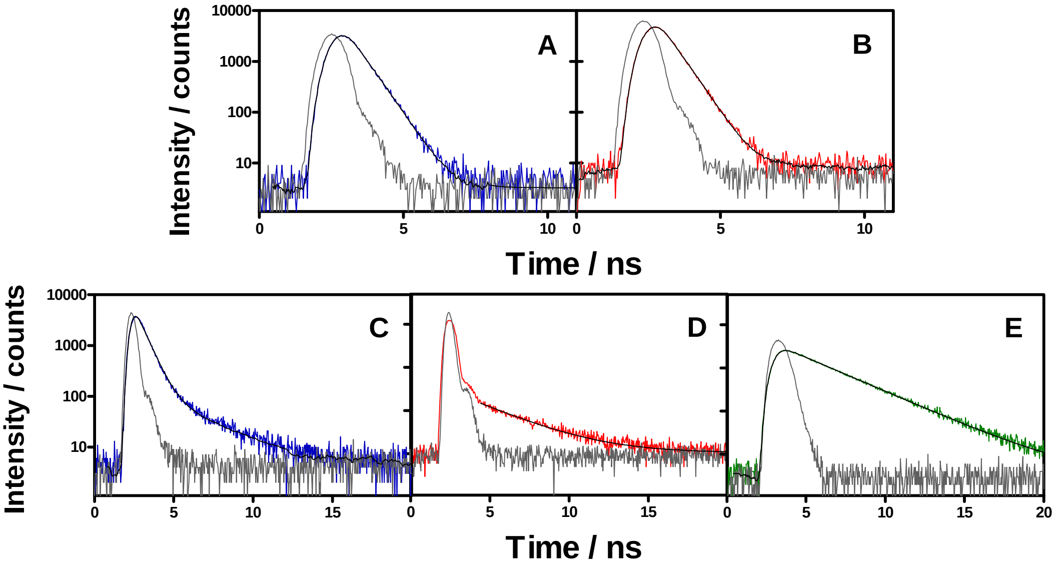

Fig. 4: Time-resolved fluorescence decay of **(A,B)** NMB at 657 nm and **(C,D,E)** ZnTMPyPz at 675 nm upon excitation at 596 nm. Signal, instrument response function, and fit in **(A,C)** PBS at pH 7.4, **(B,D)** *E. coli,* and **(E)** DMF.

Singlet oxygen kinetics in *E. coli* cells with NMB as PS

Pulsed-laser irradiation of NMB-loaded *E. coli* cells (30 min contact time; 10 µM NMB bulk concentration) suspended in buffer at pH 7.4 produced clear time-resolved $^1O_2$ phosphorescence signals at 1270 nm (Fig. 5). The contact time between the NMB solution and the bacteria had no effect on $^1O_2$ luminescence kinetics. In PBS, the signals grew with a lifetime τ_1^{PBS} = 2.5 ± 1 µs, and decayed monoexponentially with a lifetime τ_2^{PBS} = 3.7 ± 1 µs. In deuterated-PBS (D-PBS), the signal rise remained unchanged with a lifetime $\tau_1^{D\text{-}PBS}$ = 2.5 ± 1 µs, but it decayed more slowly, with a lifetime $\tau_2^{D\text{-}PBS}$ = 65 ± 2 µs. Addition of 0.75 mM bovine serum albumin (BSA), a $^1O_2$ quencher that is not able to cross the cell wall due to its size [19], clearly modified the signal: the rise of phosphorescence was now complete within the time resolution of our set-up, and the decay was also faster with lifetime τ_1^{BSA} = 7.0 ± 1 µs. Saturation of this suspension with oxygen led to a further decrease of the decay lifetime to $\tau_1^{BSA,O2}$ = 3.5 ± 1 µs. Finally, measurements in *E. coli* spheroplasts, *i.e.*, bacteria from which the cell wall had been almost completely removed, led to a 4-fold decrease in the $^1O_2$ phosphorescence signal intensity, but with the same kinetics as in intact cells.

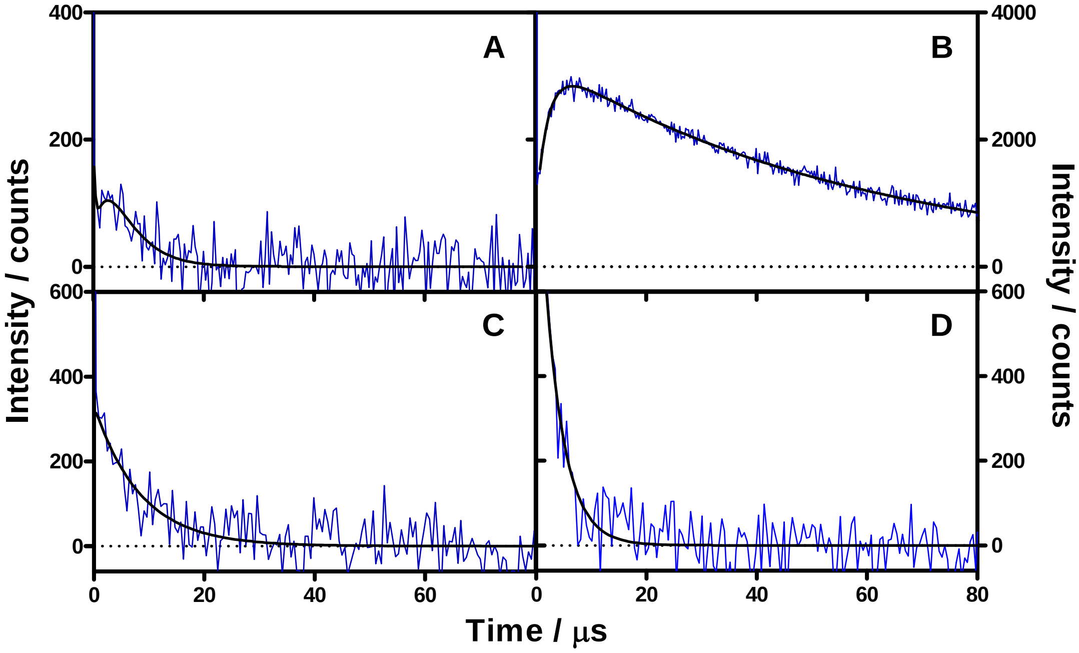

Fig. 5: Medium effects on the NMB-photosensitised singlet oxygen phosphorescence at 1270 nm in *E. coli*: **(A)** Air-saturated PBS. **(B)** Air-saturated D-PBS. **(C)** Air-saturated D-PBS with 0.75 mM BSA added. **(D)** Oxygen-saturated D-PBS with 0.75 mM BSA added.

Singlet oxygen kinetics in *E. coli* cells with ZnTMPyPz as PS

Although ZnTMPyPz is a potent $^1O_2$ photosensitiser in solution [17], irradiation of ZnTMPyPz-loaded *E. coli* cells suspended in D-PBS did not produce any clear time-resolved $^1O_2$ phosphorescence signal at 1270 nm (Fig. 6). Neither a higher contact time of ZnTMPyP (3h), nor a higher acquisition time of the $^1O_2$ phosphorescence signal (12 million laser pulses) produced any detectable signal.

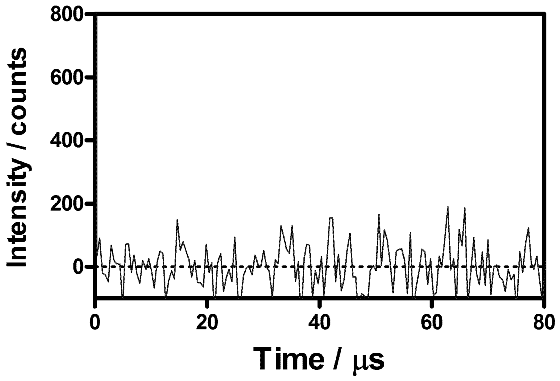

Fig. 6: Singlet oxygen phosphorescence at 1270 nm using ZnTMPyPz as photosensitiser in *E. coli* cells suspended in D-PBS.

Singlet oxygen kinetics in *E. coli* cells with ACS268 as PS

The quantum yield of singlet oxygen production (Φ_Δ) of ACS268 was measured in two different solvents, DMF and D_2O, by comparison of the signal produced by optically-matched solutions of reference PSs (phenalenone and TMPyP) [20] with that produced by ACS268. Thus, Φ_Δ values of 0.87±0.01 and 0.04±0.01 were determined in DMF and D_2O, respectively. Irradiation of ACS268-loaded *E. coli* cells produced time-resolved $^1O_2$ phosphorescence signals clearly different from those observed for NMB (Fig. 8). In PBS, the signals grew with a lifetime τ_1^{PBS} = 2.1 ± 1 μs, and decayed biexponentially with lifetimes τ_2^{PBS} = 8.6 ± 1 μs and τ_3^{PBS} = 34.1 ± 1 μs. In D-PBS, the rise of the signal was slightly slower, $\tau_1^{D\text{-}PBS}$ = 5.2 ± 1 μs, but the decay kinetics remained unchanged biexponential. Addition of 0.75 mM of BSA shortened only the slowest decay lifetime, *i.e* , τ_2^{BSA} = 8.6 ± 1 μs and τ_3^{BSA} = 34.0 ± 1 μs. Finally, measurements in *E. coli* spheroplasts led to a 3-fold decrease in the $^1O_2$ phosphorescence signal intensity, but with the same kinetics as in intact cells.

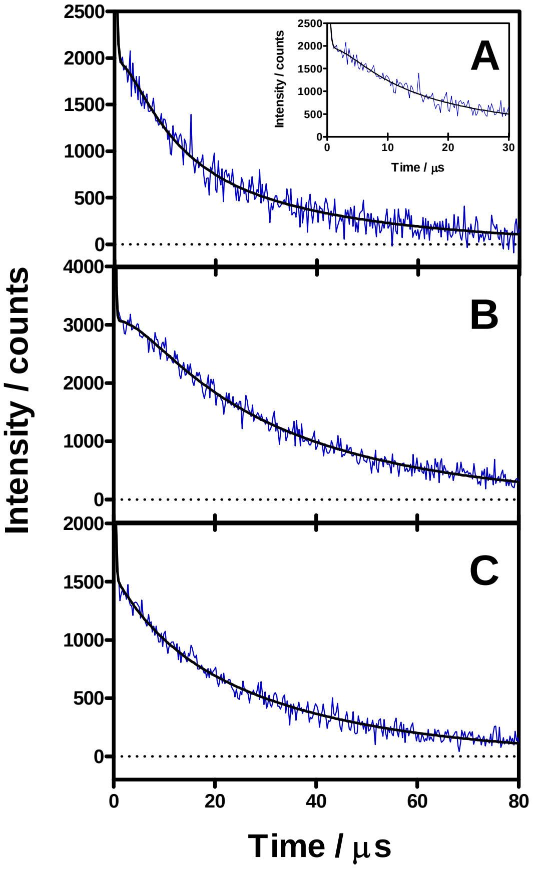

Fig. 7: Medium effect on the ACS268-photosensitised singlet oxygen phosphorescence at 1270 nm in *E. coli* cells suspended in: **(A)** PBS. Inset: Zoom of the first 30 μs , **(B)** D-PBS, **(C)** D-PBS + 0.75 mM BSA .

6.4. DISCUSSION

The main goal of this study was to seek insight into the kinetics of $^1O_2$ production and decay, thereby shedding light on the mechanism of photodynamic inactivation of gram-negative bacteria. Specifically, we were interested to learn whether representative members of three different families of photosensitisers would provide different photosensitisation kinetics.

Towards this goal, it was first essential to obtain unambiguous time-resolved $^1O_2$ phosphorescence signals from viable cells, *i.e.*, (1) to reduce to a minimum the acquisition time as the $^1O_2$ kinetics in cells changes with increasing light exposure [21,22], and (2) to identify the optimal concentration and contact time of each PS for efficient cell binding/uptake. A concentration *ca.* 10 μM, similar to the ones used in inactivation experiments for *E. coli* [18,23], and a 30 min contact time, typical in APDT [24,25], proved adequate in this respect notwithstanding the higher amount of NMB taken up at longer contact times (Fig. 2). It has been reported that, under similar experimental conditions, all these PSs do not show significant dark toxicity [18,26].

Regarding the phenothiazine group, NMB was chosen as the model due to its highest singlet oxygen quantum yield and higher hydrophobicity [27], as well as its ability to properly inactivate many bacterial species [27]. Two major changes can be observed in the absorption spectrum of NMB upon binding to *E. coli*: on one hand, the relative contribution of the dimer's band at 600 nm increases, which is consistent with the report by Usacheva *et al.* that phenothiazium dyes tend to dimerize in the presence of bacteria [28]. On the other, the monomer's band maximum shows a slight bathochromic shift that reveals a change in the NMB's microenvironment [29]. Somewhat surprisingly, such microenvironmental changes have no effect on the fluorescence spectrum, nor in the fluorescence lifetime. The fact that there is no change in the fluorescence lifetime indicates that despite the different microenvironment, NMB is still surrounded by water molecules (see *Annex*). This conclusion is supported by the $^1O_2$ phosphorescence formation and decay kinetics. Both in PBS and D-PBS, the lifetimes obtained for the $^1O_2$ phosphorescence signal matched those obtained in neat H_2O or D_2O, a 2.5 μs rise component assigned to the triplet lifetime of NMB, and a 3.7 or 65 μs component due to $^1O_2$. This indicates that NMB is localised in an aqueous-like environment and that $^1O_2$ is deactivated mainly by interactions with H_2O or D_2O [30]. Of course, it cannot be excluded that another fraction of $^1O_2$ molecules reacts with or is quenched by cell components so rapidly that it does not contribute to the observed signal. Care was taken to ensure that the signals did not originate on NMB molecules that has leaked into the bulk solution during the experiments. The supernatant solution was checked before and after the experiments and in all cases we could find no signal. Addition of BSA to the D_2O suspensions significantly changed the signal kinetics, causing both a faster rise (< 1 μs) and a faster decay (lifetime of 7 μs) in air-saturated suspensions. The latter component was decreased further to 3.5 μs upon bubbling with oxygen. These results suggest a dual effect of BSA: on one hand it quenches $^1O_2$ as one would expect [19] decreasing its lifetime below the time resolution of our setup; on the other, it interacts with NMB shielding it from oxygen [31], which effectively increases the triplet lifetime from 2.5 μs to 7 μs (in air) or 3.5 μs (under oxygen). Therefore, NMB must be located somewhere in the external structure of the cell wall, accessible to BSA, or must be able to relocate and bind to BSA upon its addition to the solution. This conclusion is consistent with Usacheva's *et al.* report that phenothiazinium dyes interact with the outer-wall bacterial lipopolisaccharides (LPS) [32,33].

Concerning the phthalocyanine family, ZnTMPyPz was chosen as a model since Dupouy *et al.* [18] had shown that, using the same uptake conditions as in this work, irradiation with visible light reduced the cell viability by 99.5%. These results can now be rationalised in the light of our findings.

First, as observed in the absorption spectrum, ZnTMPyPz is largely aggregated in *E. coli*. This aggregation would explain why no signal is observed in the $^1O_2$ luminescence experiments under conditions similar to those used for the other PSs, even increasing the contact time and the acquisition time. Spesia *et al.* showed that alterations in the cell membrane appear to be the major cause of *E. coli* inactivation upon APDT with visible light and a tetracationic zinc(II) phthalocyanine derivative ($ZnPc^{4+}$) [34]. Assuming that (1) ZnTMPyPz and $ZnPc^{4+}$ localize in a similar microenvironment because of the huge structural similarity, and that (2) ZnTMPyPz is basically aggregated like in an aqueous media, as observed by the absorption spectrum and the absence of $^1O_2$ luminescence signal, a localization to the outer structure of the cell wall, comparable to the one obtained with NMB, is tentatively attributed. This conclusion is not contradictory to the 99.5% reduction in cell viability, as there is still a small quantity of monomer, detectable by time-resolved fluorescence measurements, responsible of the production of ROS and the resulting photodynamic effect shown by ZnTMPyPz.

As to the porphyrin's family, we previously demonstrated that a tetracationic porphyrin such as TMPyP, with the cationic charges peripherically-distributed, localizes in *E. coli* at two different sites: (1) externally bound to the cell wall, probably in a similar localization as NMB and ZnTMPyPz, and (2) inside the cell, bound to the nucleic acids [14]. We hypothesize that ACS268, which has a unique cationic charge in the alkyl chain, would localize in a completely different environment than those of TMPyP, as the cationic charge is far away from the photoactive core and the lipophilicity/hydrophilicity of the molecule is completely different. The Φ_Δ values in DMF and D_2O clearly demonstrate that only when ACS268 is on its monomeric form, it is able to produce $^1O_2$.

Both the spectroscopic measurements and the $^1O_2$ phosphorescence in *E. coli* are in agreement with the aforementioned hypothesis. The bathochromic shift observed in the absorption and fluorescence spectra in *E. coli* indicates a different environment surrounding the PS relative to that in solution [29,35,36]. As for the triplet-excited state of ACS268, two components with lifetimes 8.6 μs and 34 μs are observed in the $^1O_2$ phosphorescence experiments in PBS, D-PBS and upon addition of BSA. These different lifetimes may indicate two different localizations, both clearly shielded from oxygen. Indeed, the results in spheroplasts indicate that ACS268 must be located somewhere in the external membrane of the cell wall. As regards to $^1O_2$, the τ_Δ values in *E. coli* are significantly lower (2.1 μs in PBS; 5.2 μs in D-PBS) than the ones observed in buffer (3.5 μs in PBS; 67 μs in D-PBS) [30] indicating a new competitive process of deactivation of $^1O_2$ within the cell, namely an immediate reaction of the produced $^1O_2$ with quenchers surrounding the PS molecule.

The rate constant of $^1O_2$ decay in microheterogeneous systems under exchange equilibrium conditions, k_d, is described by *Eq. 1* [37]:

$$k_d = \frac{1}{\tau_\Delta} = \frac{K_{eq} \cdot f_m \cdot k_{d,cell} + (1 - f_m) \cdot k_{d,water}}{K_{eq} \cdot f_m + (1 - f_m)} \qquad (1)$$

where $K_{eq} = [^1O_2]_{cell} / [^1O_2]_{water}$ is the partition equilibrium of $^1O_2$ between the two phases, f_m and $(1-f_m)$ are the volume fractions of the cell and aqueous phase, respectively, and $k_{d,cell}$ and $k_{d,water}$ are the decay rate constants inside and outside the cell, respectively. Assuming $K_{eq} \approx 1$ and $f_m \approx 0.0012$ for our suspensions in 5 x 10^8 CFU/mL, the lifetime of $^1O_2$ within the bacterial cell can be estimated as $\tau_{\Delta,cell} \approx 7$ ns, a value that would perfectly correlate with the $^1O_2$ phosphorescence kinetics observed upon addition of BSA.

It has previously been demonstrated that the presence of external proteins clearly modifies the effectiveness of APDT to inactivate microbial cells [38-40]. Such effect can also be observed in the kinetics of $^1O_2$ in the presence of BSA. As observed, the addition of BSA clearly modifies the $^1O_2$ phosphorescence signal produced by NMB, decreasing τ_Δ and increasing τ_T, demonstrating an interaction between NMB and BSA. However, the effect is barely observed when ACS268 is used as a PS, suggesting a deeper localization of ACS268 into the cell wall, leading to a lower accessibility towards the PS molecule and a lower $^1O_2$-quenching effect of BSA.

6.5. CONCLUSIONS

We have demonstrated that, between the different families used in the study, there are significant differences in (1) the microenvironment surrounding the PSs, *i.e.*, in their localization, and (2) the kinetics of production and decay of $^1O_2$.

When bound to *E. coli*, NMB localizes in an aqueous-like microenvironment, accessible to external proteins such as BSA and interacting with the LPS in cell-wall, ZnTMPyPz might localize similarly to NMB, where it is almost completely aggregated, and ACS268 localizes in a deeper position of the external structure of the cell wall, namely in the outer membrane, shielded from oxygen as demonstrated with the triplet lifetimes.

With regards to the $^1O_2$ produced by the PSs, $^1O_2$ generated by NMB can move freely within the cell being mainly deactivated by the aqueous phase, while a completely different scenario is observed for ACS268, suggesting that $^1O_2$ cannot escape freely from its primary site of production, and thus partially reacts with proximate cellular components. On the other hand, ZnTMPyPz did not show $^1O_2$-luminescence under conditions similar to those used for the others PSs, correlating with the lower photodynamic inactivation effect observed.

6.6. REFERENCES

1. Jori G, Fabris C, Soncin M, Ferro S, Coppellotti O, Dei D, Fantetti L, Chiti G, and Roncucci G. Photodynamic therapy in the treatment of microbial infections: Basic principles and perspective applications. *Lasers Surg Med* **2006**; 38: 468-481.

2. Wainwright M. Photoantimicrobials--so what's stopping us? *Photodiagn Photodyn Ther* **2009**; 6: 167-169.

3. Dai T, Huang YY, and Hamblin MR. Photodynamic therapy for localized infections--state of the art. *Photodiagnosis Photodyn Ther* **2009**; 6: 170-188.

4. Schweitzer C and Schmidt R. Physical mechanisms of generation and deactivation of singlet oxygen. *Chem Rev* **2003**; 103: 1685-1757.

5. Garland MJ, Cassidy CM, Woolfson D, and Donnelly RF. Designing photosensitizers for photodynamic therapy: strategies, challenges and promising developments. *Fut Med Chem* **2009**; 1: 667-691.

6. Wainwright M. Photodynamic antimicrobial chemotherapy (PACT). *J Antimicrob Chemother* **1998**; 42: 13-28.

7. Romanova NA, Brovko LY, Moore L, Pometun E, Savitsky AP, Ugarova NN, and Griffiths MW. Assessment of photodynamic destruction of *Escherichia coli* O157 : H7 and *Listeria monocytogenes* by using ATP bioluminescence. *Appl Environ Microbiol* **2003**; 69: 6393-6398.

8. Bertoloni G, Rossi F, Valduga G, Jori G, Ali H, and Vanlier JE. Photosensitizing activity of water-soluble and lipid-soluble phthalocyanines on prokaryotic and eukaryotic microbial-cells. *Microbios* **1992**; 71: 33-46.

9. Nitzan Y, Gutterman M, Malik Z, and Ehrenberg B. Inactivation of gram-negative bacteria by photosensitized porphyrins. *Photochem Photobiol* **1992**; 55: 89-96.

10. Minnock A, Vernon DI, Schofield J, Griffiths J, Parish JH, and Brown SB. Photoinactivation of bacteria. Use of a cationic water-soluble zinc phthalocyanine to photoinactivate both gram-negative and gram-positive bacteria. *J Photochem Photobiol B:Biol* **1996**; 32: 159-164.

11. Merchat M, Bertolini G, Giacomini P, Villanueva A, and Jori G. Meso-substituted cationic porphyrins as efficient photosensitizers of gram-positive and gram-negative bacteria. *J Photochem Photobiol B:Biol* **1996**; 32: 153-157.

12. Wainwright M, Phoenix DA, Marland J, Wareing DRA, and Bolton FJ. A study of photobactericidal activity in the phenothiazinium series. *FEMS Immunol Med Microbiol* **1997**; 19: 75-80.

13. Ergaieg K, Chevanne M, Cillard J, and Seux R. Involvement of both type I and type II mechanisms in gram-positive and gram-negative bacteria photosensitization by a meso-substituted cationic porphyrin. *Sol Energy* **2008**; 82: 1107-1117.

14. Ragas X, Agut M, and Nonell S. Singlet oxygen in *E. coli*: new insights for antimicrobial photodynamic therapy. *Free Rad Biol Med* **2010**; 49: 770-776..

15. Peleg AY. Optimizing therapy for *Acinetobacter baumannii*. *Sem Resp Crit Care Med* **2007**; 28: 662-671.

16. Ragàs X, Dai T, Tegos GP, Agut M, Nonell S, and Hamblin MR. Photodynamic inactivation of *Acinetobacter baumannii* using phenothiazinium dyes: *in vitro* and *in vivo* studies. *Lasers Surg Med* **2010**; 42: 384-390.

17. Martí C, Nonell S, Nicolau M, and Torres T. Photophysical properties of neutral and cationic tetrapyridinoporphyrazines. *Photochem Photobiol* **2000**; 71: 53-59.

18. Dupouy EA, Lazzeri D, and Durantini EN. Photodynamic activity of cationic and non-charged Zn(II) tetrapyridinoporphyrazine derivatives: biological consequences in human erythrocytes and *Escherichia coli*. *Photochem Photobiol Sci* **2004**; 3: 992-998.

19. Snyder JW, Skovsen E, Lambert JDC, and Ogilby PR. Subcellular, time-resolved studies of singlet oxygen in single cells. *J Am Chem Soc* **2005**; 127: 14558-14559.

20. Redmond RW and Gamlin JN. A compilation of singlet oxygen yields from biologically relevant molecules. *Photochem Photobiol* **1999**; 70: 391-475.

21. Schlothauer J, Hackbarth S, and Roder B. A new benchmark for time-resolved detection of singlet oxygen luminescence - revealing the evolution of lifetime in living cells with low dose illumination. *Laser Phys Lett* **2009**; 6: 216-221.

22. Kuimova MK, Botchway SW, Parker AW, Balaz M, Collins HA, Anderson HL, Suhling K, and Ogilby PR. Imaging intracellular viscosity of a single cell during photoinduced cell death. *Nat Chem* **2009**; 1: 69-73.

23. Harris F, Chatfield LK, and Phoenix DA. Phenothiazinium based photosensitisers - Photodynamic agents with a multiplicity of cellular targets and clinical applications. *Curr Drug Targets* **2005**; 6: 615-627.

24. Caminos DA, Spesia MB, and Durantini EN. Photodynamic inactivation of *Escherichia coli* by novel meso-substituted porphyrins by 4-(3-*N,N,N*-trimethylammoniumpropoxy)phenyl and 4-(trifluoromethyl)phenyl groups. *Photochem Photobiol Sci* **2006**; 5: 56-65.

25. Hamblin MR, O'Donnell DA, Murthy N, Rajagopalan K, Michaud N, Sherwood ME, and Hasan T. Polycationic photosensitizer conjugates: effects of chain length and Gram classification on the photodynamic inactivation of bacteria. *J Antimicrob Chemother* **2002**; 49: 941-951.

26. Phoenix DA, Sayed Z, Hussain S, Harris F, and Wainwright M. The phototoxicity of phenothiazinium derivatives against *Escherichia coli* and *Staphylococcus aureus*. *FEMS Immunol Med Microbiol* **2003**; 39: 17-22.

27. Phoenix DA and Harris F. Phenothiazinium-based photosensitizers: antibacterials of the future? *Trends Mol Med* **2003**; 9: 283-285.

28. Usacheva MN, Teichert MC, and Biel MA. The role of the methylene blue and toluidine blue monomers and dimers in the photoinactivation of bacteria. *J Photochem Photobiol B:Biol* **2003**; 71: 87-98.

29. Chirvony VS. Primary photoprocesses in cationic 5,10,15,20-meso-tetrakis(4-*N*-methylpyridiniumyl)porphyrin and its transition metal complexes bound with nucleic acids. *J Porphyrins Phthalocyanines* **2003**; 7: 766-774.

30. Michael A.J.Rodgers. Solvent-induced deactivation of singlet oxygen: additivity relationships in nonaromatic solvents. *J Am Chem Soc* **1983**; 105: 6201-6205.

31. Borissevitch IE, Tominaga TT, and Schmitt CC. Photophysical studies on the interaction of two water-soluble porphyrins with bovine serum albumin. Effects upon the porphyrin triplet state characteristics. *J Photochem Photobiol A:Chem* **1998**; 114: 201-207.

32. Usacheva MN, Teichert MC, and Biel MA. The interaction of lipopolysaccharides with phenothiazine dyes. *Lasers Surg Med* **2003**; 33: 311-319.

33. Usacheva MN, Teichert MC, Sievert CE, and Biel MA. Effect of Ca^{2+} on the photobactericidal efficacy of methylene blue and toluidine blue against gram-negative bacteria and the dye affinity for lipopolysaccharides. *Lasers Surg Med* **2006**; 38: 946-954.

34. Spesia MB, Caminos DA, Pons P, and Durantini EN. Mechanistic insight of the photodynamic inactivation of *Escherichia coli* by a tetracationic zinc(II) phthalocyanine derivative. *Photodiagn Photodyn Ther* **2009**; 6: 52-61.

35. Lee S, Lee YA, Lee HM, Lee JY, Kim DH, and Kim SK. Rotation of periphery methylpyridine of meso-tetrakis(n-*N*-methylpyridiniumyl)porphyrin (n=2, 3, 4) and its selective binding to native and synthetic DNAs. *Biophys J* **2002**; 83: 371-381.

36. De Paoli VM, De Paoli SH, Borissevitch LE, and Tedesco AC. Fluorescence lifetime and quantum yield of $TMPyPH_2$ associated with micelles and DNA. *J Alloys Compd* **2002**; 344: 27-31.

37. Lee PC and Rodgers MAJ. Singlet molecular-oxygen in micellar systems: distribution equilibria between hydrophobic and hydrophilic compartments. *J Phys Chem* **1983**; 87: 4894-4898.

38. Wilson M and Pratten J. Lethal Photosensitization of *Staphylococcus aureus in-vitro* - Effect of growth-phase, serum, and preirradation time. *Lasers Surg Med* **1995**; 16: 272-276.

39. Nitzan Y, Balzam-Sudakevitz A, and Ashkenazi H. Eradication of *Acinetobacter baumannii* by photosensitized agents *in vitro*. *J Photochem Photobiol B:Biol* **1998**; 42: 211-218.

40. Demidova TN and Hamblin MR. Photodynamic therapy targeted to pathogens. *Int J Immunopathol Pharmacol* **2004**; 17: 245-254.

6.7. Annex

Synthesis of ACS268

The synthesis of ACS268 is outlined in Fig. A1 and was performed by António Rocha Gonsalves and Arménio Serra in the University of Coimbra.

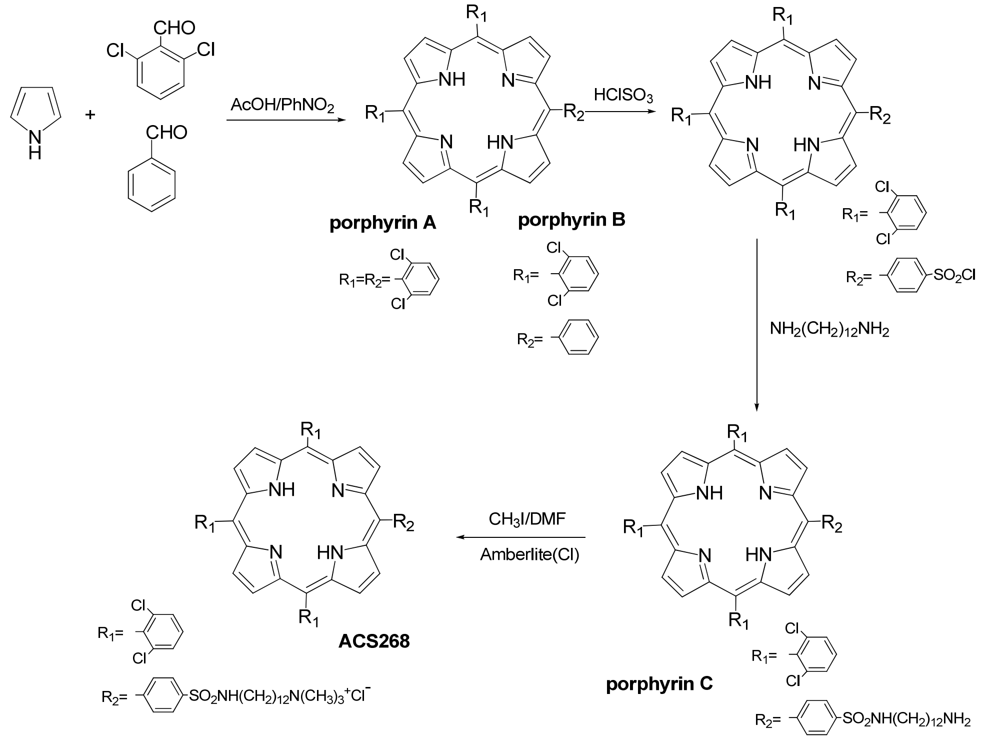
CHO
Cl
Cl
N
H
+
CHO
AcOH/PhNO2
R1
NH
N
HN
R2
porphyrin A
porphyrin B
R1=R2=
R1=
R2=
HClSO3
SO2Cl
NH2(CH2)12NH2
CH3I/DMF
Amberlite(Cl)
ACS268
porphyrin C
SO2NH(CH2)12N(CH3)3+Cl−
SO2NH(CH2)12NH2

Fig. A1: Synthethic pathway used for ACS268.

To a solution of 7.0 g (40 mmol) of 2,6-dichlorobenzaldehyde, 0.85 g (8.0 mmol) of benzaldehyde in 100 mL of acetic acid, 8 mL of acetic anhydride and 25 mL of nitrobenzene at 120 °C, 3.5 mL (50 mmol) of pyrrole were added. The reaction was maintained at this temperature for 2 hours. After cooling, 275 mg of a mixture of 5-phenyl-10,15,20-*tris*(2,6-dichlorophenyl)porphyrin (A) and tetrakis(2,6-dichlorophenyl)porphyrin (B) was obtained.

Synthesis of 5,10,15-tris(2,6-dichlorophenyl)-20-[*N*-(12-amino-dodecyl-*p*-sulphonamidophenyl]porphyrin (porphyrin C). At room temperature, 20 ml of chlorosulfonic acid was added to 250 mg of the mixture of porphyrin A and B. The solution was stirred for 2 h and then carefully poured over ice in order to precipitate the chlorosulphonylderivative of porphyrin B and unreacted porphyrin A which does not react at this temperature due to ring deactivation. The precipitate was filtered, dried, dissolved with chloroform and the solution dried with sodium sulphate (Na_2SO_4). The solution was concentrated to 30 ml and was added to 0.8 g of 1,12-diaminedodecane and pyridine (2 ml). The mixture was stirred overnight at 30 ºC and filtered. After concentration the residue was chromatographed on silica gel type 60 with particle size of 0.035-0.070 μm (Acros Organics). The porphyrin fraction was eluted first with dichloromethane and then dichloromethane/ethyl acetate/ethanol (70/30/10). Evaporation of the solvent generated 120 mg of porphyrin C (MS (ESI): *m/z* 1083 (100%, $[M+1]^+$).

Synthesis of 5,10,15-tris(2,6-dichlorophenyl)-20-[*N*-(12-trimethyl ammonium chloride)-dodecyl-*p*-sulphonamidophenyl]porphyrin (ACS268). Porphyrin C (100 mg) was dissolved in DMF (1 mL) and 2 methyl iodide (2 mL) and K_2CO_3 (150 mg) were added. The solution was stirred for 24 h at 60°C in a sealed tube and, after cooling, was poured over ice water to precipitate. The solid was filtered, dissolved in dichloromethane and dried over Na_2SO_4. Then, the solution was concentrated to 10 mL, stirred for 30 min. with Amberlite 400 (Cl), filtered and washed with methanol. Evaporation of the solvent gave a solid which was recrystallized (CH_2Cl_2/hexane) to originate 70 mg of ACS268. δ_H(400 MHz, d_6-DMSO) 8.75 (m, 8H, β-H), 8.47 (d, 2H, J= 7.2 ArH), 8.23 (d, J= 7.2 Hz, 2H, Ar-H), 8.03-7.96 (m, 9H, Ar-H), 3.12-2.90 (m, 13H, $(CH_3)_3$,CH_2N), 1.25 (m, 20H, CH_2), HRMS (ESI): m/z calc. for $C_{59}H_{57}Cl_6N_6O_2S$ (M^+) 1123.23778; found, 1123.23894.

Solvent polarity dependence of the fluorescence intensity of NMB

The fluorescence lifetime of 1 μM solutions of NMB in different solvents with increasing polarities show a clear dependence as demonstrated in Fig. A2.

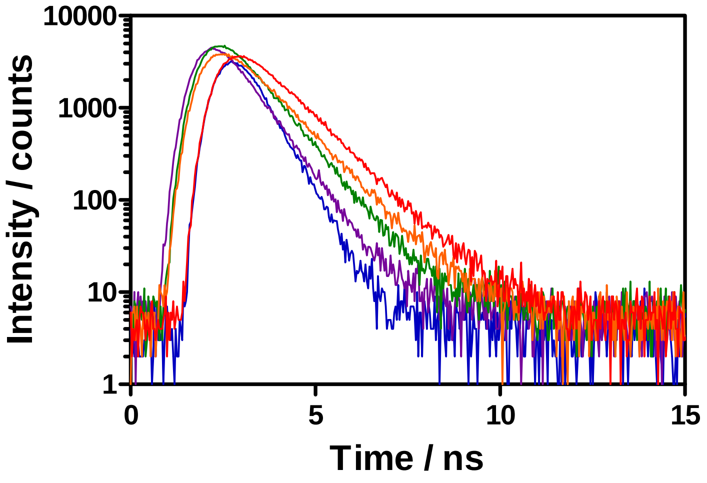

Fig. A1: Time-resolved fluorescence decay of NMB at 657 nm upon excitation at 596 nm in H_2O (0.5 ns; blue), MeOH (0.7 ns; violet), EtOH (0.8 ns; green), 1-pentanol (1.0 ns; orange) and 1-hexanol (1.1 ns; red).

Chapter 7

Singlet oxygen photosensitisation by the fluorescent probe Singlet Oxygen Sensor Green

The detection of reactive oxygen species by means of fluorescent probes is really extended. In this chapter, the ability of Singlet Oxygen Sensor Green, a fluorescein-based probe, to self-sensitize singlet oxygen under exposure to UV or visible radiation is investigated.

The work described in this chapter is adapted from Xavier Ragàs, Ana Jiménez-Banzo, David Sánchez-García, Xavier Batllori and Santi Nonell in *Chem Commun* 2009, 20, 2920-22.

7.1. INTRODUCTION

Singlet oxygen ($^1O_2$) is a highly reactive oxygen species (ROS) that can damage biological cell components such as lipids, proteins or nucleic acids. Used intentionally as a deleterious species in photodynamic therapy [1,2], its role as a biological messenger is being increasingly recognised [3-5].

Methods for $^1O_2$ detection include EPR spectroscopy using spin traps [6], phosphorescence at 1270 nm [7] and chemical trapping [8]. The current spread of fluorescence imaging techniques has lead to the development of a number of $^1O_2$ fluorescent probes such as trans-1-(2'-methoxyvinyl)pyrene (MVP) [9], dansyl-2,2,5,5-tetramethyl-2,5-dihydro-1*H*-pyrrole (DanePy) [10] or fluorescein-based probes such as DMAX or DPAX [11]. Invitrogen / Molecular Probes has recently marketed a highly selective sensor for $^1O_2$ without any appreciable response to hydroxyl radicals or superoxide under the trade name Singlet Oxygen Sensor Green (SOSG) reagent® [12]. While the exact structure of SOSG has not been disclosed, its absorption spectrum resembles that of DMAX and it may therefore be assumed that it contains a fluorescein bound to a dimethylanthracene derivative (Fig. 1).

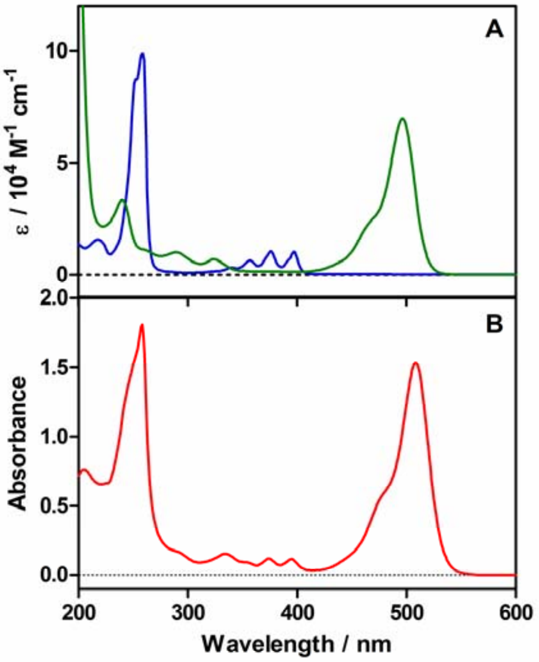

Fig. 1: UV-Visible spectrum of **(A)** dimethylanthracene (blue) and fluorescein (green) and **(B)** SOSG (red).

SOSG has been successfully applied to the detection of $^1O_2$ in fields as diverse as light-activated plant defense [13], photoinactivation of *Staphylococcus aureus* bacteria

[14], or plasmonic engineering of $^1O_2$ production [15]. A recent review compares the benefits of these probes for $^1O_2$ imaging in plants [16].

SOSG exhibits weak blue fluorescence peaks at 395 and 416 nm under excitation at 372 and 393 nm. In the presence of $^1O_2$, SOSG emits a green fluorescence with excitation and emission maxima at 504 and 525 nm, respectively [12]. This green fluorescence emission was assigned to an endoperoxide generated by the interaction of $^1O_2$ with the anthracene component of SOSG as observed for other fluorescein-anthracene probes such as DMAX or DPAX [11].

In the course of our studies using SOSG as $^1O_2$ probe, we observed the appearance of the green fluorescence under exposure of SOSG to either UV or visible radiation, even in the absence of external $^1O_2$ photosensitisers. This observation has also been reported by other authors [16,17]. Thus, the main goal of the present study is to demonstrate that SOSG is able to produce $^1O_2$ under photoirradiation.

7.2. EXPERIMENTAL SECTION

Materials

Singlet oxygen sensor green was purchased from Invitrogen (Molecular Probes, Paisley, UK). Sodium azide, 9,10-dimethylanthracene, fluorescein and 2-mercaptoethylamine (MEA) were purchased from Sigma-Aldrich (St. Louis, MO, USA). Deuterium oxide (D_2O; >99.9%), methanol, and methanol-d_4 were purchased from SDS (Solvents Documentation Synthesis, Peypin, France). Deuterated solvents were used since deuterium greatly enhances the $^1O_2$ lifetime and thus makes its detection easier.

Samples were contained in squared 1 cm optical path fused silica cuvettes (Hellma 101-QS).

Liquid chromatography conditions

Liquid Chromatography (HPLC) was performed with an Agilent 1200 series liquid chromatograph equipped with a diode array detector. SOSG was analyzed on a 12.5 mm x 4.6 mm, 5 µm particle, Lichrospher 100 RP-18 column. Detection was obtained at 254, 355 and 532 nm. All chromatography was performed at 25 ºC with a mobile phase flow rate of 1.0 mL min^{-1}. A gradient elution was performed from 40:60 to 70:30 MeOH/H_2O for the mobile phase (Table 1):

Table 1. Chromatographic conditions for the gradient elution of SOSG.

Time / min	%MeOH	% H_2O
0	40	60
2	40	60
15	70	30
20	70	30
22	40	60
27	40	60

7.3. RESULTS

Purity of SOSG

Liquid chromatography was used to assess the purity of SOSG. The sample was prepared by solving 100 µg of SOSG in 0.5 mL of MeOH / H_2O 70:30. As observed in Fig. 2, four different peaks were obtained at 254, 355 and 532 nm with relative total areas showed at Table 2.

Table 2. Relative areas of the peaks obtained by liquid chromatography of SOSG shown in Fig. 2.

Chromatogram	λ_{obs} / nm	Peak 1 (%)	Peak 2 (%)	Peak 3 (%)	Peak 4 (%)
A	254	0.1	0.2	94.9	4.8
B	355	0.1	0.2	95.3	4.4
C	532	0.1	0.2	94.9	4.8

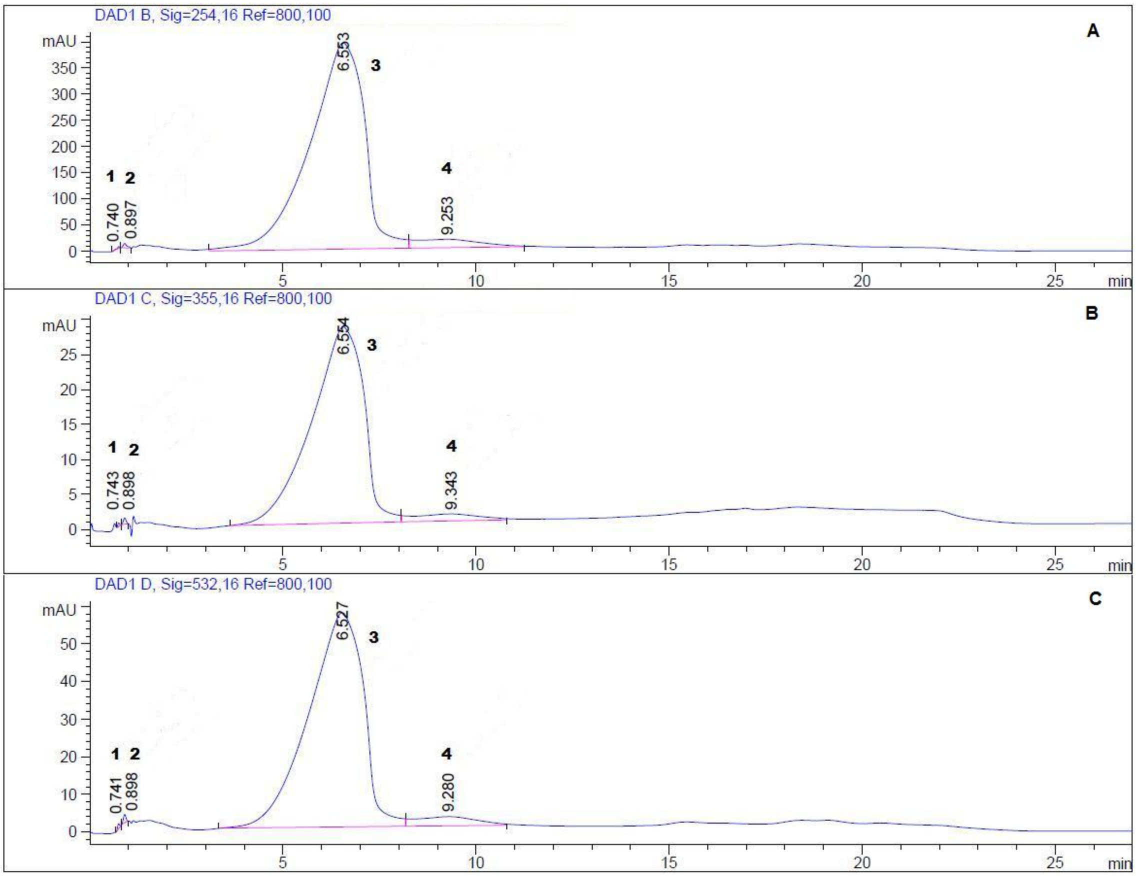

Fig. 2: Liquid chromatography of SOSG detected at (A) 254 nm, (B) 355 nm and (C) 532 nm.

Peaks **3** and **4** had the same UV-Vis spectrum as SOSG (Fig. 3) and had a total relative area better than 99%. The presence of two different peaks with the same absorption spectra could be explained by the presence of different ionization grades or different isomers of SOSG.

UV-Vis spectra of peaks **1** and **2**, corresponding to SOSG impurities or degradation products, are also presented in Fig. 3. However, sum of its relative area corresponds only to 1%.

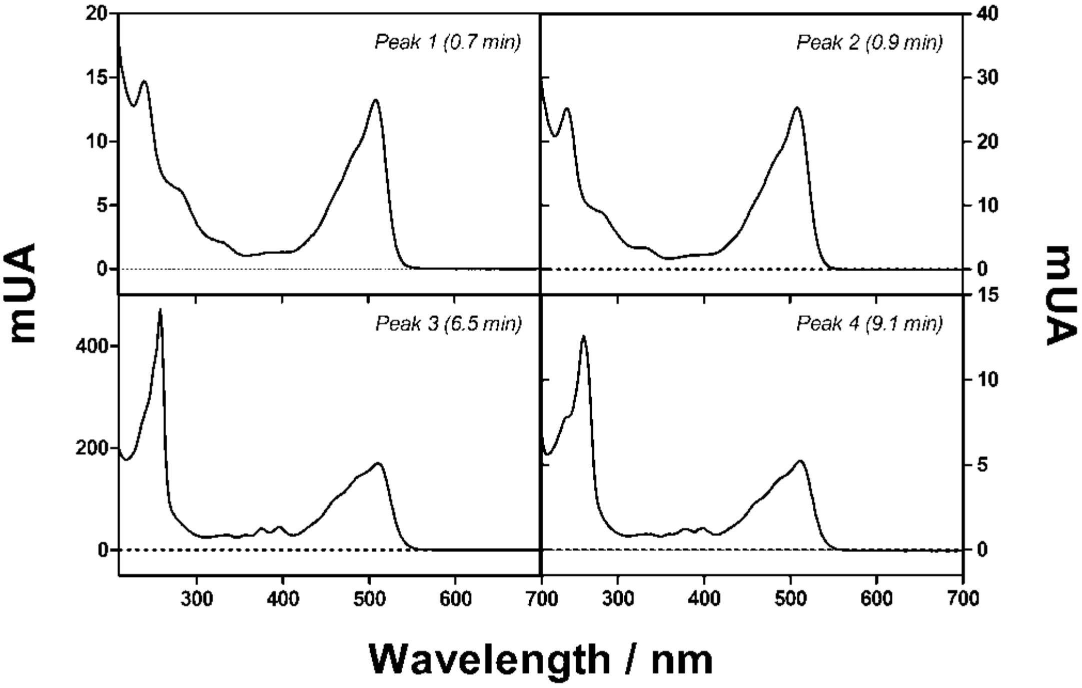

Fig. 3: Absorption spectra from 210 nm to 700 nm for the different peaks obtained by liquid chromatography and diode array detection of SOSG.

Singlet oxygen detection and control experiments

Irradiation of a methanol-d_4 SOSG solution at 355 nm produced a clear time-resolved luminescence signal with maximum intensity at 1275 nm. Substitution of air-atmosphere by bubbling during 20 min a SOSG solution with argon to remove oxygen from the solution eliminated the signal at 1275 nm (Fig. 4).

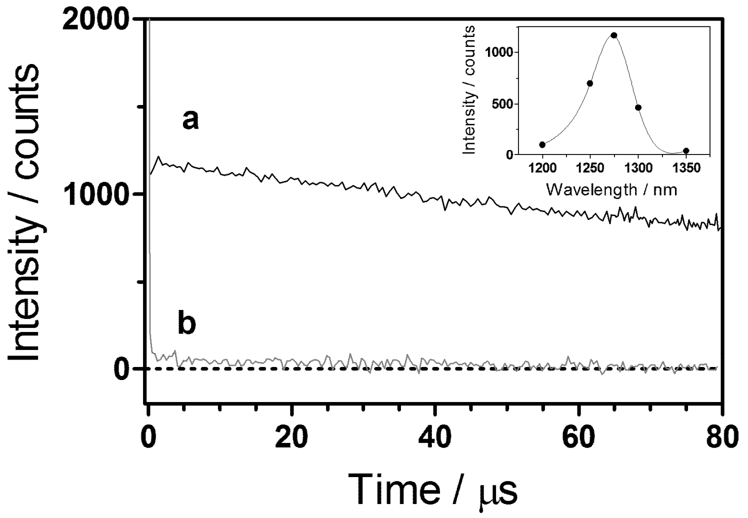

Fig. 4: Singlet oxygen phosphorescence photosensitised by SOSG in methanol-d4. The solution was irradiated with 1-ns laser pulses at 355 nm (ca. 1 μJ per pulse, repetition rate 10 kHz) and the luminescence was observed at 1275 nm. (a) Air atmosphere (b) Argon atmosphere. Inset: Spectral distribution of the photoluminescence generated by SOSG.

Addition of different volumes of a 10 mM NaN_3 solution to SOSG solved in methanol-d_4 reduced the phosphorescence decay lifetime concomitantly (Fig. 5).

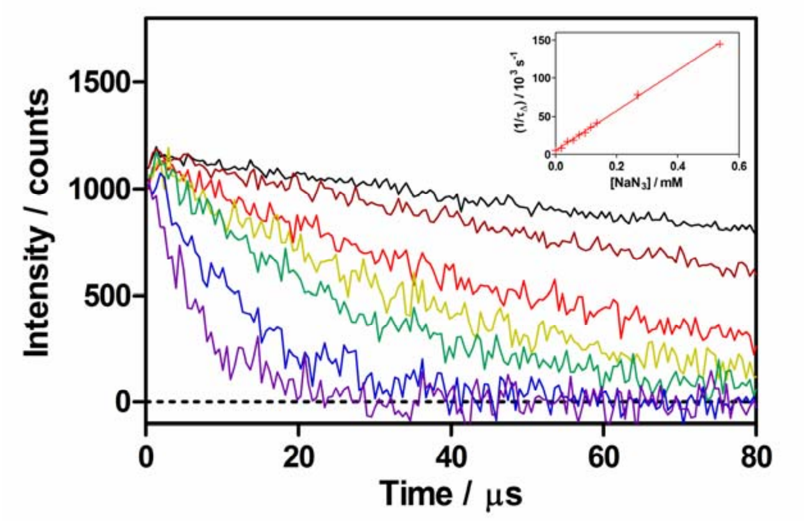

Fig. 5: Singlet oxygen phosphorescence photosensitised by SOSG in methanol-d_4, air athmosphere and sodium azide concentrations ranging from 0 mM (black curve) to 0.54 mM (pink curve). The solution was irradiated with 1-ns laser pulses at 355 nm (ca. 1 μJ per pulse, repetition rate 10 kHz) and the luminescence was observed at 1275 nm. Inset: Stern-Volmer Plot.

Likewise, removing SOSG from the solution completely eliminated the signal, demonstrating that signals did not come from an impurity due to the solvent (Fig. 6).

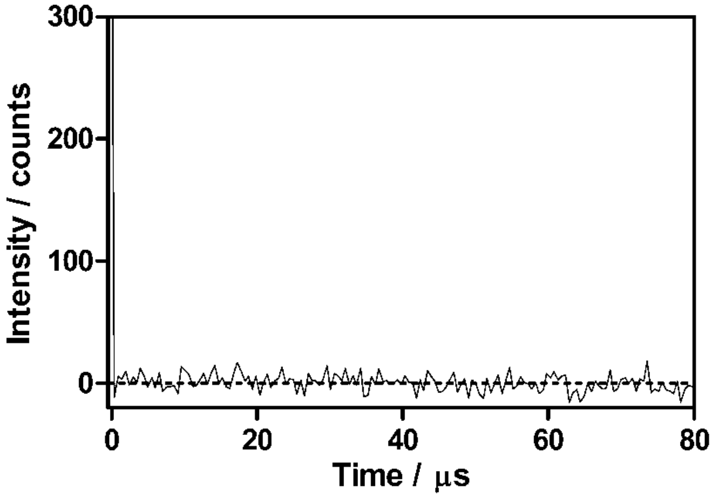

Fig. 6: Singlet oxygen phosphorescence control experiment of methanol-d$_4$ and air athmosphere. The solution was irradiated with 1-ns laser pulses at 355 nm (*ca.* 1 µJ per pulse, repetition rate 10 kHz) and the luminescence was observed at 1275 nm.

Singlet oxygen quantum yields

The $^1O_2$ production quantum yield, Φ_Δ, was determined by comparing the intensity of the $^1O_2$ signal shown by SOSG to that of optically-matched solutions of reference photosensitisers [18]. Using phenalenone and rose bengal as standards (Φ_Δ^{ref} = 0.97 and 0.75, respectively [21-23]), we obtained Φ_Δ values in methanol of 0.03 ± 0.01 and 0.009 ± 0.003 for excitation at 355 and 532 nm, respectively (Fig. 7a and 7b).

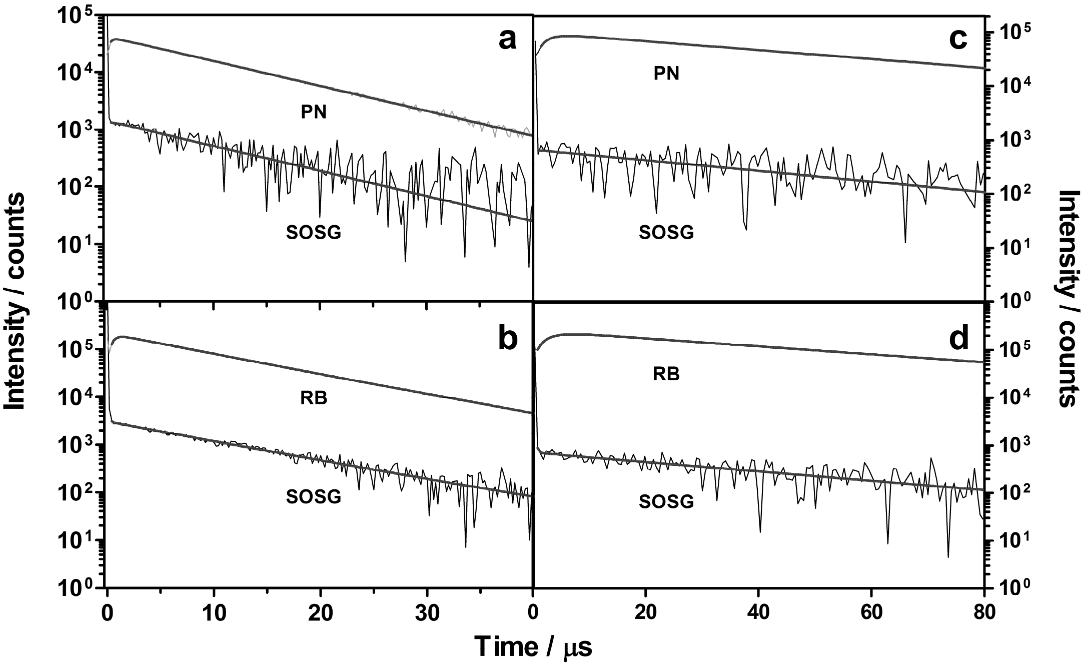

Fig. 7: Singlet oxygen phosphorescence photosensitised by SOSG in **(a,b)** MeOH and **(c,d)** D_2O-MeOH 95:5 observed at 1275 nm. The solution was irradiated with 1-ns laser pulses at **(a,c)** 355 nm using phenalenone (PN) as reference, and **(b,d)** 532 nm using rose bengal (RB) as reference.

As SOSG is intended for use in aqueous environments, Φ_Δ were also measured in 95:5 D_2O:MeOH mixtures, observing a decrease in their values dropping to 0.006 ± 0.002 at 355 nm and to 0.002 ± 0.001 at 532 nm (Fig. 7c and 7d).

Laser-induced kinetics of SOSG

Irradiation of an SOSG sample, solved in 95:5 H_2O:MeOH, at 355 nm induced very different effects: while an increase of the green fluorescence was observed at low irradiation doses, extended irradiation caused it to decrease. At the same time a fast and extensive bleaching of both the fluorescein and anthracene absorption bands could be observed. The bleaching could be slowed down by the radical quencher 2-mercaptoethylamine (MEA, 100 mM), but was insensitive to the addition of 5 mM NaN_3 (Fig. 8A and 8B).

However, irradiation at 532 nm induced different effect, namely a transient fluorescence decrease followed by a steady fluorescence rise as the dose was further increased. Interestingly, the absorbance of the fluorescein moiety increased monotonically to a final constant value, while the anthracene moiety was bleached (Fig. 8C and 8D).

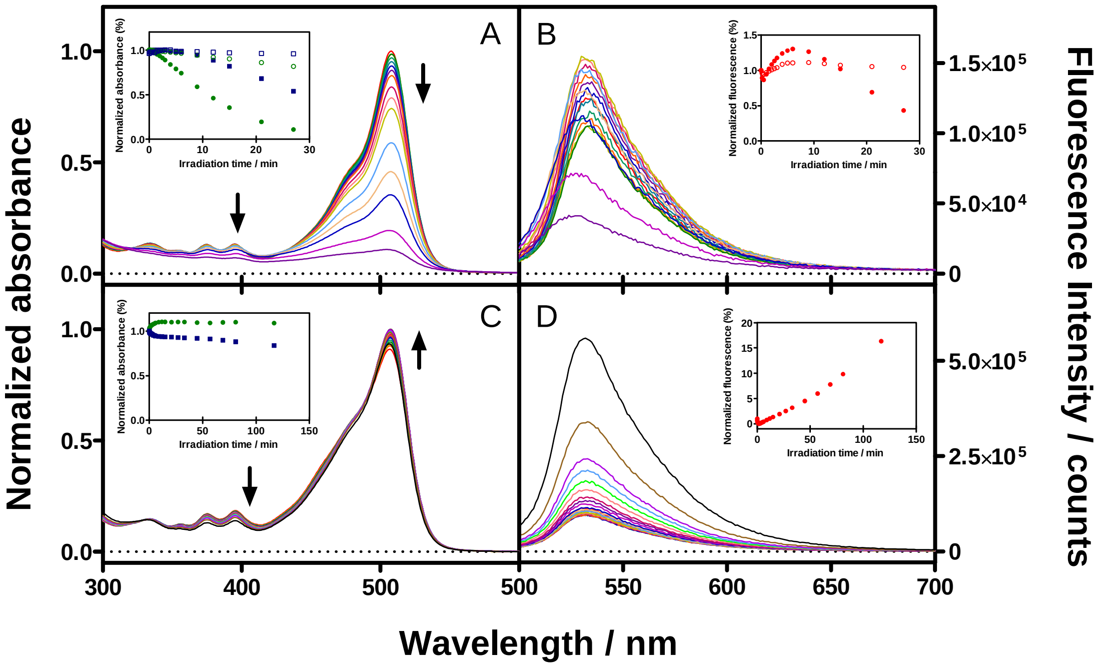

Fig. 8: Time course of the absorption **(A, C)** and fluorescence **(B, D)** spectra of SOSG upon irradiation in H_2O:MeOH (95:5) with 10-ns laser pulses at 355 nm **(A, B)** and 532 nm **(C, D)** (*ca.* 20 mJ per pulse, repetition rate 10 Hz). Insets: **(A, C)** Absorbance at 507 nm (fluorescein moiety, circles) or at 395 nm (anthracene moiety, squares) in the presence (open symbols) and absence (filled symbols) of 100 mM MEA. **(B, D)** Area under the fluorescence spectra obtained in the presence (open symbols) and absence (filled symbols) of 100 mM MEA. The samples were excited at 480 nm.

Laser flash photolysis of SOSG

Pulsed-laser irradiation at 355 nm or 532 nm of an air-saturated SOSG solution in H_2O:MeOH (95:5) produced the transient absorption signals at 428 nm shown in Fig. 9.

Excitation of SOSG at 355 nm produced a long-lived transient with maximum absorption at 428 nm that was insensitive to oxygen, but was clearly modified upon addition of 100 mM of MEA. Excitation of SOSG at 532 nm produced a long-lived transient as well, but it was much weaker than when SOSG was irradiated at 355 nm.

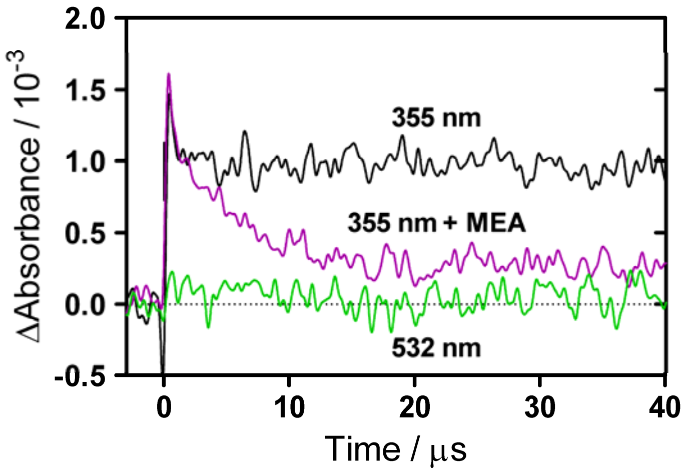

Fig. 9: Transient absorption of SOSG in air-saturated H_2O:MeOH (95:5) solutions as a function of excitation wavelength and added MEA. Observation wavelength: 428 nm.

7.4. DISCUSSION

The main goal of the present study was to demonstrate that SOSG is able to produce $^1O_2$ under photoirradiation. Therefore, it was important for us to demonstrate the purity of SOSG in the samples used for the study. Characterisation of the samples by liquid chromatography probed adequate to this respect, showing that both the spectra and the relative areas of the different peaks observed were due to the same product with a relative area >99%. Mass spectrometry was also performed providing a major signal of m/z = 601.1050 correspondent to an empirical formula of $C_{36}H_{22}ClO_7$ (see *Annex*). Additionally, NMR experiments were also performed and are also given in the *Annex*.

Formation of $^1O_2$ by SOSG has been assessed by time-resolved near-IR phosphorescence detection [18,19]. Many control experiments have been performed to demonstrated that it was indeed $^1O_2$ photosensitised by SOSG the source of the luminescence observed at 1275 nm: (1) the addition of NaN_3 reduced the phosphorescence decay lifetime, providing a quenching rate of 2.6 x 10^8 $M^{-1}s^{-1}$, in perfect agreement with bibliographic values [20]. Removing (2) oxygen or (3) SOSG from the solution completely eliminated the signal

The Φ_Δ values are modest but non negligible, particularly as SOSG is used as a $^1O_2$ probe. This is particularly important when UV radiation is used or when the photosensitisers under scrutiny show low $^1O_2$ quantum yields, e.g., as for the enhanced green fluorescent protein (EGFP) [7]. The excitation wavelength dependence of the Φ_Δ values indicates that different photochemical processes arise upon excitation of the anthracence or fluorescein moieties. In agreement with this observation, the absorbance and green fluorescence intensity of SOSG changed in a different fashion upon irradiation of either the anthracene-moiety (355 nm) or the fluorescein-moiety (532 nm). While the results upon irradiation at 532 nm are consistent with a steady production of $^1O_2$ upon irradiation, confirming the time-resolved near-IR luminescence results, irradiation at 355 nm induced very different effects. The fact that the bleaching of the fluorescein moiety could be slowed down by the radical quencher MEA, but not by NaN_3 suggests that the bleaching is mediated by radical species but not by $^1O_2$. This observation agrees with an earlier report on the photobleaching of fluorescein [24] and with our experiments performed by laser flash photolysis.

All these results can be rationalised using the energy diagram depicted in Fig. 10, under the assumption that the excited-state energy levels and redox potentials of

SOSG are close to those of fluorescein and dimethylanthracene [25-27]. Irradiation at 355 nm and at 532 nm trigger different photochemical pathways.

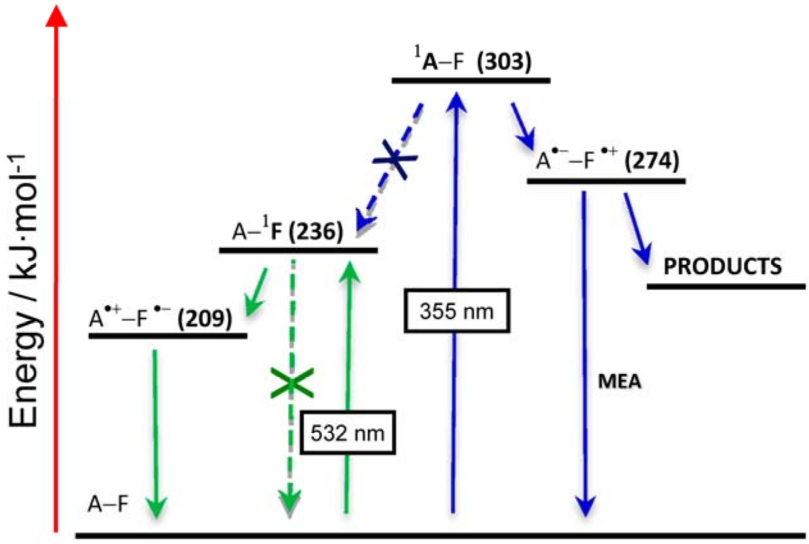

Fig. 10: Energy diagram of the dimethylanthracene – fluorescein photosystem and suggested deactivation pathways following excitation at 355 and 532 nm.

Thus, irradiation at 532 pumps the fluorescein to its singlet excited state, which is followed by a fast electron transfer from anthracene to fluorescein. As long as the anthracene moiety is intact, this pathway competes efficiently with SOSG fluorescence and the probe is silent. In the presence of $^1O_2$, anthracene is oxidised and this deactivation pathway is no longer available, rendering SOSG fluorescent. However, when intact SOSG is exposed to UV radiation an additional photochemical pathway becomes possible, namely electron transfer from fluorescein to anthracene, which leads to its irreversible bleaching. The observation of a long-lived transient at 428 nm in the laser flash photolysis experiments is consistent with the formation of the semioxidised form of fluorescein in this case [24].

7.5. CONCLUSIONS

The results above show that SOSG is able to act as $^1O_2$ photosensitiser, particularly under UV radiation. Furthermore, UV irradiation leads to its photobleaching due to the formation of radical species. While SOSG remains a useful $^1O_2$ probe, these results should be taken into account by users of this probe for the design of appropriate controls and care must be exercised when using it, particularly in combination with UV sources.

7.6. REFERENCES

1. Dolmans DEJG, Fukumura D, and Jain RK. Photodynamic therapy for cancer. *Nat Rev Cancer* **2003**; 3: 380-387.
2. Jori G, Fabris C, Soncin M, Ferro S, Coppellotti O, Dei D, Fantetti L, Chiti G, and Roncucci G. Photodynamic therapy in the treatment of microbial infections: Basic principles and perspective applications. *Lasers Surg Med* **2006**; 38: 468-481.
3. Flors C and Nonell S. Light and singlet oxygen in plant defense against pathogens: Phototoxic phenalenone phytoalexins. *Acc Chem Res* **2006**; 39: 293-300.
4. Beck CF. Signaling pathways from the chloroplast to the nucleus. *Planta* **2005**; 222: 743-756.
5. Bhattacharjee S. Reactive oxygen species and oxidative burst: Roles in stress, senescence and signal transduction in plants. *Curr Sci India* **2005**; 89: 1113-1121.
6. Hideg E, Spetea C, and Vass I. Singlet oxygen production in thylakoid membranes during photoinhibition as detected by EPR spectroscopy. *Photosynth Res* **1994**; 39: 191-199.
7. Jimenez-Banzo A, Nonell S, Hofkens J, and Flors C. Singlet oxygen photosensitization by EGFP and its chromophore HBDI. *Biophys J* **2008**; 94: 168-172.
8. Telfer A, Bishop SM, Phillips D, and Barber J. Isolated photosynthetic reaction-center of photosystem-II as a sensitizer for the formation of singlet oxygen - Detection and quantum yield determination using a chemical trapping technique. *J Biol Chem* **1994**; 269: 13244-13253.
9. Thompson A, Seliger HH, and Posner GH. Chemiluminescent probes for singlet oxygen in biological reactions. *Methods Enzymol* **1986**; 133: 569-584.
10. Kalai T, Hideg E, Vass I, and Hideg K. Double (fluorescent and spin) sensors for detection of reactive oxygen species in the thylakoid membrane. *Free Rad Biol Med* **1998**; 24: 649-652.

11. Tanaka K, Miura T, Umezawa N, Urano Y, Kikuchi K, Higuchi T, and Nagano T. Rational design of fluorescein-based fluorescence probes. Mechanism-based design of a maximum fluorescence probe for singlet oxygen. *J Am Chem Soc* **2001**; 123: 2530-2536.

12. Molecular Probes product information, **2004**.

13. Flors C, Fryer MJ, Waring J, Reeder B, Bechtold U, Mullineaux PM, Nonell S, Wilson MT, and Baker NR. Imaging the production of singlet oxygen in vivo using a new fluorescent sensor, Singlet Oxygen Sensor Green®. *J Exp Bot* **2006**; 57: 1725-1734.

14. Maisch T, Baier J, Franz B, Maier M, Landthaler M, Szeimies RM, and Baumler W. The role of singlet oxygen and oxygen concentration in photodynamic inactivation of bacteria. *Proc Natl Acad Sci USA* **2007**; 104: 7223-7228.

15. Zhang Y, Aslan K, Previte MJR, and Geddes CD. Plasmonic engineering of singlet oxygen generation. *Proc Natl Acad Sci USA* **2008**; 105: 1798-1802.

16. Hideg E. A comparative study of fluorescent singlet oxygen probes in plant leaves. *Cent Eur J Biol* **2008**; 3: 273-284.

17. Chignel CF and Bilski P, personal communication.

18. Nonell S and Braslavsky SE Time-resolved singlet oxygen detection. *Methods Enzymol* **2000**; 319: 37-49.

19. Jimenez-Banzo A, Ragas X, Kapusta P, and Nonell S. Time-resolved methods in biophysics. 7. Photon counting vs. analog time-resolved singlet oxygen phosphorescence detection. *Photochem Photobiol Sci* **2008**; 7: 1003-1010.

20. Wilkinson F, Helman WP, and Ross AB. Rate constants for the decay and reactions of the lowest electronically excited singlet state of molecular oxygen in solution. An expanded and revised compilation. *J Phys Chem Ref Data* **1995**; 24: 663-1021.

21. Schmidt R, Tanielian C, Dunsbach R, and Wolff C. Phenalenone, a universal reference compound for the determination of quantum yields of singlet oxygen $O_2(^1\Delta_g)$ sensitization. *J Photochem Photobiol A:Chem* **1994**; 79: 11-17.

22. Martí C, Jürgens O, Cuenca O, Casals M, and Nonell S. Aromatic ketones as standards for singlet molecular oxygen $O_2(^1\Delta_g)$ photosensitization. Time-resolved photoacoustic and NIR emission studies. *J Photochem Photobiol A:Chem* **1996**; 97: 11-18.

23. Wilkinson F, Helman WP, and Ross AB. Quantum yields for the photosensitized formation of the lowest electronically excited singlet state of molecular oxygen in solution. *J Phys Chem Ref Data* **1993**; 22: 113-262.

24. Song LL, Varma CAGO, Verhoeven JW, and Tanke HJ. Influence of the triplet excited state on the photobleaching kinetics of fluorescein in microscopy. *Biophys J* **1996**; 70: 2959-2968.

25. Murov SL, Carmichael I, and Hug GL. Ionization energies, electron affinities, and redox potentials of organic compounds. In: Handbook of Photochemistry, Marcel Dekker, Inc., New York, 2nd ed., **1993**.

26. Urano Y, Kamiya M, Kanda K, Ueno T, Hirose K, and Nagano T. Evolution of fluorescein as a platform for finely tunable fluorescence probes. *J Am Chem Soc* **2005**; 127: 4888-4894.

27. Zhang HP, Zhou YL, Zhang MH, Shen T, Li YL, and Zhu DB. Photoinduced interaction between fluorescein ester derivatives and CdS colloid. *J Colloid Interf Sci* **2003**; 264: 290-295.

7.6. ANNEX

Mass spectrometry

High resolution mass spectrometry was done to know the exact mass of SOSG. A TOF spectrometer with ESI gave a major peak of m/z = 601.1050 (Fig. A1) correspondent to an empirical formula of $C_{36}H_{22}ClO_7$.

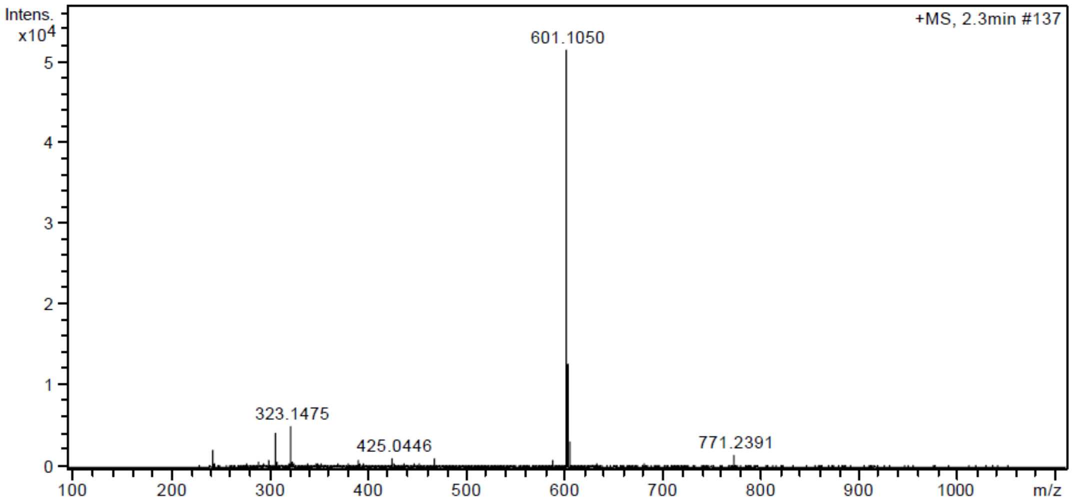

Fig. A1: ESI-TOF high resolution mass spectrometry of SOSG.

^{1}H-NMR

δ_H (800 MHz; methanol-d_4) 3.10 (6 H_{ant}, s, Me), 6.47 (1 H_{fluo}, s), 6.50 (1 H_{fluo}, s), 6.72 (1 H_{fluo}, s), 6.74 (1 H_{fluo}, s), 6.94 (1 H_{fluo}, s), 6.95 (1 H_{fluo}, s), 7.01 (1 H_{fluo}, s), 7.02 (1 H_{fluo}, s), 7.20 (1 H_{ant}, dd), 7.23 (1 H_{ant}, dd), 7.32 – 7.43 (7 $H_{6ant + 1fluo}$, m), 7.47 (2 H_{ant}, dd), 7.56 (1 H_{ant}, d), 7.58 (1 H_{ant}, d), 7.90 (1 H_{fluo}, d), 7.91 (1 H_{fluo}, d), 8.16 (1 H_{fluo}, d), 8.30 (2 H_{ant}, d), 8.32 (1 H_{fluo}, d), 8.34 (2 H_{ant}, d), 8.43 (1 H_{fluo}, s).

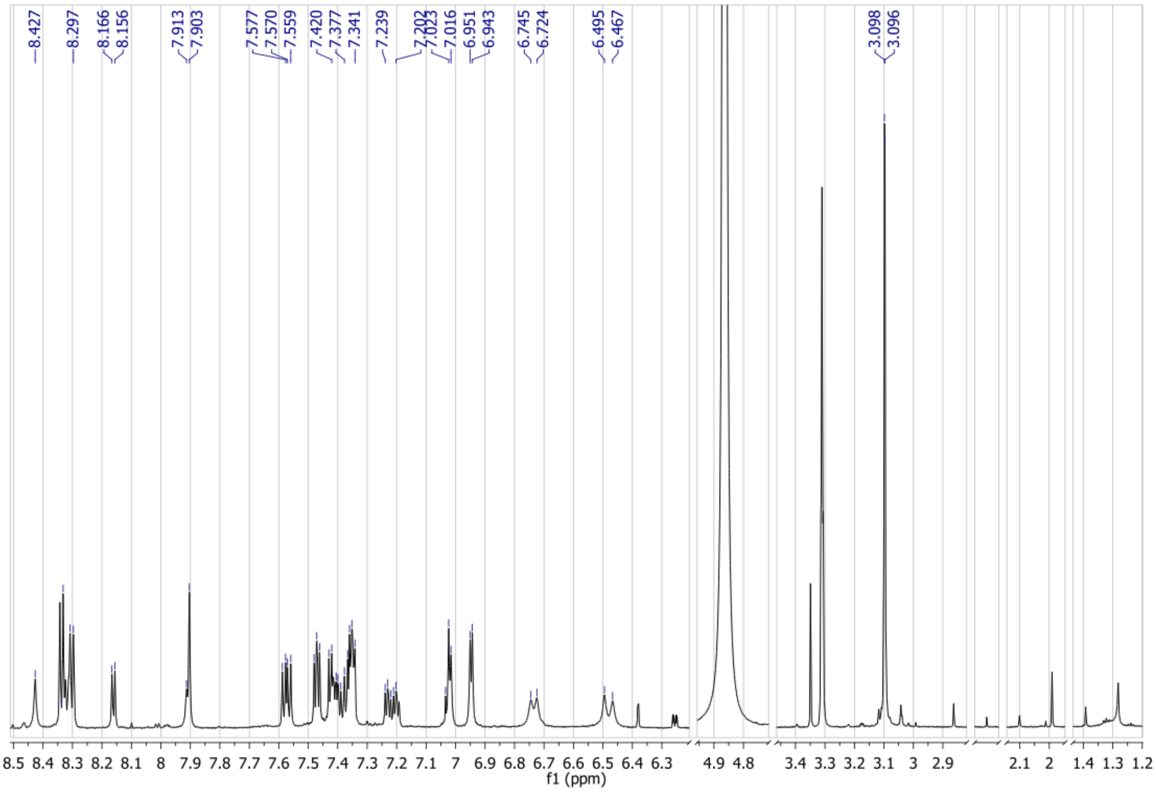

Fig. A2: ^{1}H-RMN of SOSG in methanol-d$_4$.

2D-COSY

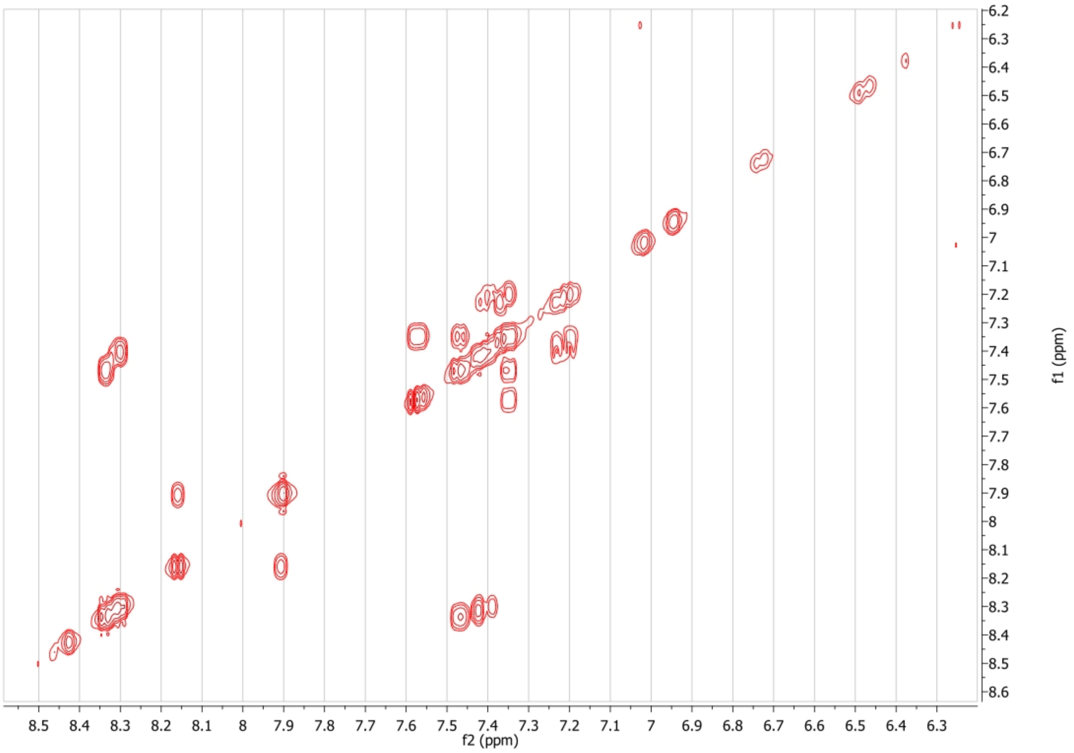

Fig. A3: 2D-COSY of SOSG in methanol-d$_4$.

^{1}H-^{13}C HSQC

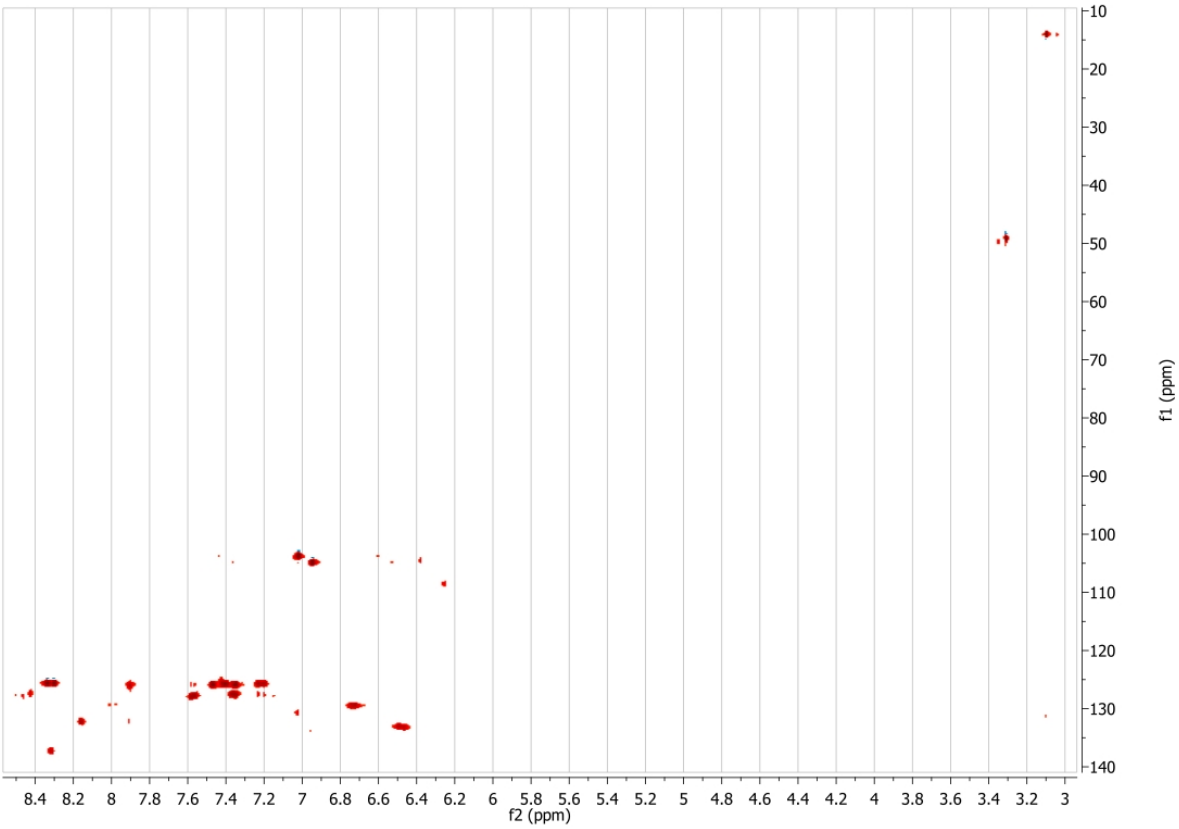

Fig. A4: ^{1}H-^{13}C HSQC of SOSG in methanol-d$_4$.

Chapter 8

Genetically-encoded singlet oxygen production by a red fluorescent protein

The role of reactive oxygen species (ROS), e.g. singlet oxygen, in chromophore-assisted light inactivation (CALI) by fluorescent proteins has been demonstrated. In this chapter, we investigate the ability of a red fluorescent protein to photoproduce ROS using time-resolved detection of the NIR phosphorescence of $^1O_2$ and specific fluorescent probes for the detection of ROS.

The work described in this chapter is adapted from X. Ragàs, L. P. Cooper, J. H. White, S. Nonell and C. Flors, *Angew Chem Int Ed,* 2010, submitted.

8.1. INTRODUCTION

Chromophore-assisted laser inactivation (CALI) is a useful technique used to specifically inactivate the function of target proteins or organelles by producing photochemical damage [1]. CALI is generally achieved by the photosensitised production of reactive oxygen species (ROS) [2] by photoactive dyes such as malachite green or fluorescein isothiocyanate. The usefulness of CALI has been demonstrated against many cellular functional proteins, e.g., β-galactosidase, alkaline phosphatase, acetylcholinesterase [3,4], and nuclear Ki-67 protein [5].

One of the problems of the CALI technique is the non-specific binding of the current dyes, which often induce uncontrolled photodamage. An alternative approach could be the use of fluorescent proteins (FPs), which can be fully genetically encoded and therefore expressed at predetermined sites to avoid non-specific damage. Unfortunately, all fluorescent proteins tested so far have proven less efficient than the typical CALI dyes. Recently, KillerRed, a protein derived from the GFP-like hydrozoan chromoprotein anm2CP, was specifically evolved to produce phototoxicity [6]. The main mechanism of KillerRed's phototoxicity involves the generation of the superoxide radical anion [7] by photoinduced electron transfer between the excited triplet state of the chromophore (at the site of its exocyclic double bond) and molecular oxygen [8]. The presence of a long water-filled channel that connects the chromophore with the external solvent, which facilitates the diffusion of molecular oxygen and ROS, is also crucial in the properties of KillerRed [8,9]. Another important ROS such as singlet oxygen ($^1O_2$) has also been detected from KillerRed, though to a lesser extent [6], and it does not play a major role in the KillerRed CALI effect [7].

Singlet oxygen, however, seems to be the main ROS that participates in CALI when using other FPs such as the enhanced (E)GFP. By following the CALI effect in the presence of several selective ROS quenchers, a recent study points to $^1O_2$ being the main ROS produced and responsible for observed EGFP-CALI effect [10]. Consistent with this observation , we have recently shown by means of time-resolved NIR detection of $^1O_2$ phosphorescence (TRPD) at 1275 nm that EGFP is able to photosensitise singlet oxygen [11]. Our previous work also provided a first quantification of the lifetime of $^1O_2$ produced by a FP. However, we were not able to quantify a quantum yield of photosensitised $^1O_2$ (Φ_Δ), presumably due to the low amount produced.

In this chapter, we investigate the ROS photosensitising properties of the red FP TagRFP, which absorbs at 555 nm and emits at 584 nm (Fig. 1) [12]. This particular protein caught our attention because its photobleaching rate showed a clear oxygen dependence [13]. This is unusual, and it is commonly accepted that FP photobleaching occurs by light-induced decarboxylation [14] and $^1O_2$ participates only marginally [15]. We thus anticipated that TagRFP could be a reasonably good $^1O_2$ photosensitiser within the FP family.

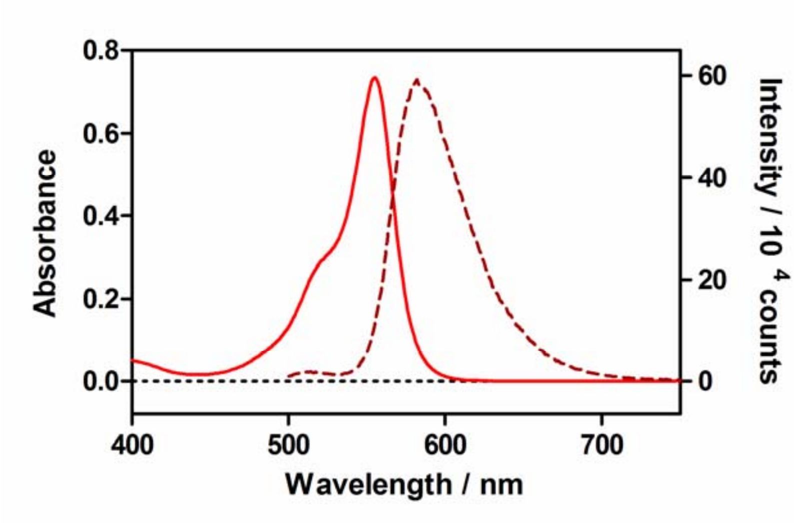

Fig. 1: Absorption (solid line) and fluorescence (dashed line) spectra of TagRFP.

8.2. EXPERIMENTAL SECTION

Materials

Plasmid TagRFP-N was obtained from Evrogen (Moscow, Russia) and expressed in *E. coli* BL21 cells by Flors *et al.* in the University of Edinburgh. Singlet oxygen sensor green (SOSG) and dihydroethidium (DHE) were purchased from Invitrogen (Molecular Probes, Paisley, UK). Sodium azide and potassium dioxide were purchased from Sigma-Aldrich (St. Louis, MO, USA). Deuterium oxide (D_2O; >99.9%), was purchased from SDS (Solvents Documentation Synthesis, Peypin, France).

Samples were contained in squared 1 cm optical path fused silica cuvettes (Hellma 101-QS).

8.3. RESULTS

Time-resolved singlet oxygen detection

Pulsed laser irradiation at 532 nm of a 14.5 µM solution of TagRFP in an air-saturated mixture of PBS, glycerol and deuterated (D)-PBS (1:1:20) allowed the detection of $^1O_2$ phosphorescence at 1270 nm (Fig. 2A). The signal, fitted with a biexponential function, rose with a lifetime of about 1.1 µs and decayed in 3.0 µs. The addition of 10 mM NaN_3, increased the rate of the rise component and only a decay of 2.8 µs could be resolved (Fig. 2B). Observation of the luminescence at 1140 nm did not provide any significant signal (Fig. 2C).

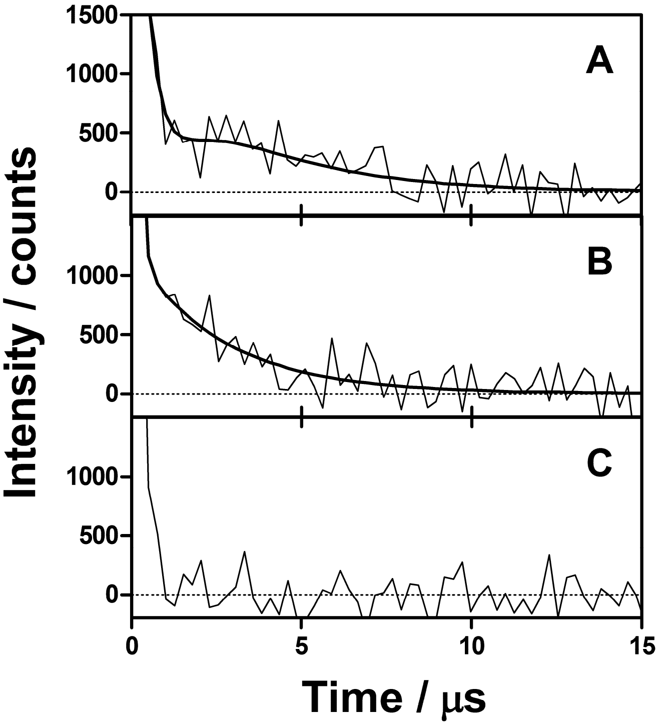

Fig. 2: Singlet oxygen phosphorescence photosensitised by TagRFP in a PBS:Glycerol:D-PBS mixture (1:1:20) upon irradiation with 1-ns laser pulses at 532 nm (*ca.* 1 µJ per pulse, repetition rate 10 kHz). (**A**) Luminescence at 1270 nm and no sodium azide (**B**) Luminescence at 1270 nm with 10 mM sodium azide (**C**) Luminescence at 1140 nm and no sodium azide.

Quantum yield of singlet oxygen production

SOSG is a $^1O_2$ probe that becomes fluorescent when it reacts with $^1O_2$. Indeed, we found that SOSG fluorescence was enhanced in the presence of TagRFP and light, to a substantially greater extent than in the presence of TagRFP or light alone. Comparison of the SOSG fluorescence enhancement upon irradiation of TagRFP and a known $^1O_2$ photosensitiser yields the Φ_Δ value of TagRFP. Fig. 3A shows the fluorescence (λ_{ex} = 480 nm) of air-saturated solutions of SOSG (10 μM) and TagRFP (14.5 μM) after different pulsed laser irradiation times. The samples were excited at 532 nm, where only TagRFP absorbs. It can be observed that the SOSG emission band at 527 nm increased while the TagRFP fluorescence band at about 590 nm decreased and shifted slightly to the blue.

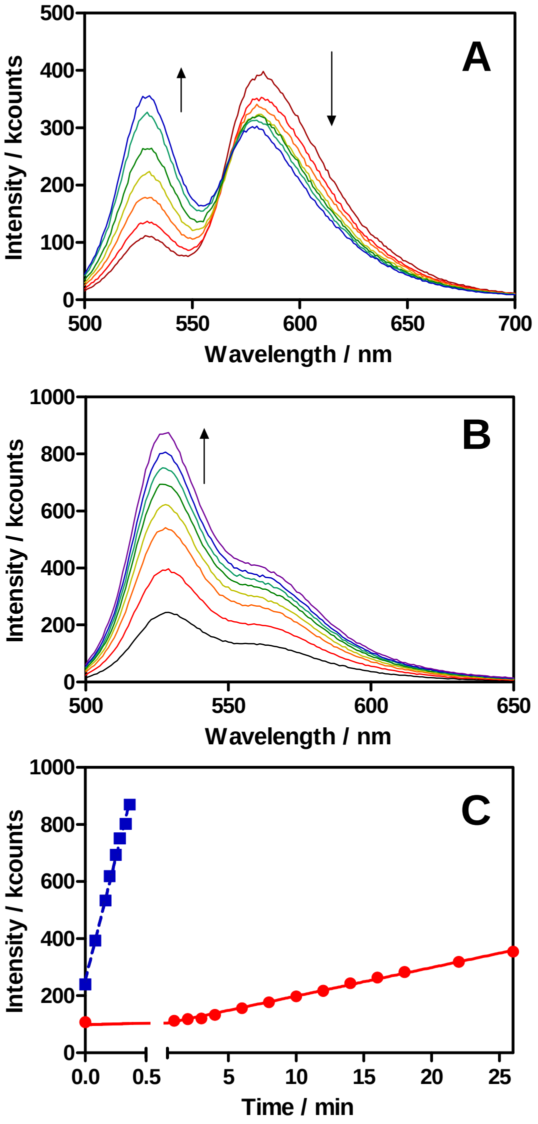

Fig. 3: Time course of the fluorescence spectra of optically matched solutions at 532 nm of (**A**) SOSG and TagRFP, and (**B**) SOSG and Rose Bengal in a PBS:Glycerol:D-PBS mixture (1:1:20) upon irradiation with 1-ns laser pulses at 532 nm (*ca.* 1 µJ per pulse, repetition rate 10 kHz). (**C**) Intensity of fluorescence of SOSG at 527 nm and linear fit of TagRFP (circles) and Rose bengal (squares) solutions upon irradiation at 532 nm.

Irradiation at 532 nm of an optically matched solution of Rose bengal in the same PBS:Glycerol:D-PBS mixture showed a significant increase of the SOSG fluorescence signal already at lower irradiation doses (Fig. 3B). Fig. 3C shows the SOSG fluorescence intensity at 527 nm for both TagRFP and rose bengal at the different irradiation times, with the linear fits to the data.

Control solutions of SOSG and TagRFP alone were irradiated under the same conditions providing a slight increase and decrease in the fluorescence emission at 527 nm, respectively (Fig. 4).

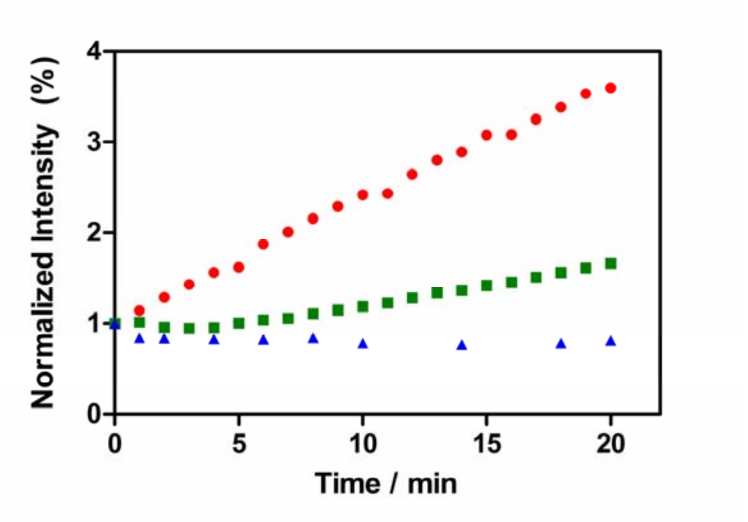

Fig. 4: Normalized fluorescence intensity at 527 nm of TagRFP with SOSG (circles), SOSG alone (squares) and TagRFP alone (triangles) in a PBS:Glycerol:D-PBS mixture (1:1:20) upon irradiation with 1-ns laser pulses at 532 nm (*ca.* 1 μJ per pulse, repetition rate 10 kHz)

Superoxide production by TagRFP

Pulsed laser irradiation at 532 nm of a 14.5 μM solution of TagRFP in an air-saturated mixture of PBS, glycerol and deuterated (D)-PBS (1:1:20) in the presence of dihydroethidium, a superoxide probe, did not show any evidence of superoxide. As observed in the Inset of Fig. 5, the solution fluorescence was not affected by the presence of TagRFP.

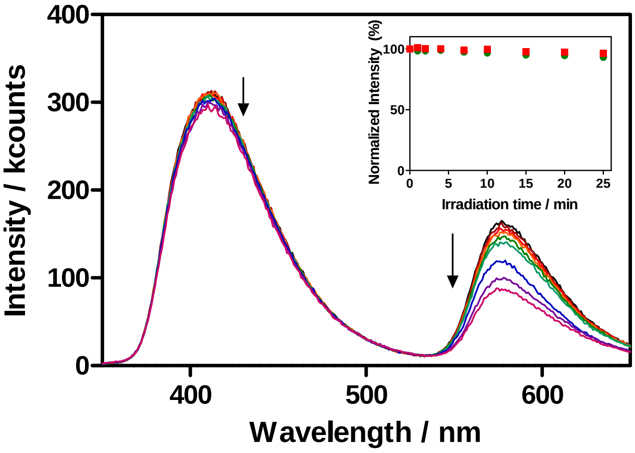

Fig. 5: Time course of the fluorescence spectra of dihydroethidium (DHE) and TagRFP in a PBS:Glycerol:D-PBS mixture (1:1:20) upon irradiation during 25 minutes with 1-ns laser pulses at 532 nm (*ca.* 1 µJ per pulse, repetition rate 10 kHz) Inset: Normalized fluorescence at 410 nm of a TagRFP solution with DHE (squares) and DHE alone (circles).

In order to demonstrate that the blue fluorescence exhibited by DHE in solution correlated with the amount of superoxide, a positive control was performed by adding different amounts of potassium superoxide to the DHE solution (Fig. 6).

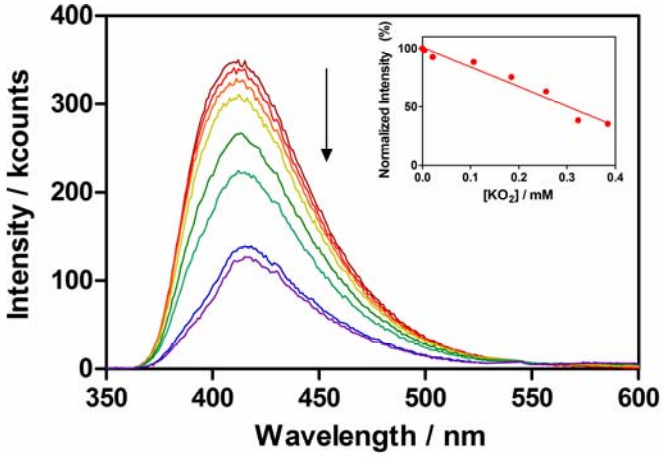

Fig. 6: Effect of KO_2 in the fluorescence spectrum of dihydroethidium in a PBS:Glycerol:D-PBS mixture (1:1:20) upon excitation at 330 nm. Inset: Normalized fluorescence intensity at 410 nm.

8.4. DISCUSSION

The main goal of this chapter was to assess the potential of TagRFP as a genetically-encoded PS for the production of reactive oxygen species. Thus, TRPD and SOSG as a $^1O_2$ fluorescent probe probed adequate to this respect.

Irradiation of TagRFP allowed the detection of $^1O_2$ phosphorescence, providing a 1.1 μs component that we attribute to $^1O_2$ and a 3 μs component due to the triplet state of TagRFP on account of all the experiments carried out. This counterintuitive kinetic inversion has been seen before for EGFP and indicates that $^1O_2$ is shorter-lived than its precursor, the FP triplet [11]. The lifetime of the triplet state of TagRFP is thus much shorter than that of EGFP (~25 μs) [11], suggesting better access of molecular oxygen to the chromophore inside the beta-barrel. The $^1O_2$ lifetime is also shorter than that in the case of EGFP (4 μs), which points to additional quenching by the chromophore or the aminoacids in close contact with it. It is worth noting that no signal was detected at other NIR wavelengths such as 1140 nm, ruling out other potential signal sources such as FP phosphorescence and, therefore, supporting the assignment of the signal to $^1O_2$ emission.

Photosensitisation of $^1O_2$ by TagRFP was further confirmed by trapping it with the specific fluorescent probe Singlet Oxygen Sensor Green (SOSG) [16,17]. The decrease and hypsochromic shift of the fluorescent band of TagRFP indicate that photobleaching and/or photoconversion of the FP may be occurring. Comparison of the slope in the SOSG fluorescence produced by TagRFP and by Rose bengal, as a reference [18], allows us to estimate a Φ_Δ value for TagRFP of 0.004 ± 0.001 after substracting (see *Annex*) the contribution of self-sensitised SOSG production of $^1O_2$ [17]. This value is, however, a lower limit of Φ_Δ, as only the $^1O_2$ that is able to escape the barrel and react with SOSG will be detected. However, diffusion of singlet oxygen, and presumably also $^1O_2$, across the β-barrel seems to be easier in TagRFP compared to EGFP, as suggested by the shorter triplet lifetime (*vide supra*). In any case, it is only the $^1O_2$ that does escape the barrel which is relevant in applications such as CALI.

The Φ_Δ estimated above for TagRFP is very similar to that measured for the EGFP fluorophore 4-hydroxybenzylidene-1,2-dimethylimidazoline (HBDI). Although it might be quite modest, it is certainly not insignificant. For comparison, EGFP photobleaches with a quantum yield of about 8 x 10^{-6} [19] and DsRed has two photobleaching processes with about 10^{-6} and 10^{-7} quantum yields [20]. This is the first estimation of Φ_Δ for a fluorescent protein.

We also tested if, like KillerRed, TagRFP was able to generate superoxide by using the probe dihydroethidium (DHE) [21,22] under the same conditions than the ones used for SOSG. No evidence of superoxide was found as the same effect produced upon photosensitisation of TagRFP was observed with DHE alone.

Nevertheless, it is possible to estimate the upper limit of the quantum yield of superoxide photosensitisation (Φ_{SO}) assuming that the decrease in the blue fluorescence band of DHE was due to its reaction with superoxide. Thus, Φ_{SO} is defined as the number of superoxide molecules produced per absorbed photon. By means of the number of photons given to TagRFP, the absorbance of the sample, and the calibration curve of the fluorescence decrease of DHE with KO_2, it is possible to estimate that $\Phi_{SO} < 0.0002$, one order of magnitude below Φ_Δ.

Given the results above, it is expected that TagRFP will be useful for CALI applications. This protein has excellent photophysical and biochemical properties, including high brightness, long lifetime, complete chromophore maturation and high pH stability [12,23]. More specifically, and in comparison with other FPs used for CALI such as EGFP, its longer excitation wavelength will minimize non-specific photodamage. This is important since high light intensities are needed in FP-CALI experiments. Another important advantage related to the latter point is that TagRFP has the highest two-photon excitation cross section and brightness of all orange and red FPs tested [24], which would be particularly useful for CALI. Multiphoton CALI has already been demonstrated with EGFP [25]. From the biochemical point of view, TagRFP is monomeric, as opposed to the dimeric KilledRed, and is thus a better fusion partner.

8.5. CONCLUSIONS

As discussed before [10,11], the interplay of several factors affects the efficiency of FP-CALI. The quantification of each factor is thus essential to understand and compare CALI effects. In this work, we have demonstrated that TagRFP is able to sensitise $^1O_2$ but it is not able to produce superoxide. Besides, we have quantified for the first time the amount of $^1O_2$ that is able to escape the barrel in TagRFP, providing a Φ_Δ value of 0.004. Moreover, we have shown that the FP triplet state lifetime can provide information about the oxygen accessibility of the chromophore.

Thus, our results provide important photophysical insight that allows the understanding of the mechanism behind CALI, and will aid to direct the evolution of new and more efficient mutants.

8.6. REFERENCES

1. Beermann AEL and Jay DG. Chromophore-assisted laser inactivation of cellular proteins. In: Methods in cell biology. San Diego: Academic press inc. **1994**: 715-732.

2. Jacobson K, Rajfur Z, Vitriol E, and Hahn K. Chromophore-assisted laser inactivation in cell biology. *Trends Cell Biol* **2008**; 18: 443-450.

3. Jay DG. Selective Destruction of Protein Function by Chromophore-Assisted Laser Inactivation. *Proc Natl Acad Sci USA* **1988**; 85: 5454-5458.

4. Liao JC, Roider J, and Jay DG. Chromophore-assisted laser inactivation of proteins is Mediated by the photogeneration of free-radicals. *Proc Natl Acad Sci USA* **1994**; 91: 2659-2663.

5. Rahmanzadeh R, Huttmann G, Gerdes J, and Scholzen T. Chromophore-assisted light inactivation of pKi-67 leads to inhibition of ribosomal RNA synthesis. *Cell Proliferation* **2007**; 40: 422-430.

6. Bulina ME, Chudakov DM, Britanova OV, Yanushevich YG, Staroverov DB, Chepurnykh TV, Merzlyak EM, Shkrob MA, Lukyanov S, and Lukyanov KA. A genetically encoded photosensitizer. *Nat Biotechnol* **2006**; 24: 95-99.

7. Serebrovskaya EO, Edelweiss EF, Stremovskiy OA, Lukyanov KA, Chudakov DM, and Deyev SM. Targeting cancer cells by using an antireceptor antibody-photosensitizer fusion protein. *Proc Natl Acad Sci USA* **2009**; 106: 9221-9225.

8. Carpentier P, Violot S, Blanchoin L, and Bourgeois D. Structural basis for the phototoxicity of the fluorescent protein KillerRed. *FEBS Lett* **2009**; 583: 2839-2842.

9. Pletnev S, Gurskaya NG, Pletneva NV, Lukyanov KA, Chudakov DM, Martynov VI, Popov VO, Kovalchuk MV, Wlodawer A, Dauter Z, and Pletnev V. Structural basis for phototoxicity of the genetically encoded photosensitizer KillerRed. *J Biol Chem* **2009**; 284: 32028-32039.

10. Mclean MA, Rajfur Z, Chen ZZ, Humphrey D, Yang B, Sligar SG, and Jacobson K. Mechanism of chromophore assisted laser inactivation employing fluorescent proteins. *Anal Chem* **2009**; 81: 1755-1761.

11. Jimenez-Banzo A, Nonell S, Hofkens J, and Flors C. Singlet oxygen photosensitization by EGFP and its chromophore HBDI. *Biophys J* **2008**; 94: 168-172.

12. Merzlyak EM, Goedhart J, Shcherbo D, Bulina ME, Shcheglov AS, Fradkov AF, Gaintzeva A, Lukyanov KA, Lukyanov S, Gadella TWJ, and Chudakov DM. Bright monomeric red fluorescent protein with an extended fluorescence lifetime. *Nat Methods* **2007**; 4: 555-557.

13. Shaner NC, Lin MZ, McKeown MR, Steinbach PA, Hazelwood KL, Davidson MW, and Tsien RY. Improving the photostability of bright monomeric orange and red fluorescent proteins. *Nat Methods* **2008**; 5: 545-551.

14. van Thor JJ, Gensch T, Hellingwerf KJ, and Johnson LN. Phototransformation of green fluorescent protein with UV and visible light leads to decarboxylation of glutamate 222. *Nat Struct Biol* **2002**; 9: 37-41.

15. Bell AF, Stoner-Ma D, Wachter RM, and Tonge PJ. Light-driven decarboxylation of wild-type green fluorescent protein. *J Am Chem Soc* **2003**; 125: 6919-6926.

16. Flors C, Fryer MJ, Waring J, Reeder B, Bechtold U, Mullineaux PM, Nonell S, Wilson MT, and Baker NR. Imaging the production of singlet oxygen in vivo using a new fluorescent sensor, Singlet Oxygen Sensor Green$^{®}$. *J Exp Bot* **2006**; 57: 1725-1734.

17. Ragas X, Jimenez-Banzo A, Sanchez-Garcia D, Batllori X, and Nonell S. Singlet oxygen photosensitisation by the fluorescent probe Singlet Oxygen Sensor Green (R). *Chem Commun* **2009**; 2920-2922.

18. Redmond RW and Gamlin JN. A compilation of singlet oxygen yields from biologically relevant molecules. *Photochem Photobiol* **1999**; 70: 391-475.

19. Peterman EJG, Brasselet S, and Moerner WE. The fluorescence dynamics of single molecules of green fluorescent protein. *J Phys Chem A* **1999**; 103: 10553-10560.

20. Lounis B, Deich J, Rosell FI, Boxer SG, and Moerner WE. Photophysics of DsRed, a red fluorescent protein, from the ensemble to the single-molecule level. *J Phys Chem B* **2001**; 105: 5048-5054.

21. Wardman P. Fluorescent and luminescent probes for measurement of oxidative and nitrosative species in cells and tissues: Progress, pitfalls, and prospects. *Free Rad Biol Med* **2007**; 43: 995-1022.

22. Gomes A, Fernandes E, and Lima JLFC. Fluorescence probes used for detection of reactive oxygen species. *J Biochem Biophys Methods* **2005**; 65: 45-80.

23. Day RN and Davidson MW. The fluorescent protein palette: tools for cellular imaging. *Chem Soc Rev* **2009**; 38: 2887-2921.

24. Drobizhev M, Tillo S, Makarov NS, Hughes TE, and Rebane A. Absolute two-photon absorption spectra and two-photon brightness of orange and red fluorescent proteins. *J Phys Chem B* **2009**; 113: 855-859.

25. Tanabe T, Oyamada M, Fujita K, Dai P, Tanaka H, and Takamatsu T. Multiphoton excitation-evoked chromophore-assisted laser inactivation using green fluorescent protein. *Nat Methods* **2005**; 2: 503-505.

8.7. Annex

Correction of quantum yield of singlet oxygen production

The Φ_Δ value was determined by comparison of the slope in the fluorescence intensity of SOSG produced by optically matched solutions of TagRFP and a reference, Rose Bengal, under the same conditions, namely with the same amount of SOSG and in the same solvent mixture (Eq. 1).

$$\Phi'_\Delta(\mathrm{TagRFP}) = \frac{\mathrm{Slope}_{\mathrm{TagRFP}}}{\mathrm{Slope}_{\mathrm{ref}}} \cdot \Phi'_\Delta(\mathrm{ref}) \quad (1)$$

$$\Phi'_\Delta(\mathrm{sample}) = \frac{A^{532}_{\mathrm{Sample}}}{A^{532}_{\mathrm{Total}}} \cdot \Phi_\Delta(\mathrm{sample}) + \frac{A^{532}_{\mathrm{SOSG}}}{A^{532}_{\mathrm{Total}}} \cdot \Phi_\Delta(\mathrm{SOSG}) \quad (2)$$

As it has been demonstrated that SOSG is able to self-sensitise singlet oxygen, and the absorption at 532 nm due to SOSG was not negligible (Fig. A1), Eq (2) was used to calculate the corrected singlet oxygen quantum yield (Φ'_Δ):

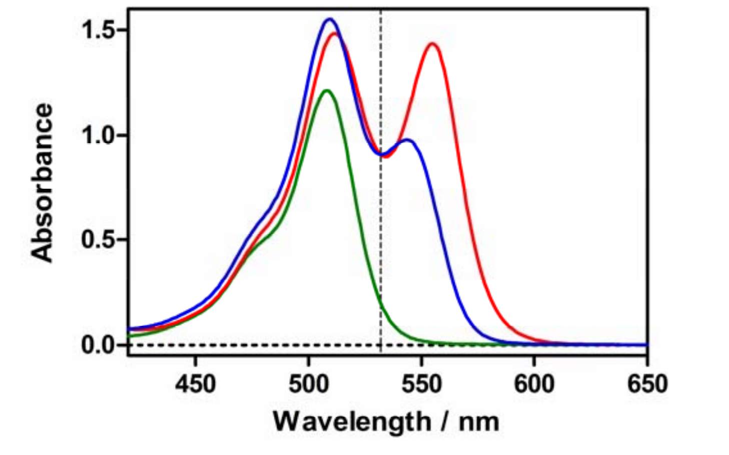

Fig. A1: Absorption spectra of the solutions used to quantify the singlet oxygen quantum yield: TagRFP with SOSG (red), Rose Bengal with SOSG (blue) and SOSG alone (green).

Chapter 9

Singlet oxygen enhancement by silver islands films

Metallic surfaces, colloids and islands are able to induce significant changes on the emissive rates of organic species. Thus, processes such as metal-enhanced fluorescence or phosphorescence have been described. In this chapter, we investigate the ability of silver island films to induce a plasmonic effect on singlet oxygen using time-resolved detection of the NIR phosphorescence of $^1O_2$.

The work described in this chapter will be submitted for publication to *Chem Mater* in collaboration with Prof. Chris D. Geddes laboratory's results. Manuscript in preparation.

9.1. INTRODUCTION

Singlet molecular oxygen ($^1O_2$) is a reactive oxygen species (ROS) involved in a variety of biological processes and known by its high reactivity with many cellular components [1]. This makes its detection important in order to gain insights into the mechanism of $^1O_2$-based clinical therapies such as photodynamic therapy (PDT) [2,3]. Many different possibilities have been reported to indirectly detect singlet molecular oxygen, including EPR spectroscopy using spin traps [4], chemical trapping [5], and fluorescent probes [6-8]. However, the most unambiguous way to detect is by monitoring its phosphorescence at 1270 nm [9], which is very weak because the overall deactivation is overwhelmingly dominated by non-radiative pathways, invariably providing for an extremely low phosphorescence quantum yield [10].

$^1O_2$ is commonly produced *via* photosensitization processes. Thus, the electronically-excited states of the photosensitiser (PS), produced upon light absorption, are efficiently quenched by molecular oxygen, particularly the longer-lived triplet state. Energy transfer between the two species results in the production of $^1O_2$ as outlined in the following scheme:

$$PS + h\nu \rightarrow {}^1PS^*$$
$${}^1PS^* \rightarrow {}^3PS^*$$
$${}^3PS^* + {}^3O_2 \rightarrow PS + {}^1O_2$$

Over the last years, it has been demonstrated that metallic surfaces, including colloids and islands are able to induce significant changes on the emissive rates of organic species [11]. Thus, processes such as metal-enhanced fluorescence (MEF) [12] and metal-enhanced phosphorescence (MEP) [13,14] have been described. Such effects can be explained by a non-radiative energy transfer from excited distal luminophores to the surface plasmon electrons in non-continous films, followed by radiation of the photophysical characteristics of the coupling luminophores by the surface plasmons themselves [15]. Therefore, the application of the plasmon-coupling effect in the generation and emission of $^1O_2$ is interesting and potentially important for $^1O_2$ direct detection.

Different strategies can be used to enhance the $^1O_2$ production. On the one hand, Toftegaard *et al.* [16] reported an enhancement factor of 3.5 of the radiative rate of $^1O_2$ by means of gold nanodiscs of a controlled size coated with polystyrene doped with tetraphenylporphyrine as PS. On the other hand, Zhang *et al.* [17] demonstrated that the extent of $^1O_2$ enhancement produced by silver island films (SIFs) is inversely proportional to the free space in the $^1O_2$ quantum yield (Φ_Δ), a direct result of MEP and the ability of surface plamons to pump triplet states and subsequently generate more $^1O_2$. Interestingly, the extent of $^1O_2$ generation falls off exponentially with distance from the surface, suggesting that an enhanced excitation rate (enhanced absorbance cross-section) is the underlying mechanism for enhanced $^1O_2$ generation [18].

Thus, the goal of this study is to provide direct evidence of the plasmonic effect caused by SIFs of different sizes on the $^1O_2$ production by means of time-resolved singlet oxygen luminescence detection.

9.2. EXPERIMENTAL SECTION

Materials

Silver island films were prepared by Prof. Chris D. Geddes *et al.* of the University of Maryland Biotechnology Institute by means of the protocol described in [12].

Fullerene (C_{60}) and carbon disulfide were purchased in Sigma-Aldrich Co. (St. Louis, MO, USA). The C_{60} films were formed by means of a KW-4A Spin Coater (SPI Supplies, West Chester, PA, USA) at 4000 rpm for 50 s.

Statistics

Values are expressed as means ± standard error of the mean (SEM) of three independent samples.

9.3. RESULTS

SIFs characterization

Different SIFs were produced at different formation times. In all cases SIFs exhibited a plasmonic band *ca.* 380 nm, whose absorption maxima and intensity shifted hypsochromically and increased concomitantly when the formation time was increased. Both of them showed a similar trend as observed in the inset of Fig. 1A. These observations were reported recently, for different size silver-islands providing for a range of conditions for MEF [19].

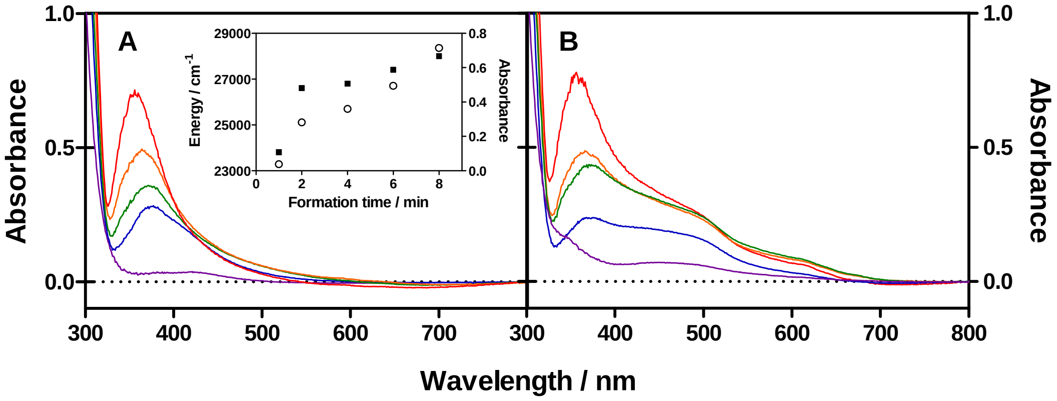

Fig. 1: (A) Absorption spectra of silver island films (SIFs) at 1 (violet), 2 (blue), 4 (green), 6 (orange) and 8 (red) min formation times. Inset: Energy (squares) and absorbance (circles) of the maximum of absorption at each formation time. **(B)** Absorption spectra of the same SIFs spin-coated with C_{60} from a 3 mg·mL^{-1} solution. The spectra are not the simple sum of the individual SIF and C_{60} spectra.

When a C_{60} film was coating the SIFs, the absorption spectra changed significantly, showing a new band at *ca.* 500 nm, whose absorption did not correlate with the sum of the absorption of C_{60} plus the absorption of SIFs (Fig. 1B), but is in fact thought due to the change in refractive index above the SIFs by the sample.

Singlet oxygen production by a C_{60} film

Fig. 2 shows the time-resolved $^1O_2$ phosphorescence produced by a C_{60} film on a quartz slide. As observed, the atmosphere that surrounded the sample strongly affected the phosphorescence signal produced by $^1O_2$ modifying the intensity. The spectrum of the signal clearly demonstrated that the transient observed is due to $^1O_2$. The decays kinetics are multiexponential, requiring typically three exponential terms to provide acceptable fits.

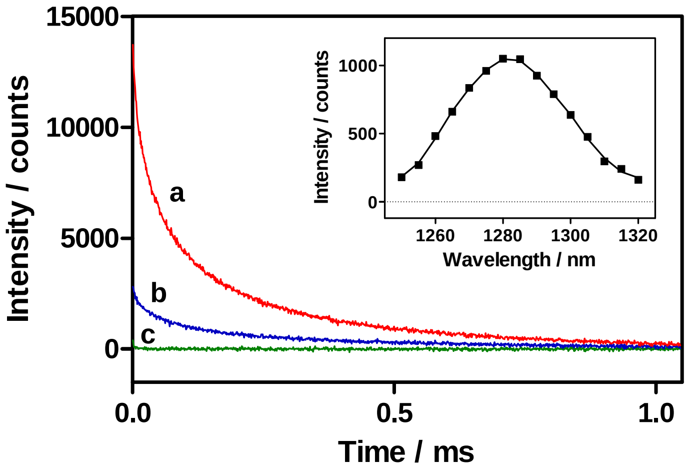

Fig. 2: Singlet oxygen phosphorescence at 1270 nm photosensitized by a C_{60} film on a quartz slide. **(a)** Oxygen-saturated atmosphere. **(b)** Air-saturated atmosphere. **(c)** Argon-saturated atmosphere. Inset: Spectral distribution of the photoluminescence, which matches the phosphorescence spectrum of singlet oxygen.

Effect of the concentration of C_{60}

Different concentrations of C_{60} ranging from 0.5 to 5 mg·mL^{-1} were tested in the $^1O_2$ measurements. As observed in Fig. 3A, the decay kinetics were not affected by the amount of C_{60}, as no significant change was observed in the lifetime values. With regards to the intensity of the signal, as observed in Fig. 3B, the phosphorescence signal produced by C_{60} on glass slides increases with the C_{60} concentration concomitantly. However, when the signal is produced on SIFs, a significant intensity enhancement is observed, , the enhancement clearly decreasing from a 32-fold factor to a 7-fold factor when the amount of C_{60} is increased (Fig. 3C).

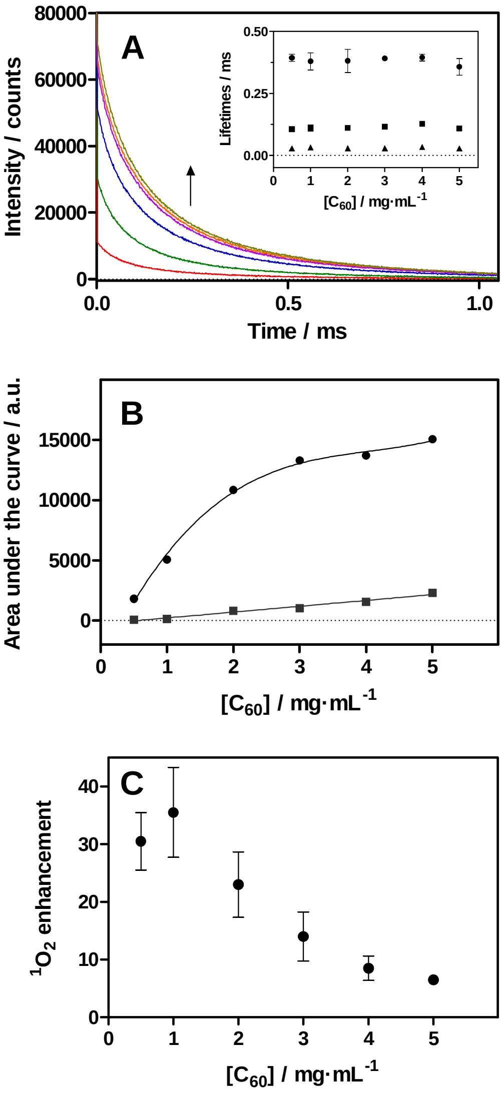

Fig. 3: Effect of the concentration of C_{60} (0.5, 1, 2, 3, 4, and 5 mg·mL^{-1}) on the 1270-nm singlet oxygen phosphorescence from silver islands films. **(A)** Singlet oxygen kinetics on a 2 min silver island film at increasing concentrations of C_{60}. Inset: Lifetimes of the three components observed for the singlet oxygen luminescence signals. **(B)** Area under the singlet oxygen luminescence curves (circles). Values for C_{60} films on glass slides without silver islands are shown for comparison (squares). **(C)** Enhancement of the singlet oxygen luminescence signal observed with increasing concentrations of C_{60}

Effect of SIFs' formation time

The formation time and experimental conditions determines the size of the SIFs' nanoparticle [19]. SIFs with different sizes were obtained for deposition times ranging from 1 to 8 min. As observed in Fig. 4A, the $^1O_2$ phosphorescence signal produced by C_{60} on SIFs shows an emission maximum for SIFs with 2 min formation time. In addition, the decay kinetics showed no correlation with the nanoparticle size.

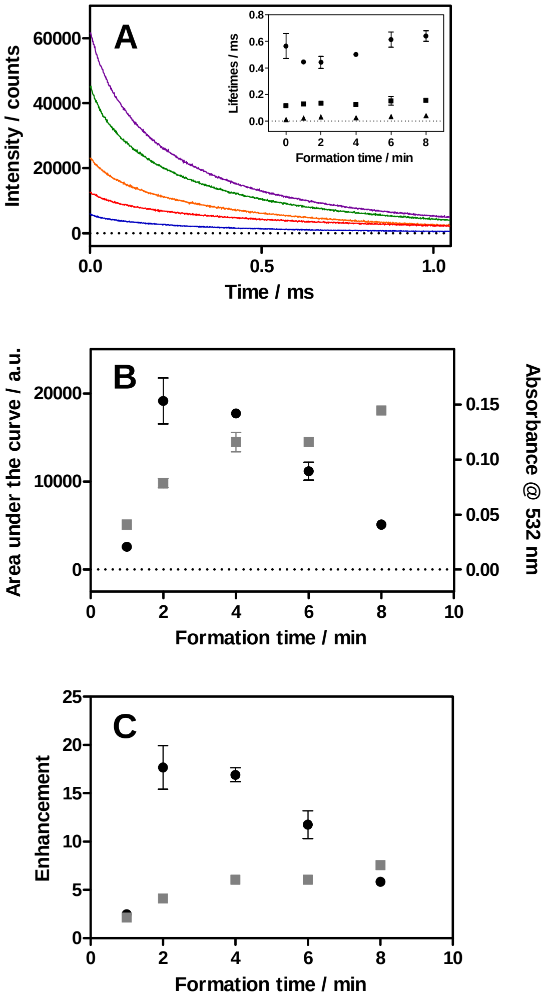

Fig. 4: Effect of the silver island size on the singlet oxygen luminescence**. (A)** Singlet oxygen kinetics as a function of the silver island formation time: 1 min (blue), 2 min (violet), 4 min (green), 6 min (orange), and 8 min (red). The concentration of C_{60} was 3 mg·mL^{-1}. Inset: Lifetimes of the three components observed for the singlet oxygen luminescence signals. **(B)** Area under the singlet oxygen luminescence curves (circles) and absorbance of C_{60} at 532 nm (squares) with SIFs at different formation times with a 3 mg·mL^{-1} concentration of C_{60}. **(C)** Enhancement of the singlet oxygen luminescence signal (circles) and the absorption at 532 nm (squares) observed with SIFs at different formation times with a 3 mg·mL^{-1} concentration of C_{60}.

As observed in Fig. 4B, the absorption of C_{60} at 532 nm and the $^1O_2$ luminescence intensity does not correlate with the SIFs' size either. When compared to the signal produced by a C_{60} film alone, a maximum in the $^1O_2$ enhancement factor is observed at 2 min formation time with a value *ca.* 18-fold, close to the one observed with the 4 min SIFs (Fig. 4C). With regard to the absorption at 532 nm of C_{60}, the trend is significantly different and the signal increases with the SIFs formation time up to *ca.* a 7-fold increment for the 8 min SIFs.

Stability and reproducibility

The stability of the samples was measured as a function of the irradiation cycles with the same C_{60} film. Fig. 5A shows the stability of the $^1O_2$ luminescence signal produced upon irradiation of a C_{60} film with and without SIFs. When the signal produced by a C_{60} film is measured, the signal is stable and no trend is observed when increasing the irradiation cycles of the same film. However, in the presence of SIFs, the higher the number of irradiation cycles, the lower the signal.

With regard to the reproducibility of the luminescence measurements with SIFs (Fig. 5B), there is not any trend in the signal, demonstrating that they can be reused because there is not any degradation of the SIFs when the irradiation cycles are increased.

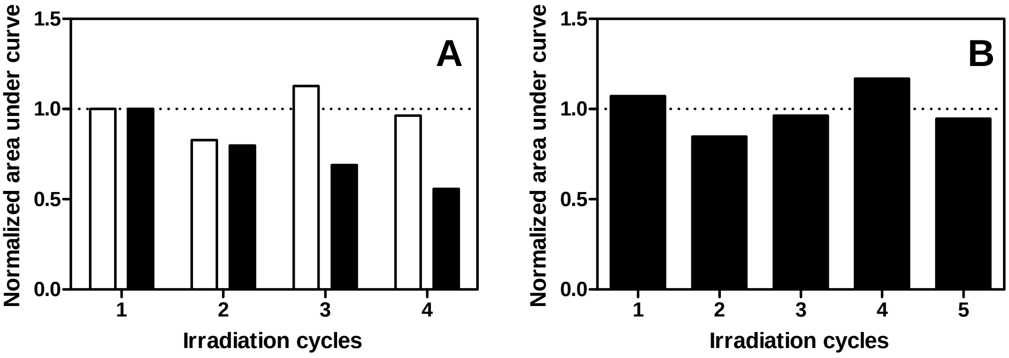

Fig. 5: Stability and reproducibility of the singlet oxygen luminescence produced by C_{60}-coated SIFs. **(A)** Normalized area under the decay curve *vs.* number of irradiation cycles (5 minutes each) for C_{60} films coated on glass slides (white) or silver islands (black). **(B)** Same as in panel **A** but with a C_{60} film freshly coated after each cycle.

9.4. DISCUSSION

C_{60} is a well-known photosensitizer with a quantum yield of $^1O_2$ production (Φ_Δ) upon excitation at 532 nm *ca.* 1 in solution and, consequently, a triplet quantum yield close to 1 [20]. However, in films, the intensity depends markedly on the concentration of oxygen, suggesting an inefficient trapping of the precursor triplet excited state of C_{60} in air-saturated films and, consequently, a reduction of Φ_Δ.

As demonstrated with Fig. 3C and 4C, the $^1O_2$ phosphorescence signal produced by a C_{60} film is significantly enhanced. According to the photosensitization mechanism of $^1O_2$ formation, the potential causes for an increased $^1O_2$ phosphorescence can be: (1) an enhanced plasmon-induced absorption by C_{60}, (2) an enhanced intersystem crossing from the singlet excited-state to the triplet excited-state of C_{60}, or (3) an enhanced metal-PS coupled system radiative decay of $^1O_2$.

According to our results, the $^1O_2$ enhancement observed is partially due to an enhanced plasmon-induced absorption by C_{60}. The absorption at 532 nm produced by a 3 $mg \cdot mL^{-1}$ C_{60} film on SIFs does not correlate with the sum of the absorption due to C_{60} film alone plus the absorption due to SIFs. Thus, the C_{60} absorption enhancement factor increases hyperbolically with the SIFs formation time up to 7-fold (8 min SIFs formation time). Such an increase in the absorption of C_{60} should lead to a similar increase in the fluorescence signal. Some attempts of measuring the weak fluorescence exhibited by the C_{60} films -fullerene shows a fluorescent quantum yield *ca.* 3×10^{-4} in different solvents [21]- were made but no fluorescence, neither on SIFs nor on glass slides, was observed around 750 nm.

Therefore, an additional explanation of the $^1O_2$ enhancement factor is considered. Assuming that the triplet quantum yield of C_{60} films is still close to 1, an enhanced intersystem crossing might be excluded.

The fact that the $^1O_2$ enhancement factor vs. SIFs formation time curve shows a maximum might be explained by a compromise between two antagonic effects. On one hand, the intensity of the plasmon increases at higher deposition times, which would result in an increase of the plasmon-induced absorption by C_{60}. On the other hand, the energy of the plasmon increases at higher deposition times and therefore becomes less resonant to the $S_0 \rightarrow S_1$ absorption transition of C_{60}, reducing it.

In addition, it has been previously reported by means of FDTD calculations that the plasmonic coupling and enhancing effects are extended only through a few nanometers from the nanoparticle [17]. This is consistent with our results with increasing concentrations of C_{60}, where a decrease in the enhancement is observed at high C_{60} concentrations, induced by larger distances of the C_{60} molecules to the SIFs as additional C_{60} layers are being deposited in the solid phase samples.

Finally, it is interesting to comment on why the extent of $^1O_2$ decreases when the irradiation cycles are increased. At first one may consider the oxidation of SIFs and the expected loss of Plasmon resonance to be the explanation. However, as shown in Fig. 5B, fresh coatings of C_{60} films provide for very similar extents of $^1O_2$ generation. Subsequently, this suggests that the surface remains unperturbed and that $^1O_2$ decreases as the number of cycles is increased, due to C_{60} film photophysics, such as self photo oxidation. Given the enhanced absorption cross-sections, coupled with the significant generation of $^1O_2$, then this result is not surprising.

9.5. CONCLUSIONS

We have demonstrated that silver nanoparticles are able to enhance the $^1O_2$ luminescence signal produced by C_{60} films with a maximum increase *ca.* 35-fold, obtained with the 2 min formation time SIF and with a C_{60}-concentration of 1 mg·mL^{-1}.

As deduced from our results, the effect is partially mediated by an enhanced plasmon-induced absorption of C_{60}, which increases at higher SIFs formation times, and by an enhanced radiative decay of $^1O_2$.

Such effect is interesting to be used both in the $^1O_2$ detection field, *i.e.*, allowing the measurements of $^1O_2$ kinetics in shorter periods of time, or even opening the possibility to boost the detection of this reactive oxygen species *in vivo*, and in the photodynamic therapy field, allowing a reduction of the light-dose or the drug-dose in APDT treatments, or increasing the effectiveness of commonly used PSs by conjugation of nanoparticles with ability to produce such plasmonic effect with commonly used photosensitisers.

9.6. REFERENCES

1. Wilkinson F, Helman WP, and Ross AB. Rate constants for the decay and reactions of the lowest electronically excited singlet state of molecular oxygen in solution. An expanded and revised compilation. *J Phys Chem Ref Data* **1995**; 24: 663-1021.

2. Jimenez-Banzo A, Sagrista ML, Mora M, and Nonell S. Kinetics of singlet oxygen photosensitization in human skin fibroblasts. *Free Rad Biol Med* **2008**; 44: 1926-1934.

3. Ragàs X, Agut M, and Nonell S. Singlet oxygen in *E. coli*: new insights for antimicrobial photodynamic therapy. *Free Rad Biol Med* **2010**; 49: 770-776.

4. Hideg E, Spetea C, and Vass I. Singlet oxygen production in thylakoid membranes during photoinhibition as detected by EPR spectroscopy. *Photosynth Res* **1994**; 39: 191-199.

5. Telfer A, Bishop SM, Phillips D, and Barber J. Isolated photosynthetic reaction-center of photosystem-II as a sensitizer for the formation of singlet oxygen - Detection and quantum yield determination using a chemical trapping technique. *J Biol Chem* **1994**; 269: 13244-13253.

6. Ragàs X, Jimenez-Banzo A, Sánchez-García D, Batllori X, and Nonell S. Singlet oxygen photosensitisation by the fluorescent probe Singlet Oxygen Sensor Green®. *Chem Commun* **2009**; 2920-2922.

7. Flors C, Fryer MJ, Waring J, Reeder B, Bechtold U, Mullineaux PM, Nonell S, Wilson MT, and Baker NR. Imaging the production of singlet oxygen in vivo using a new fluorescent sensor, Singlet Oxygen Sensor Green®. *J Exp Bot* **2006**; 57: 1725-1734.

8. Tanaka K, Miura T, Umezawa N, Urano Y, Kikuchi K, Higuchi T, and Nagano T. Rational design of fluorescein-based fluorescence probes. Mechanism-based design of a maximum fluorescence probe for singlet oxygen. *J Am Chem Soc* **2001**; 123: 2530-2536.

9. Jimenez-Banzo A, Ragàs X, Kapusta P, and Nonell S. Time-resolved methods in biophysics. 7. Photon counting vs. analog time-resolved singlet oxygen phosphorescence detection. *Photochem Photobiol Sci* **2008**; 7: 1003-1010.

10. Schweitzer C and Schmidt R. Physical mechanisms of generation and deactivation of singlet oxygen. *Chem Rev* **2003**; 103: 1685-1757.

11. Lakowicz JR. Radiative decay engineering: Biophysical and biomedical applications. *Anal Biochem* **2001**; 298: 1-24.

12. Geddes CD and Lakowicz JR. Metal-enhanced fluorescence. *J Fluorescence* **2002**; 12: 121-129.

13. Zhang YX, Aslan K, Malyn SN, and Geddes CD. Metal-enhanced phosphorescence (MEP). *Chem Phys Lett* **2006**; 427: 432-437.

14. Zhang YX, Aslan K, Previte MJR, Malyn SN, and Geddes CD. Metal-enhanced phosphorescence: Interpretation in terms of triplet-coupled radiating plasmons. *J Phys Chem B* **2006**; 110: 25108-25114.

15. Lakowicz JR. Radiative decay engineering 5: metal-enhanced fluorescence and plasmon emission. *Anal Biochem* **2005**; 337: 171-194.

16. Toftegaard R, Arnbjerg J, Daasbjerg K, Ogilby PR, Dmitriev A, Sutherland DS, and Poulsen L. Metal-enhanced 1270 nm singlet oxygen phosphorescence. *Angew Chem Int Ed* **2008**; 47: 6025-6027.

17. Zhang Y, Aslan K, Previte MJR, and Geddes CD. Plasmonic engineering of singlet oxygen generation. *Proc Natl Acad Sci USA* **2008**; 105: 1798-1802.

18. Geddes CD. Metal-enhanced fluorescence: Progress towards a unified plasmon fluorophore description. In: Metal-enhanced fluorescence. New Jersey: John Wiley and Sons. **2010**: 1-24.

19. Pribik R, Dragan AI, Zhang Y, Gaydos C, and Geddes CD. Metal-Enhanced Fluorescence (MEF): Physical characterization of Silver-island films and exploring sample geometries. *Chem Phys Lett* **2009**; 478: 70-74.

20. Arbogast JW, Darmanyan AP, Foote CS, Rubin Y, Diederich FN, Alvarez MM, Anz SJ, and Whetten RL. Photophysical properties of C_{60}. *J Phys Chem* **1991**; 95: 11-12.

21. Ma B and Sun Y-P. Fluorescence spectra and quantum yields of [60] fullerene and [70] fullerene under different solvent conditions. A quantitative examination

using a near-infrared-sensitive emission spectrometer. *J Chem Soc Perkin Trans 2* **1996**; 2157-2162.

Chapter 10

General Discussion

An overall discussion of the work described in the previous chapters is given. The implications in antimicrobial photodynamic therapy, and some suggestions for future research in this field are given in this chapter.

10.1. DISCUSSION

On the basis of the work presented in the previous chapters, we have gained insight into three different questions that need to be answered when a therapy is proposed: (1) does it work, (2) how does it work, and (3) what can we do to improve it.

With regards to the first question, the answer has been divided into two different sections. On the one hand, one of the main advantages of APDT, discussed in *Chapter 1,* is that it is able to inactivate even pandrug- or multidrug-resistant bacterial strains under similar conditions than those used for “typical” bacterial strains [1,2]. So, we have performed some *in vitro* and *in vivo* studies against *A. baumanii,* one of these “superbugs”, observing that NMB is the most active dye among all tested phenothiazinium dyes. However, only MB and TBO, the PSs with the lowest inactivation efficiency, are actually being used in APDT agents in clinical applications. These results support the idea expressed by Garland *et al.* that many of the APDT agents used in the clinical practice may not be the most appropriate within a given class [3]. Therefore, based on the efficacy pattern obtained in this study, we propose to clinically test NMB as a potential PS against a wide range of localized infections. Besides, we have demonstrated that, in the *in vivo* studies*,* it is interesting to give an extra dose of light in order to preclude the regrowth of the infection, one of the most important problems found for APDT [4].

On the other hand, it is also interesting that the PSs used in APDT can act against a wide range of microbial infections [5]. Our group has focused its interest in the porphycene family. Since the synthesis of the first porphycene in 1986 [6], a variety of substituted derivatives have been prepared, including the 2,7,12,17-tetraphenylporphycene [7], as well as several of its metal-ion complexes [8]. However, it has not been possible until now to synthesize the first aryl cationic porphycene in order to test it as an APDT agent. Caminos *et al.* showed that, in porphyrins with cationic (A) and non-cationic (B) groups, the photosensitized inactivation of *E. coli* cellular suspensions follows the order: $A_3B^{3+} > A_4^{4+} >> ABAB^{2+} > AB_3^{+}$ [9]. Therefore, we decided to perform the inactivation experiments with a porphycene molecule following the structure A_3B^{3+}. Thus, as shown in *Chapter 4*, aryl cationic porphycenes can be used as potential PSs in APDT against a wide range of microbial cells such as gram-positive bacteria, gram-negative bacteria and fungal cells. Indeed, it has been successfully used *in-vivo* against MRSA.

Nevertheless, as this is only the first step in the development of porphycene compounds as APDT agents, it would probably be interesting to synthesize and test new porphycene compounds with (a) a higher number of cationic charges, as it has been demonstrated with cationic fullerenes that the higher number of charges, the higher inactivation of bacterial strains such as *P. aeruginosa* [10], or (b) hydrocarbon chains of different length on the amino nitrogens [11], as alkyl are not as rigid as pyridyl groups and may affect the kinetics and extent of binding with microbial cells [5].

Some answers to the second question, “how does it work?”, have been found by means of a mechanistic study performed with paradigm PS representative of the different families used in APDT, and a gram-negative bacterium such as *E. coli*. This study has been possible as the state of the art for $^1O_2$ phosphorescence detection has improved during the last years [12]. Three main conclusions have been found to this respect.

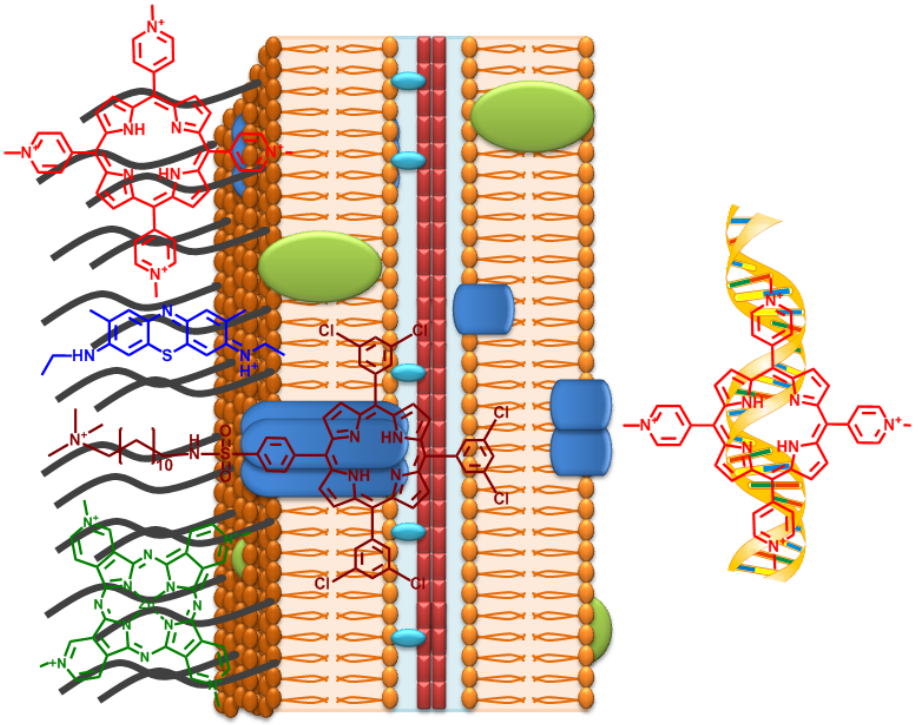

Fig. 1: Pictorial representation of the localization of the model PSs used in the mechanistic study: TMPyP (red); NMB (blue); ACS268 (maroon); ZnTMPyPz (green).

Firstly, it is worth noting that it has been difficult to assess the localization of PSs in APDT as, because of the bacterial size –in the range of 1-10 µM– and the resolution of current microscopes, it is not possible to use fluorescence microscopy as for eukaryotic cells [13]. Thus, we present a combination of spectroscopic and time-resolved photophysical techniques that can be used as an alternative to ascertain the localization of the PSs. As observed in *Chapters 5 and 6* (Fig. 1), we found that PSs with charged photoactive centers –TMPyP, NMB and ZnTMPyPz– localize in the external structure of the cell wall, accessible to external proteins such as BSA. Additionally, it has also been observed that TMPyP is partially internalized, therefore having a second location inside the cell, bound to the nucleic acids. However, when the cationic charge is far from the photoactive center –ACS268– a different localization is observed, suggesting an oxygen-shielded position, namely inside the outer membrane.

Secondly, the production and fate of $^1O_2$ clearly depend on the PS internalization and localization, thereby on the PS structure. Two different scenarios have been observed. While the $^1O_2$ produced in the outer structure of the cell wall by TMPyP and NMB is mainly deactivated by the aqueous phase (τ_Δ ~ 67 µs in D-PBS), equilibrium between cell-deactivation and solvent-deactivation pathways is suggested for ACS268 in order to explain the singlet oxygen kinetics (τ_Δ ~ 5 µs in D-PBS; Fig. 2). Thus, in order to increase the singlet oxygen reactive efficiency with cellular components, it may be interesting to develop asymmetric compounds where the hydrophilic and hydrophobic (chromophore) parts of the structure can be differentiated.

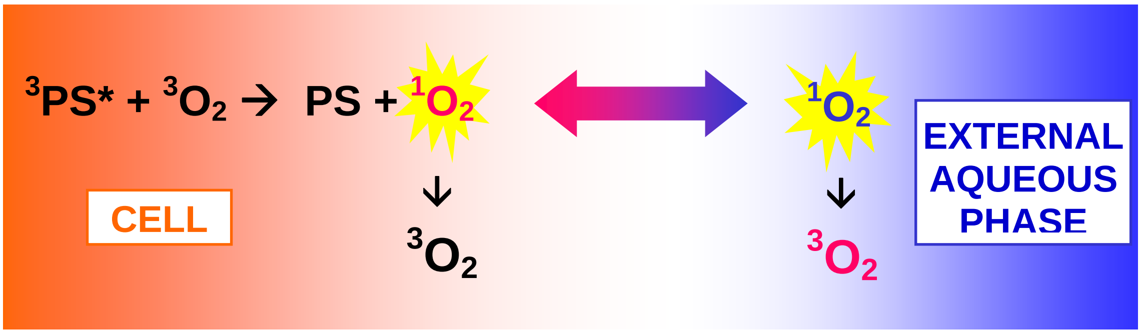

Fig. 2: Proposed mechanism for the $^1O_2$ formation and decay in *E. coli*.

Likewise, we have demonstrated that $^1O_2$ is able to cross the bacterial cell wall and move “freely” within the cell. Thus, as shown in *Chapter 5*, $^1O_2$ produced by both localizations of TMPyP is mainly deactivated by the external aqueous phase, as observed upon addition of BSA and when the experiments where performed in *E. coli* spheroplasts. This is an important conclusion as some evidences had been previously described in eukaryotic cells [14,15] but not in prokaryotic cells. Additionally, strengths the view that APDT is not likely to develop resistance in microorganisms as it provides direct evidence for the observation that the PS does not need to be internalized for inflicting photodamage on vital structures of the cell [16].

The third question refers to the future directions of APDT. As mentioned in *Chapter 1*, a possible direction, still in its initial steps, is the development of genetically-encoded PS. In 2006, Bulina *et al.* demonstrated the utility of Killer Red for light-induced killing of *E. coli* and eukaryotic cells [17]. Since then, the research and development of new GFP-mutants with optimal structure and properties to produce ROS has increased. Our group reported in 2008, the Φ_Δ value of HBDI, the GFP-chromophore, and the kinetics of $^1O_2$ production by EGFP. However, it was not possible to estimate the Φ_Δ value for EGFP using time-resolved detection of the NIR phosphorescence of $^1O_2$.

An alternative detection method is the use of fluorescent probes such as SOSG to detect ROS species [18,19]. However, as demonstrated in *Chapter 7*, care must be taken when using it, as it is able to self-sensitise $^1O_2$ in the absence of external photosensitisers, under exposure to either UV or, to a lesser extent, visible radiation. It is therefore important to measure negative controls when using SOSG to detect small amounts of $^1O_2$, as false-positive results can be obtained, especially in combination with UV light sources.

The knowledge of this fluorescent probe has been used in our studies with red fluorescent proteins. The clear oxygen dependence in the photobleaching curves shown by TagRFP caught our attention [20]. Thus, as shown in *Chapter 8,* TagRFP is able to photosensitise $^1O_2$ with a Φ_Δ value of 0.004, similar to the one shown by HBDI in basic-D_2O [21]. To our knowledge, this is the first estimation of a Φ_Δ value for a GFP-like photosensitiser. Likewise, it only represents a minimum value for Φ_Δ, as only the $^1O_2$ that escapes from the β-can reacts with SOSG.

A possible future improvement in APDT may be the use of the plasmonic effect produced by silver nanoparticles in two different topics. On the one hand, a 35-fold increase in the $^1O_2$ luminescence signal may be interesting to increase the detection limit of $^1O_2$ with the current methods, therefore, allowing the measurements of $^1O_2$ kinetics in shorter periods of time, or even opening the possibility to boost the detection of this reactive oxygen species *in vivo*. On the other hand, as there is an enhancement effect in the absorption of the PS, the photosensitisation of ROS may be increased, allowing a reduction of the light-dose or the drug-dose in APDT treatments, or increasing the effectiveness of commonly used PSs. In this regard, Narband *et al.* recently demonstrated that gold nanoparticles enhance the antimicrobial effectiveness of Toluidine blue O [22].

10.2. REFERENCES

1. Maisch T. A new strategy to destroy antibiotic resistant microorganisms: antimicrobial photodynamic treatment. *Mini-Rev Med Chem* **2009**; 9: 974-983.

2. Tang HM, Hamblin MR, and Yow CM. A comparative *in vitro* photoinactivation study of clinical isolates of multidrug-resistant pathogens. *J Infect Chemother* **2007**; 13: 87-91.

3. Garland MJ, Cassidy CM, Woolfson D, and Donnelly RF. Designing photosensitizers for photodynamic therapy: strategies, challenges and promising developments. *Fut Med Chem* **2009**; 1: 667-691.

4. Hamblin MR and Hasan T. Photodynamic therapy: a new antimicrobial approach to infectious disease? *Photochem Photobiol Sci* **2004**; 3: 436-450.

5. Jori G, Fabris C, Soncin M, Ferro S, Coppellotti O, Dei D, Fantetti L, Chiti G, and Roncucci G. Photodynamic therapy in the treatment of microbial infections: Basic principles and perspective applications. *Lasers Surg Med* **2006**; 38: 468-481.

6. Vogel E, Kocher M, Schmickler H, and Lex J. Porphycene - A novel porphin isomer. *Angew Chem Int Ed Engl* **1986**; 25: 257-259.

7. Nonell S, Bou N, Borrell JI, Teixido J, Villanueva A, Juarranz A, and Canete M. Synthesis of 2,7,12,17-tetraphenylporphycene (TPPo) - First aryl-substituted porphycene for the photodynamic therapy of tumors. *Tetrahedron Lett* **1995**; 36: 3405-3408.

8. Cañete M, Ortiz A, Juarranz A, Villanueva A, Nonell S, Borrell JI, Teixido J, and Stockert JC. Photosensitizing properties of palladium-tetraphenylporphycene on cultured tumour cells. *Anti-Cancer Drug Des* **2000**; 15: 143-150.

9. Caminos DA, Spesia MB, and Durantini EN. Photodynamic inactivation of *Escherichia coli* by novel meso-substituted porphyrins by 4-(3-*N,N,N*-trimethylammoniumpropoxy)phenyl and 4-(trifluoromethyl)phenyl groups. *Photochem Photobiol Sci* **2006**; 5: 56-65.

10. Tegos GP, Demidova TN, Arcila-Lopez D, Lee H, Wharton T, Gali H, and Hamblin MR. Cationic fullerenes are effective and selective antimicrobial photosensitizers. *Chem Biol* **2005**; 12: 1127-1135.

11. Segalla A, Borsarelli CD, Braslavsky SE, Spikes JD, Roncucci G, Dei D, Chiti G, Jori G, and Reddi E. Photophysical, photochemical and antibacterial photosensitizing properties of a novel octacationic Zn(II)-phthalocyanine. *Photochem Photobiol Sci* **2002**; 1: 641-648.

12. Jimenez-Banzo A, Ragas X, Kapusta P, and Nonell S. Time-resolved methods in biophysics. 7. Photon counting vs. analog time-resolved singlet oxygen phosphorescence detection. *Photochem Photobiol Sci* **2008**; 7: 1003-1010.

13. Stockert JC, Juarranz A, Villanueva A, Nonell S, Horobin RW, Soltermann AT, Durantini EN, Rivarola V, Colombo LL, Espada J, and Cañete M. Photodynamic therapy: selective uptake by photosensitising drugs into tumor cells. *Curr Top Pharmacol* **2004**; 8: 185-217.

14. Snyder JW, Skovsen E, Lambert JDC, and Ogilby PR. Subcellular, time-resolved studies of singlet oxygen in single cells. *J Am Chem Soc* **2005**; 127: 14558-14559.

15. Jimenez-Banzo A, Sagrista ML, Mora M, and Nonell S. Kinetics of singlet oxygen photosensitization in human skin fibroblasts. *Free Rad Biol Med* **2008**; 44: 1926-1934.

16. Dahl TA, Midden WR, and Hartman PE. Pure Singlet oxygen cytotoxicity for bacteria. *Photochem Photobiol* **1987**; 46: 345-352.

17. Bulina ME, Chudakov DM, Britanova OV, Yanushevich YG, Staroverov DB, Chepurnykh TV, Merzlyak EM, Shkrob MA, Lukyanov S, and Lukyanov KA. A genetically encoded photosensitizer. *Nat Biotechnol* **2006**; 24: 95-99.

18. Hideg E. A comparative study of fluorescent singlet oxygen probes in plant leaves. *Cent Eur J Biol* **2008**; 3: 273-284.

19. Wardman P. Fluorescent and luminescent probes for measurement of oxidative and nitrosative species in cells and tissues: Progress, pitfalls, and prospects. *Free Rad Biol Med* **2007**; 43: 995-1022.

20. Shaner NC, Lin MZ, McKeown MR, Steinbach PA, Hazelwood KL, Davidson MW, and Tsien RY. Improving the photostability of bright monomeric orange and red fluorescent proteins. *Nat Methods* **2008**; 5: 545-551.

21. Jimenez-Banzo A, Nonell S, Hofkens J, and Flors C. Singlet oxygen photosensitization by EGFP and its chromophore HBDI. *Biophys J* **2008**; 94: 168-172.

22. Narband N, Tubby S, Parkin IP, Gil-Tomas J, Ready D, Nair SP, and Wilson M. Gold nanoparticles enhance the toluidine blue-induced lethal photosensitisation of *Staphylococcus aureus*. *Curr Nanosci* **2008**; 4: 409-414.

Chapter 11

Conclusions

1. Among the photosensitisers tested in this thesis, new methylene blue is the most active phenothiazinium dye *in vitro* against multidrug-resistant *Acinetobacter baumanii*, being also able to succesfully treat burn infections of *A. baumanii in vivo* in a mouse model.

2. Aryl cationic porphycenes are promising photosensitisers for antimicrobial photodynamic therapy due to their efficacy *in vitro* and *in vivo* against a broad-spectrum of prototypical human pathogenic microbes including bacteria and yeasts.

3. The localization of antimicrobial photodynamic therapy cationic photosensitisers in gram-negative bacteria depends on the number and topology of the positive charges. While photosensitisers with charged photoactive centers localize in the external structure of the cell wall, hydrophobic photosensitisers with positive charges far from the chromophore localize in oxygen-shielded sites, possibly inside the outer membrane.

4. The kinetics of singlet oxygen deactivation in *E. coli* depends on the internalisation's degree of the photosensitiser. On one hand, singlet oxygen produced in the external structure of the cell wall is mainly deactivated by the external aqueous phase, while singlet oxygen produced within the outer membrane shows equilibrium between cell-deactivation and solvent-deactivation pathways. On the other hand, singlet oxygen produced inside the cell is able to cross the cell wall, supporting the idea that the PS does not need to be internalized for inflicting photodamage on vital structures of the cell.

5. The ability of the fluorescent probe Singlet Oxygen Sensor Green to self-sensitise the production of singlet oxygen upon irradiation with UV and, to a lesser extent, visible light implies that care must be exercised when using this probe to ascertain the presence of singlet oxygen in a photosystem.

6. The ability of fluorescent proteins to photosensitise the production of singlet oxygen pave the way for the development of genetically-encoded photosensitisers for chromophore-assisted laser inactivation purposes. Specifically, the production of singlet oxygen has been quantified for the first time for the red fluorescent protein TagRFP, which shows a quantum yield of singlet oxygen production $\Phi_\Delta = 0.004 \pm 0.001$, but does not produce superoxide radical to any measurable extent.

7. The surface plasmon effect generated by silver island films enhances the phosphorescence of singlet oxygen opening the possibility to boost the detection of this reactive oxygen species *in vivo*. Likewise, the also enhanced production of this reactive oxygen species shed light into a new alternative to improve the effectiveness of commonly used antimicrobial photodynamic therapy agents by conjugation with plasmon-active nanoparticles.

List of contributions to other articles

During the development of the thesis, some contributions to other articles that do not belong to the present work have been performed:

1. Jimenez-Banzo A, Ragàs X, Kapusta P, and Nonell S. Time-resolved methods in biophysics. 7. Photon counting vs. analog time-resolved singlet oxygen phosphorescence detection. *Photochem Photobiol Sci* **2008**; 7: 1003-1010.

2. Jimenez-Banzo A, Ragàs X, Abbruzzetti S, Viappiani C, Campanini B, Flors C, and Nonell S. Singlet oxygen photosensitisation by GFP mutants: Oxygen accessibility to the chromophore. *Photochem Photobiol Sci* **2010**, DOI:10.1039/C0PP00125B.

3. Hahn U, Setaro F, Ragàs X, Gray-Weale A, Nonell S, and Torres T. Microenvironment switchable singlet oxygen generation by axially-coordinated hydrophilic ruthenium phthalocyanine dendrimers. *Phys Chem Chem Phys* **2010**, submitted.